HOMOGENEOUS CATALYSTS FOR THE HYDROLYSIS OF SODIUM BOROHYDRIDE: SYNTHESIS, CHARACTERIZATION AND CATALYTIC USE

A THESIS SUBMITTED TO
THE GRADUATE SCHOOL OF NATURAL AND APPLIED SCIENCES
OF
MIDDLE EAST TECHNICAL UNIVERSITY

BY

MEHDI MASJEDI

IN PARTIAL FULFILLMENT OF THE REQUIREMENTS
FOR
THE DEGREE OF DOCTOR OF PHILOSOPHY
IN
CHEMISTRY

AUGUST 2010

Approval of the thesis:

HOMOGENEOUS CATALYSTS FOR THE HYDROLYSIS OF SODIUM BOROHYDRIDE: SYNTHESIS, CHARACTERIZATION AND CATALYTIC USE

submitted by **MEHDI MASJEDI** in partial fulfillment of the requirements for the degree of **Doctor of Philosophy in Chemistry Department, Middle East Technical University** by,

Prof. Dr. Canan Özgen _____
Dean, Graduate School of **Natural and Applied Sciences**

Prof. Dr. İlker Özkan _____
Head of Department, **Chemistry**

Prof. Dr. Saim Özkar
Supervisor, **Chemistry Dept., METU** _____

Examining Committee Members:

Prof. Dr. Hüseyin İşçi _____
Chemistry Dept., METU

Prof. Dr. Saim Özkar _____
Chemistry Dept., METU

Prof. Dr. Ceyhan Kayran _____
Chemistry Dept., METU

Assoc. Prof. Dr. Ayşen Yilmaz _____
Chemistry Dept., METU

Prof. Dr. Yavuz İmamoğlu _____
Chemistry Dept., Hacettepe University

Date: 13.08.2010

I hereby declare that all information in this document has been obtained and presented in accordance with academic rules and ethical conduct. I also declare that, as required by these rules and conduct, I have fully cited and referenced all material and results that are not original to this work.

Name, Last name: MEHDI MASJEDI

Signature

ABSTRACT

HOMOGENEOUS CATALYSTS FOR THE HYDROLYSIS OF SODIUM BOROHYDRIDE: SYNTHESIS, CHARACTERIZATION AND CATALYTIC USE

Masjedi, Mehdi

Ph.D., Department of Chemistry

Supervisor: Prof. Dr. Saim Özkar

August 2010, 120 pages

Recent study has shown that ruthenium(III) acetylacetonate acts as a homogeneous catalyst in the hydrolysis of sodium borohydride. When two equivalents of trimethylphosphite per ruthenium is added to the reaction solution containing sodium borohydride and ruthenium(III) acetylacetonate in the mixture of water and tetrahydrofuran, the rate of hydrogen generation is practically stopped (or reduced to the level of self hydrolysis). However, the catalytic hydrogen evolution of sodium borohydride restarts at an unexpectedly high rate in a certain period of time (induction time) after addition of trimethylphosphite. Consequently, trimethylphosphite known to be a poison in the hydrolysis, is involved in the formation of a new active catalyst (ruthenium species containing trimethylphosphite ligands) which has much higher catalytic activity in comparison with sole ruthenium(III) acetylacetonate. The same rate enhancement is observed by addition of two equivalents of triphenylphosphite per ruthenium into the medium. Varying the phosphorus compound affects not only the life time of catalyst but also the kinetic and activation parameters of the hydrolysis of sodium borohydride. However,

varying the mole ratio of phosphorus compound to ruthenium does not affect the rate of hydrolysis or in other words, the rate of hydrogen generation is independent of phosphite concentration.

Trans- and cis-[Ru(acac)$_2${P(OMe)$_3$}$_2$] complexes do not show significant catalytic activity in hydrogen generation of sodium borohydride. However, catalytic activity of cis-isomer is highly increased in the presence of two equivalents of trimethylphosphite, showing that the active catalyst formed during hydrolysis of sodium borohydride starting with Ru(acac)$_3$ or cis-[Ru(acac)$_2${P(OMe)$_3$}$_2$], has more than two phosphine ligands. For the first time, a ruthenium(I) complex was isolated from aqueous solution after finishing the catalytic hydrolysis of sodium borohydride starting with ruthenium(III) acetylacetonate and trimethylphosphite. Hydridotetrakis(trimethylphosphite)ruthenium(I), [Ru{P(OMe)$_3$}$_4$H] was isolated and characterized by single crystal X-ray diffraction, Mass, UV-visible, FTIR, ^{1}H, ^{13}C and ^{31}PNMR spectroscopy. Following the catalytic reaction by UV-Visible spectroscopy shows in-situ formation of a Ru(II) species which is mostly converted back to ruthenium(III) acetylacetonate after hydrolysis reaction along with formation of [Ru{P(OMe)$_3$}$_4$H] complex as a minor product. Although Ru(II) species could not be isolated, adding 1 equivalent of 2,2'-bipyridine yielded [Ru(acac)(bipy){P(OMe)$_3$}H] complex which could be isolated and characterized by Mass, UV-Visible, FTIR, ^{1}H, ^{13}C and ^{31}PNMR spectroscopy. In-situ generated Ru(II) species has much higher catalytic activity in comparison with its stabilized form [Ru(acac)(bipy){P(OMe)$_3$}H] or [Ru{P(OMe)$_3$}$_4$H] complex. Conclusively, the fac-[Ru(acac){P(OMe)$_3$}$_3$H] complex is believed to be the in-situ generated Ru(II) species and the active catalyst in the hydrolysis of sodium borohydride.

Keywords: Ruthenium; Acetylacetonate; Phosphine; Sodium borohydride; Hydrolysis; Homogeneous catalysis.

ÖZ

SODYUM BORHİDRÜRÜN HİDROLİZİ İÇİN HOMOJEN KATALİZÖR: SENTEZİ, YAPISAL TANIMLANMASI VE KATALİTİK ETKİNLİĞİ

Masjedi, Mehdi
Doktora, Kimya Bölümü
Tez Yöneticisi: Prof. Dr. Saim Özkar

2010, 120 sayfa

Son zamanlarda yapılan bir çalışma, rutenyum(III) asetil asetonatın sodyum borhidrürün hidrolizinde homojen katalizör olarak davrandığını göstermiştir. Sodyum borhidrür ve rutenyum(III) asetil asetonat içeren tetrahidrofuran ve su karışımındaki tepkime çözeltisine, her bir rutenyum için iki eşdeğer trimetilfosfit eklenmesi, hidrojen üretimini durdurmaktadır (veya öz hidroliz seviyesine düşürmektedir). Bununla birlikte, trimetilfosfit ilavesinden sonra, sodyum bor hidrürün katalitik hidrojen oluşumu, belli bir süre içinde (oluşum süresi) yüksek bir hızla yeniden başlamaktadır. Sonuç olarak, hidrolizde bir zehir olarak bilinen trimetilfosfit, rutenyum(III) asetil asetonat ile karşılaştırıldığında çok daha yüksek katalitik etkinliğe sahip olan yeni bir etkin katalizörün (trimetilfosfit ligandlarını içeren rutenyum türü) oluşumuna yol açmaktadır. Aynı hız artışı, ortamdaki her rutenyum için iki eşdeğer trifenilfosfit ilavesinde de gözlenmektedir. Fosforlu bileşiği değiştirmek sadece katalizörün ömrünü etkilemekle kalmayıp aynı zamanda sodyum borhidrürün hidrolizinin kinetik ve aktivasyon parametrelerini de etkilemektedir. Fosforlu bileşiğin rutenyuma karşı mol oranının arttırılması,

hidrolizin hızını etkilememekte veya bir başka ifadeyle, hidrojen üretim hızı fosfit derişiminden bağımsız olmaktadır.

Sodyum borhidrürün hidrolizinden hidrojen üretiminde trans- ve cis-[Ru(acac)$_2${P(OMe)$_3$}$_2$] kompleksleri önemli bir katalitik etkinlik göstermemektedir. Ancak, cis-izomerin katalitik etkinliği iki eşdeğer trimetilfosfit eşliğinde oldukça artmaktadır. Ru(acac)$_3$ veya cis-[Ru(acac)$_2${P(OMe)$_3$}$_2$] ile başlayan sodyum bor hidrürün hidrolizi esnasında oluşan aktif katalizörün ikiden fazla fosfit ligandına sahip olduğu görülmektedir. Rutenyum(III) asetilasetonat ve trimetilfosfit ile başlayan sodyum bor hidrürün hidrolizinin katalitik tepkimesi bittikten sonra, ilk kez bir rutenyum(I) kompleksi sulu çözeltiden ayrılmıştır. Hidridotetrakis(trimetilfosfit)rutenyum(I), [Ru{P(OMe)$_3$}$_4$H] kompleksi izole edilmiş ve bu kompleks tek kristal X-ışını kırınımı, Kütle, UV-Görünür, FTIR, ^{1}H, ^{13}C ve ^{31}P NMR spektroskopisi ile tanımlanmıştır. UV-Görünür spektroskopisi ile katalitik tepkime takip edildiğinde, hidrojen üretimi bittikten sonra, ürün olarak az miktardaki [Ru{P(OMe)$_3$}$_4$H] kompleksinin oluşmasıyla birlikte, ortamda bulunan rutenyum(II) kompleksinin çoğunlukla rutenyum(III) asetilasetonata yeniden dönüştüğü görülmektedir. Ru(II) kompleksinin izole edilememesine rağmen, bir eşdeger 2,2'-bipiridin eklenmesi ile oluşan [Ru(acac)(bipy){P(OMe)$_3$}H] kompleksi izole edilebilmiştir ve Kütle, UV-Görünür, FTIR, ^{1}H, ^{13}C ve ^{31}P NMR spektroskopisi ile tanımlanmıştır. Kararlaştırılmış hali olan [Ru(acac)(bipy){P(OMe)$_3$}H] kompleksi veya [Ru{P(OMe)$_3$}$_4$H] kompleksi ile karşılaştırıldığında, Ru(II) türü çok daha yüksek katalitik etkinliğe sahiptir. Sonuç olarak, fac-[Ru(acac){P(OMe)$_3$}$_3$H] kompleksinin sodyum borhidrürün hidrolizinde aktif katalizör olduğuna inanılmaktadır.

Anahtar Kelimeler: Rutenyum, Asetil asetonat, Fosfin, Sodyum bor hidrür, Hidroliz, Homojen kataliz.

To all, who understand the real value of science and sacrifice themselves for that.

ACKNOWLEDGEMENT

I would like to express my sincere gratitude to my supervisor Prof. Dr. Saim Ozkar for his continuous guidance, great support, patience and encouragement through this research work. It was a great pleasure for me to learn lots of things about organometallic synthesis and homogeneous catalysis.

My extensive thanks are offered to Professor Leyla Tatar Yildirim for her sincere cooperation regarding single crystal X-ray diffraction analysis.

Thanks also extended to Mr. Bunyamin Cosut from Gebze Institute of Technology for performing mass analysis.

I would like to thank to Meryem Seda Karayılan and Zehra Uzunoğlu from Chemistry Department in METU for performing NMR analysis.

I would like to thank the Technological and Scientific Research Council of Turkey (TUBITAK) for awarding me a PhD fellowship for 4 years.

I would like to express my sincere gratitude to my family for their great support and considerations within my PhD studies. Without their help and understanding, starting PhD studies would have not been possible for me.

I would like to express my special thanks to all the members of Nanoclusters and Organometallic research laboratory for their caring and friendship.

I would like to express my sincere gratitude to Department of Chemistry, METU for giving me the chance of becoming a PhD student and providing me the required lab facilities.

TABLE OF CONTENTS

ABSTRACT iv
ÖZ vi
ACKNOWLEDGEMENT ix
TABLE OF CONTENTS x
LIST OF FIGURES xiv
LIST OF SCHEMES xix
LIST OF TABLES xx
CHAPTERS
1. INTRODUCTION 1
2. EXPERIMENTAL 14
2.1 Materials 14
2.2 Equipment 14
2.3 Self hydrolysis of sodium borohydride. 16
2.4 Catalytic activity of ruthenium(III)acetylacetonate in the hydrolysis of sodium borohydride in the presence of trimethylphosphite 16
2.5 Catalytic activity of ruthenium(III)acetylacetonate in the hydrolysis of sodium borohydride in the presence of triphenylphosphite 17
2.6 Catalytic lifetime of ruthenium(III)acetylacetonate in the presence of different phosphorus ligands 18
2.7 Poisoning experiment 18
2.8 Preparation of cis-$[Ru(acac)_2(\eta^2\text{-}C_8H_{14})_2]$ complex 19
2.9 preparation of trans and cis-$[Ru(acac)_2\{P(OMe)_3\}_2]$ complexes 19
2.10 Crystal structure analysis of trans and cis-$[Ru(acac)_2\{P(OMe)_3\}_2]$ complexes 20

2.11 Catalytic activity of trans and cis-[$Ru(acac)_2\{P(OMe)_3\}_2$] in the hydrolysis of sodium borohydride 21
2.12 Catalytic activity of trans and cis-[$Ru(acac)_2\{P(OMe)_3\}_2$] in the hydrolysis of sodium borohydride in the presence of trimethylphosphite 21
2.13 Catalytic activity of $Ru(acac)_3$ in the hydrolysis of sodium borohydride.... 22
2.14 Isolation of monohydrotetrakis(trimethylphosphite)ruthenium(I) complex, [$Ru\{P(OMe)_3\}_4H$] 22
2.15 Single crystal X-ray diffraction analysis of [$Ru\{P(OMe)_3\}_4H$] 23
2.16 Catalytic activity of [$Ru\{P(OMe)_3\}_4H$] in the hydrolysis of sodium borohydride 24
2.17 UV-Visible spectroscopic measurements during hydrolysis of sodium borohydride catalyzed by $Ru(acac)_3$ and $P(OMe)_3$ 24
2.18 Stabilization of catalytically very active in-situ Ru(II) species by 2,2'-bipyridine in the form of [$Ru(acac)(bipy)\{P(OMe)_3H\}$]. 25
2.19 Catalytic activity of stabilized active catalyst with 2,2'-bipyridine in the hydrolysis of sodium borohydride plus UV-visible spectroscopic measurements 26
2.20 Preparation of 1,2-bis(diphenylphosphinoborane)ethane, $dppe(BH_3)_2$.....27
2.21 Single crystal X-ray diffraction analysis of 1,2-bis(diphenylphosphinoborane)ethane, $[Ph_2P(BH_3)CH_2]_2$ 28
3. RESULTS AND DISCUSSION ..... .29
3.1 Self hydrolysis of sodium borohydride 29
3.2 Ruthenium(III)acetylacetonate: a homogeneous catalyst in the hydrolysis of sodium borohydride 30
3.3 Catalytic activity of $Ru(acac)_3$ for the hydrolysis of $NaBH_4$ in the presence of trimethylphosphite 32
3.4 Catalytic activity of $Ru(acac)_3$ for the hydrolysis of $NaBH_4$ in the presence of triphenylphosphite 35
3.5 The effect of phosphorus concentration on catalytic activity of $Ru(acac)_3$ for the hydrolysis of $NaBH_4$ 36

3.6 Kinetic study of the hydrolysis of sodium borohydride catalyzed by $Ru(acac)_3$ plus 2 equivalents of $P(OMe)_3$ 39
3.6.1 The rate law for the hydrolysis of sodium borohydride catalyzed by Ruthenium(III)acetylacetonate plus 2 equivalents of $P(OMe)_3$ 39
3.6.2 Activation parameters for the hydrolysis of $NaBH_4$ catalyzed by $Ru(acac)_3$ plus 2 equivalents of $P(OMe)_3$ 43
3.7 The catalytic lifetime of ruthenium(III)acetylacetonate and 2 equivalents of $P(OMe)_3$ per ruthenium... 47
3.8 Kinetic study of the hydrolysis of sodium borohydride catalyzed by $Ru(acac)_3$ plus 2 equivalents of $P(OPh)_3$ 49
3.8.1 The rate law for the hydrolysis of sodium borohydride catalyzed by Ruthenium(III)acetylacetonate plus 2 equivalents of $P(OPh)_3$ 49
3.8.2 Activation parameters for the hydrolysis of $NaBH_4$ catalyzed by $Ru(acac)_3$ plus 2 equivalents of $P(OPh)_3$ 53
3.9 The catalytic lifetime of ruthenium(III)acetylacetonate and 2 equivalents of $P(OPh)_3$ per ruthenium..... 57
3.10 Activation parameters for the hydrolysis of $NaBH_4$ catalyzed by $Ru(acac)_3$ in the presence of different phosphorus compounds 58
3.11 The catalytic lifetime of ruthenium(III)acetylacetonate in the presence of different phosphorus compounds..... 60
3.12 Synthesis of trans- and cis-$[Ru(acac)_2\{P(OMe)_3\}_2]$ complexes 61
3.12.1 Characterization of trans- and cis-$[Ru(acac)_2\{P(OMe)_3\}_2]$ complexes by UV-Visible, Mass, ^1H, ^{13}C and ^{31}PNMR Spectroscopy 64
3.12.2 Crystal structure of trans- and cis-$[Ru(acac)_2\{P(OMe)_3\}_2]$. 71
3.13 Catalytic activity of trans- and cis-$[Ru(acac)_2\{P(OMe)_3\}_2]$ in hydrogen generation from the hydrolysis of sodium borohydride..... 76
3.14 Attempts to isolate the active catalyst after finishing the catalytic hydrolysis of sodium borohydride starting with $Ru(acac)_3$ and $P(OMe)_3$ along with UV-Visible spectroscopic mesurements during the catalytic reaction 78
3.15 Isolation and characterization of $[Ru\{P(OMe)_3\}_4H]$ complex..... 82

3.16 Testing catalytic activity of [Ru{P(OMe)$_3$}$_4$H] complex as a homogeneous catalyst in hydrogen generation from the hydrolysis of sodium borohydride....92
3.17 Stabilization, isolation and characterization of catalytically very active in-situ Ru(II) species formed temporarily during catalytic hydrolysis of sodium borohydride starting with Ru(acac)$_3$ and P(OMe)$_3$....93
3.18 Comparison the catalytic activity of in-situ active catalyst without stabilization, [Ru{P(OMe)$_3$}$_3$(acac)H], and in the case of stabilization by 2,2'-bipyridine, [Ru(bipy){P(OMe)$_3$}(acac)H], in hydrogen generation of sodium borohydride....100
3.19 Preparation, characterization and single crystal X-ray diffraction of 1,2-bis(diphenylphosphinoborane)ethane....101
4. CONCLUSION....108
REFERENCES....112

LIST OF FIGURES

FIGURES

Figure 1.1 : Comparison the hydrogen conent and hydrolysis heat of $NaBH_4$ with other chemical hydrides……3

Figure 1.2 : $Ru(acac)_3$ is acting as a homogeneous catalyst in the hydrolysis of sodium borohydride……6

Figure 1.3 : Plot of the volume of hydrogen generated versus time for the hydrolysis of $NaBH_4$ at 25 ºC in 50 mL THF/water (1/9) solution starting with [$NaBH_4$] = 450 mM, [$Ru(acac)_3$] = 3 mM, and (trimethylphosphite [$P(OMe)_3$] or triphenylphosphite [$P(OPh)_3$] = 6 mM) added at the beginning of catalytic reaction……..…..8

Figure 1.4 : Plot of hydrogen generation rate versus mole ratio of phosphine to ruthenium in the hydrolysis of $NaBH_4$ catalyzed by $Ru(acac)_3$ plus a phosphine. [$NaBH_4$] = 450 mM, [Ru] = 2.0 mM, T = 25 ºC……..9

Figure 2.1 : The experimental setup used in the measurement of the volume of hydrogen generated from the hydrolysis of sodium borohydride…….…..15

Figure 3.1 : plot of hydrogen volume versus time in the self hydrolysis of sodium borohydride starting with 450 mM $NaBH_4$ in 50 mL H_2O at 25°C……29

Figure 3.2 : Plots of hydrogen volume versus time for the self hydrolysis of sodium borohydride and hydrolysis of sodium borohydride catalyzed by $Ru(acac)_3$. [$NaBH_4$] = 450 mM, [$Ru(acac)_3$] = 2 mM, T = 25°C……30

Figure 3.3 : Plot of the relative rate versus the moles of $P(OCH_3)_3$/the moles of $Ru(acac)_3$ in the hydrolysis of sodium borohydride……...…32

Figure 3.4 : Plot of the volume of hydrogen generated versus time for the hydrolysis of $NaBH_4$ at 25 ºC in 50 mL THF/water (1/9) solution starting with [$NaBH_4$] = 450 mM, [$Ru(acac)_3$] = 2 mM and [$P(OMe)_3$] = 4 mM added at the beginning of catalytic reaction……..…….33

Figure 3.5 : Plot of the volume of hydrogen generated versus time for the hydrolysis of $NaBH_4$ at 25 ºC in 50 mL THF/water (1/9) solution starting with [$NaBH_4$] = 450 mM, [$Ru(acac)_3$] = 2 mM, and trimethylphosphite ([$P(OMe)_3$] = 4 mM) added in 80

minutes after the start of reaction. The addition of trimethylphosphite first stops the reaction completely. The reaction restarts at a faster rate in 75 minutes after the addition of $P(OMe)_3$……34

Figure 3.6 : Plot of the volume of hydrogen generated versus time for the hydrolysis of $NaBH_4$ at 25 ºC in 50 mL THF/water (1/9) solution starting with $[NaBH_4]$ = 450 mM, $[Ru(acac)_3]$ = 2 mM and $[P(OPh)_3]$ = 4 mM……..35

Figure 3.7 : Plot of hydrogen volume versus time in the hydrolysis of sodium borohydride starting with a solution containing 450 mM $NaBH_4$ and 2 mM $Ru(acac)_3$ plus different equivalents of $P(OCH_3)_3$ per ruthenium at 25°C……..36

Figure 3.8 : Plot of hydrogen volume versus time in the hydrolysis of sodium borohydride starting with a solution containing 450 mM $NaBH_4$ and 2 mM $Ru(acac)_3$ plus different equivalents of $P(OPh)_3$ per ruthenium at 25°C……37

Figure 3.9 : Plot of hydrogen generation rate versus mole ratio of phosphine to ruthenium in the hydrolysis of $NaBH_4$ catalyzed by $Ru(acac)_3$ plus a phosphine. $[NaBH_4]$ = 450 mM, [Ru] = 2.0 mM, T = 25 ºC……38

Figure 3.10 : The volume of H_2 versus time plots during the hydrolysis of $NaBH_4$ solution (450 mM) catalyzed by $Ru(acac)_3$ and 2 equivalents of $P(OMe)_3$ in different ruthenium concentration at 25°C……40

Figure 3.11 : The graph of ln (rate) versus ln [Ru] for the hydrolysis of sodium borohydride catalyzed by different concentrations of $Ru(acac)_3$ and 2 equivalents of $P(OMe)_3$ per ruthenium at 25°C……41

Figure 3.12 : The volume of H_2 versus time plot during the hydrolysis of sodium borohydride solution catalyzed by 2 mM $Ru(acac)_3$ and 2 equivalents of $P(OMe)_3$ in different sodium borohydride concentrations at 25°C……42

Figure 3.13 : The graph of ln (rate) versus ln $[NaBH_4]$ for the hydrolysis of sodium borohydride with different concentrations (in the range of 300-1500 mM) catalyzed by a constant concentration of $Ru(acac)_3$ (2 mM) and 2 equivalents of $P(OMe)_3$ at 25.0°C……43

Figure 3.14 : Plot of hydrogen volume generated versus time for the hydrolysis of sodium borohydride (450 mM) catalyzed by 2 mM $Ru(acac)_3$ and 2 equivalents of $P(OMe)_3$ per ruthenium at various temperatures……44

Figure 3.15 : Arrhenius plot for the hydrolysis of sodium borohydride (450 mM) catalyzed by 2 mM $Ru(acac)_3$ and 2 equivalents of $P(OMe)_3$ per ruthenium at various temperatures……46

Figure 3.16 : Eyring plot for the hydrolysis of sodium borohydride (450 mM) catalyzed by 2 mM $Ru(acac)_3$ and 2 equivalents of $P(OMe)_3$ per ruthenium at various temperatures……47

Figure 3.17 : Plot of total turnover number versus time for hydrogen generation from the catalytic hydrolysis of sodium borohydride starting with 2 mM $Ru(acac)_3$, 2 equivalents of $P(OMe)_3$ per ruthenium and 450 mM $NaBH_4$ in 50 mL H_2O-THF solution at 25.0°C……...…48

Figure 3.18 : The volume of hydrogen versus time plots during the hydrolysis of $NaBH_4$ solution (450 mM) catalyzed by $Ru(acac)_3$ and 2 equivalents of $P(OPh)_3$ in different ruthenium concentration at 25°C…….50

Figure 3.19 : The graph of ln (rate) versus ln [Ru] for the hydrolysis of sodium borohydride catalyzed by different concentrations of $Ru(acac)_3$ and 2 equivalents of $P(OPh)_3$ per ruthenium at 25°C……...……51

Figure 3.20 : The volume of H_2 versus time plot during the hydrolysis of sodium borohydride solution catalyzed by 2 mM $Ru(acac)_3$ and 2 equivalents of $P(OPh)_3$ in different sodium borohydride concentrations at 25°C……52

Figure 3.21 : The graph of ln (rate) versus ln [$NaBH_4$] for the hydrolysis of sodium borohydride with different concentrations (in the range of 300-1500 mM) catalyzed by a constant concentration of $Ru(acac)_3$ (2 mM) and 2 equivalents of $P(OPh)_3$ at 25.0°C…….53

Figure 3.22 : Plot of hydrogen volume generated versus time for the hydrolysis of sodium borohydride (450 mM) catalyzed by 2 mM $Ru(acac)_3$ and 2 equivalents of $P(OPh)_3$ per ruthenium at various temperatures…….54

Figure 3.23 : Arrhenius plot for the hydrolysis of sodium borohydride (450 mM) catalyzed by 2 mM $Ru(acac)_3$ and 2 equivalents of $P(OPh)_3$ per ruthenium at various temperatures……56

Figure 3.24 : Eyring plot for the hydrolysis of sodium borohydride (450 mM) catalyzed by 2 mM $Ru(acac)_3$ and 2 equivalents of $P(OPh)_3$ per ruthenium at various temperatures……57

Figure 3.25 : Plot of total turnover number versus time for hydrogen generation from the catalytic hydrolysis of sodium borohydride starting with 2 mM $Ru(acac)_3$, 2 equivalents of $P(OPh)_3$ per ruthenium and 450 mM $NaBH_4$ in 50 mL H_2O-THF solution at 25.0°C……...…58

Figure 3.26 : Plots of total turnover number versus time for hydrogen generation from the catalytic hydrolysis of sodium borohydride starting with 2 mM $Ru(acac)_3$, 2 equivalents of phosphine per ruthenium and 450 mM $NaBH_4$ in 50 mL H_2O-THF solution at 25.0 °C for all of the phosphines……..…….61

Figure 3.27 : ^{1}HNMR of trans-$[Ru(acac)_2\{P(OMe)_3\}_2]$ complex……..…65

Figure 3.28 : ^{1}HNMR of cis-$[Ru(acac)_2\{P(OMe)_3\}_2]$ complex……..……65

Figure 3.29 : ^{13}CNMR of trans-[Ru(acac)$_2${P(OMe)$_3$}$_2$] complex……66

Figure 3.30 : ^{13}CNMR of cis-[Ru(acac)$_2${P(OMe)$_3$}$_2$] complex……67

Figure 3.31 : ^{31}PNMR spectrum of trans-[Ru(acac)$_2${P(OMe)$_3$}$_2$] complex…….68

Figure 3.32 : ^{31}PNMR spectrum of cis-[Ru(acac)$_2${P(OMe)$_3$}$_2$] complex……68

Figure 3.33 : FAB-Mass spectrum of trans- or cis-[Ru(acac)$_2${P(OMe)$_3$}$_2$] complexes……...…69

Figure 3.34 : UV spectrum of trans-[Ru(acac)$_2${P(OMe)$_3$}$_2$] complex…….……70

Figure 3.35 : UV spectrum of cis-[Ru(acac)$_2${P(OMe)$_3$}$_2$] complex…….……70

Figure 3.36 : ORTEP drawing of the title compounds with the atomic numbering scheme Displacement ellipsoids are drawn at the 30% probability level for trans -[Ru(acac)$_2${P(OMe)$_3$}$_2$], where (i: -x, -y, -z)……..73

Figure 3.37 : ORTEP drawing of the title compounds with the atomic numbering scheme Displacement ellipsoids are drawn at the 30% probability level for cis -[Ru(acac)$_2${P(OMe)$_3$}$_2$], where (i: -x, -y, -z)……..73

Figure 3.38 : Basal planes of the coordination geometry for the Ru(II) ion in the trans (a) and in the cis (b) structures……74

Figure 3.39 : Volume of hydrogen versus time for the hydrolysis of sodium borohydride using compounds : a) *cis*-[Ru(acac)$_2${P(OMe)$_3$}$_2$], b) *trans*-[Ru(acac)$_2${P(OMe)$_3$}$_2$], c) *trans*-[Ru(acac)$_2${P(OMe)$_3$}$_2$] plus 2 equivalents of P(OMe)$_3$, d) [Ru(acac)$_3$], e) [Ru(acac)$_3$] plus 2 equivalents of P(OMe)$_3$, f) *cis*-[Ru(acac)$_2${P(OMe)$_3$}$_2$] plus 2 equivalents of P(OMe)$_3$……78

Figure 3.40 : ^{1}HNMR spectroscopy of combined paramagnetic Ru(acac)$_3$ and ruthenium complex with trimethylphosphite ligands……79

Figure 3.41 : ^{13}CNMR spectroscopy of combined paramagnetic Ru(acac)$_3$ and ruthenium complex with trimethylphosphite ligands……80

Figure 3.42 : UV-Visible spectroscopic measurements during hydrolysis of $NaBH_4$ (450 mM) starting with 2 mM Ru(acac)$_3$ and P(OMe)$_3$ (4-8 mM) in THF-H_2O (1:9) at 25 °C……..…….81

Figure 3.43 : X-ray crystal structure of [Ru{P(OMe)$_3$}$_4$H] complex……83

Figure 3.44 : Projection of the crystal structure of [Ru{P(OMe)$_3$}$_4$H] complex…...84

Figure 3.45 : ^{1}HNMR spectrum of [Ru{P(OMe)$_3$}$_4$H] complex……...…87

Figure 3.46 : ^{13}CNMR spectrum of [Ru{P(OMe)$_3$}$_4$H] complex……..88

Figure 3.47 : ^{31}PNMR spectrum of [Ru{P(OMe)$_3$}$_4$H] complex……...…89

Figure 3.48 : UV-Visible spectrum of [Ru{P(OMe)$_3$}$_4$H] complex…….……90

Figure 3.49 : FTIR spectrum of [Ru{P(OMe)$_3$}$_4$H] complex taken by ATR/FTIR spectrometer ……...……91

Figure 3.50 : Mass spectrum of [Ru{P(OMe)$_3$}$_4$H] complex……91

Figure 3.51 : Volume of hydrogen versus time for the hydrolysis of $NaBH_4$ (450 mM) using 0.6 mM of ruthenium compounds : a) *cis*-[Ru(acac)$_2${P(OMe)$_3$}$_2$], b) *trans*-[Ru(acac)$_2${P(OMe)$_3$}$_2$], c) *trans*-[Ru(acac)$_2${P(OMe)$_3$}$_2$] plus 2 equivalents of P(OMe)$_3$, d) [Ru{P(OMe)$_3$}$_4$H] e) [Ru(acac)$_3$], f) [Ru(acac)$_3$] plus 2 equivalents of P(OMe)$_3$, g) *cis*-[Ru(acac)$_2${P(OMe)$_3$}$_2$] plus 2 equivalents of P(OMe)$_3$……..92

Figure 3.52 : UV-Visible spectroscopic measurements during hydrolysis of $NaBH_4$ (450 mM) starting with 2 mM Ru(acac)$_3$ and 3 equivalents of P(OMe)$_3$ along with stabilization by 2,2´-bipyridine (2.5 mM)……..….94

Figure 3.53 : ^{1}HNMR spectrum of [Ru(acac)(bipy){P(OMe)$_3$}H] complex…….95

Figure 3.54 : ^{13}CNMR spectrum of [Ru(acac)(bipy){P(OMe)$_3$}H] complex……....96

Figure 3.55 : ^{31}PNMR spectrum of [Ru(acac)(bipy){P(OMe)$_3$}H] complex……....97

Figure 3.56 : FTIR spectrum of [Ru(acac)(bipy){P(OMe)$_3$}H] complex……..…98

Figure 3.57 : Mass spectrum of [Ru(acac)(bipy){P(OMe)$_3$}H] complex……..…98

Figure 3.58 : Volume of H_2 versus time for the hydrolysis of $NaBH_4$ (450 mM) starting with 2 mM Ru(acac)$_3$ in the case of a) in-situ active catalyst, [Ru(acac){P(OMe)$_3$}$_3$H], b) active catalyst stabilized by 2,2´-bipyridine, [Ru(acac)(bipy){P(OMe)$_3$}H]…….……..……...…100

Figure 3.59 : ORTEP drawing of the title compound with the atomic numbering scheme for DPPE(BH$_3$)$_2$ complex……104

Figure 3.60 : ^{1}HNMR of DPPE(BH$_3$)$_2$…….105

Figure 3.61 : ^{13}CNMR of DPPE(BH$_3$)$_2$……106

Figure 3.62 : ^{31}PNMR of DPPE(BH$_3$)$_2$……106

Figure 3.63 : ^{11}BNMR of DPPE(BH$_3$)$_2$……107

LIST OF SCHEMES

Scheme 3.1 : Suggested pathway for fomation of trans- and cis-[$Ru(acac)_2L_2$] from cis-[$Ru(acac)_2(\eta^2\text{-}C_8H_{14})L$]…….64

LIST OF TABLES

TABLES

Table 3.1. Rate constant valuse for the hydrolysis of sodium borohydride (450 mM) catalyzed by 2 mM $Ru(acac)_3$ and 2 equivalents of $P(OMe)_3$ per ruthenium at various temperatures……45

Table 3.2. Rate constant valuse for the hydrolysis of sodium borohydride (450 mM) catalyzed by 2 mM $Ru(acac)_3$ and 2 equivalents of $P(OPh)_3$ per ruthenium at various temperatures……55

Table 3.3. The rate constant values k in (mmol H_2). (mmol Ru)$^{-1}$. s^{-1} at various temperatures and the activation parameters (Ea in kJ.mol^{-1}, A, $\Delta H^{\#}$ in kJ.mol^{-1}, and $\Delta S^{\#}$ in J.mol^{-1}.K^{-1}) for the hydrolysis of sodium borohydride catalyzed by $Ru(acac)_3$ plus 2 equivalents of phosphine per ruthenium starting with a solution of 450 mM $NaBH_4$ and 2 mM $Ru(acac)_3$……59

Table 3.4. Crystal data and results of structure refinement for trans- and cis-$[Ru(acac)_2\{P(OMe)_3\}_2]$ complexes……72

Table 3.5. Selected bond lengths and angles for compounds (Å,°)……75

Table 3.6. Hydrogen-bonding geometry (Å,°)……76

Table 3.7. Crystal data and experimental details of the title compound……85

Table 3.8. Selected/average bond length [Å] and angles [°] for the three asymmetric units of $[Ru\{P(OMe)_3\}_4H]$……86

Table 3.9. Crystal data and structure refinement for $DPPE(BH_3)_2$……102

Table 3.10. Selected bond length [Å] and angles [°] for two asymmetric units of $DPPE(BH_3)_2$……103

Table 3.11. Structural parameters of pi-ring interaction geometry (Å,°) for the title compound……103

CHAPTER 1

INTRODUCTION

From the beginning of industrialization, human kind has been consuming natural resources without thinking about the environmental impact and possible consequences of their exhaustion. A major effect of using fossil fuels is global warming, which causes hundreds of deaths in warm climate countries, increasing levels of sea water worldwide which threatens seaside cities and numerous other natural disasters such as floods, hurricanes, forest fires and so on. To solve the problems of global warming, clean energy technologies such as solar energy, wind power, hydropower, biomass energy, geothermal energy, tidal energy and wave power technologies are improving very rapidly. The main problem with these technologies is that energy produced from these sources is difficult to store or transport. It is obvious that an energy career is needed for all of these energy sources, which will be hydrogen [1], giving its name to the new era coming soon- The Hydrogen Era. Although hydrogen is the most abundant element in the universe, it has to be produced, since on earth it only occurs in the form of water and hydrocarbons [2].

Hydrogen can be produced by numerous techniques, with no emission of pollutants and green house gases. Hydrogen has a number of attractive advantages such as high energy density, non-toxic reaction products and abundant natural resources. Hydrogen is produced from various energy sources, stored, transported and used in industries, homes, automobiles, airplanes and factories or used as electricity generations [3]. Especially, proton exchange membrane (PEM) fuel cells

are attractive and alternative options for producing clean energy for on-board system. However, the major hurdle for commercialization of systems with PEM fuel cell is how to generate and supply pure hydrogen gas directly [4] where low system weight and portability are important. Hence, fuel cells which store hydrogen and operate by using it as fuel, have been under development. Such a fuel cell is a battery which is actuated with a gas. Energy obtained upon a reaction of hydrogen and oxygen is directly converted into electric energy [5]. Since such a fuel cell has an efficiency much higher than that of conventional combustion engines, fuel cell vehicle (FCV) is expected as a car having high efficiency [6,7]. Recently, studies of the fuel cells of the type which employ a hydrogen-containing hydrocarbon compound such as methane, propane, methanol, hydrazine and ammonia, have been developed [8,9]. However, these fuel cells have the disadvantages that they require high temperature (e.g., 100 – 300 °C) for effective oxidation/reduction reactions of hydrogen/oxygen, so that the reaction rate is very slow. The main challenge for the widespread application of hydrogen is its real-time production and its safe and convenient storage. H_2 has low density which makes it difficult to store in compressed or liquid form. Carbon nanotubes have received considerable research interests as a probably better hydrogen storage materials [10], but their unusually high hydrogen absorption capacity can only be realized under extreme conditions such as low temperatures and high pressures. The hydrogen-storing alloy is considered to play an important role in fuel cell vehicle (FCV). For the hydrogen-storing alloy, however, there are also many problems to overcome, such as its heaviness (small amount of storage per unit weight) due to its nature as an alloy and deterioration (the alloy turning into finer particles or changing its structure) upon repeated storage and release [11]. Attention has recently been given to the generation of pure hydrogen and without any fuel-cell poisons [12,13] by the hydrolysis of alkaline or alkaline earth metal hydrides [14]. As a new fueling concept, it can be suggested that the chemical hydrides ($NaBH_4$, KBH_4, LiH, NaH, etc.) act as new fuel media supplying hydrogen at normal temperature [15,16,17]. Chemical hydrides are very reactive with water, which results in releasing a large amount of H_2. Among these chemical hydrides, sodium borohydride ($NaBH_4$) is safe and practical means of storing hydrogen and it is desirable due to its high hydrogen content of 10.57 wt.%, moderate heat of

hydrolysis in comparison with other chemical hydrides (Figure 1.1) and the excellent stability of its alkaline solutions [18].

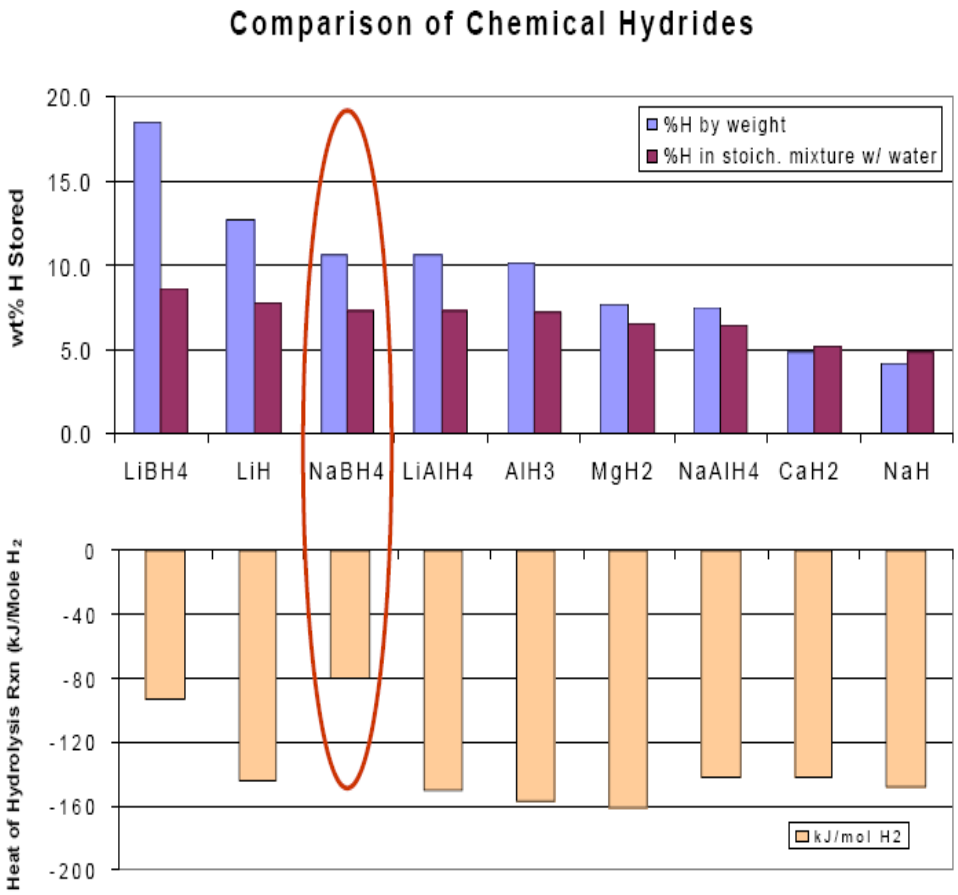

Fig 1.1. Comparison the hydrogen content and hydrolysis heat of $NaBH_4$ with other chemical hydrides.

Sodium borohydride has been considered as hydrogen storage material [2,15,16,17,19] in the use of renewable energy sources [1] on the way towards sustainable energy of the future [20,21,22,23]. A stabilized aqueous solution of sodium borohydride is a safe, simple and compact source of high-purity hydrogen [24]. The hydrolysis reaction is exothermic and proceeds according to equation:

$$NaBH_4(aq) + 2H_2O(l) \xrightarrow{\text{catalyst}} NaBO_2(aq) + 4H_2(g) \qquad (1.1)$$

Hydrolysis of $NaBH_4$ produces hydrogen gas and water-soluble sodium metaborate, $NaBO_2$, as a side product. Generating H_2 catalytically from $NaBH_4$

solutions has the following adavantages: $NaBH_4$ solutions are nonflammable and stable in air for months, H_2 generation only occurs in the presence of selected catalysts, the only other product in the gas stream is water vapor, reaction products are environmentally safe, H_2 generation rates are easily controlled, volumetric and gravimetric H_2 storage efficiencies are high, the reaction products can be recycled and H_2 can be generated even at 0°C [16]. At ordinary temperatures, only a small fraction of the theoretical amount of hydrogen is liberated after the sodium borohydride and water have been mixed [12,14]. The decrease in the initial rate of hydrogen evolution is due to the increasing pH of the solution which in turn caused by the formation of the basic metaborate ion. Such a hydrolysis of sodium borohydride has been known to be accelerated by catalysts, by acid [25] or under elevated temperature [12].

The first study on catalytic hydrolysis of sodium borohydride was performed by Schlesinger in 1953 using platinum and rhodium salts as catalyst [26], followed by Pecsok [27], L. Brown [28], C. Brown (iron, ruthenium, palladium, osmium, iridium, and platinum salts) [29], Stockmayer [30], Davis [31,32], Mesmer [33], Gardiner [34], Sen (nickel, Raney nickel, and bulk cobalt) [35], Amendola (bulk ruthenium) [15], Kojima (mixed metal/metal oxides such as Pt-$LiCoO_2$) [5,36,37], Hanxi (nickel boride) [38], Lee [39], Wu [40,41], Kim [3], Yang [42] (filamentary nickel-cobalt).

Homogeneous catalysts applied in the hydrolysis of sodium borohydride are rare. One of the pioneer works on the catalyzed $NaBH_4$ hydrolysis by Schlesinger and co-workers [26] examined a number of metal salts and estabilished relative rates for hydrogen generation using these homogeneous catalysts. In their studies, aqueous solutions of the metal salts were added to aqueous solutions of $NaBH_4$ at 25°C. Ruthenium and rhodium salts showed the best catalytic activity. Chloride salts of manganese, iron, cobalt, nickel and copper were also demonstrated to be active for catalytic hydrolysis of sodium borohydride to produce hydrogen at room temperature. Almost all of other catalysts applied in the hydrolysis of sodium borohydride so far are bulk metals and they act as heterogeneous catalysts [4,5

,43,44]. The limited surface area of the heterogeneous catalysts causes lower catalytic activity as the activity of catalyst is directly related to its surface area. Thus, the use of metal nanoparticles with large surface area provides potential route to increase the catalytic activity. Ruthenium(0) nanoclusters have been reported as the first transition metal nanoclusters used as catalysts in the hydrolysis of sodium borohydride at ambient temperature with an appreciable rate of hydrogen generation [45]. Ruthenium nanoparticles generated from the reduction of ruthenium(III) chloride by sodium borohydride in water and stabilized by using acetate anion, provide the lowest activation energy ever found for the hydrolysis of sodium borohydride [46]. As another example, water-dispersible nickel(0) nanoclusters prepared from the reduction of nickel(II) acetylacetonate by sodium borohydride in aqueous solution and stabilized by hydrogenphospate anion [47], are highly active catalysts even at room temperature, providing 1450 total turnovers in the hydrolysis of sodium borohydride over 4 h, before they are deactivated. Moreover, low-cost and reusable intrazeolite cobalt(0) nanoclusters with total turnovers of 36000 in basic sodium borohydride solution [48] and poly(N-vinyl-2-pyrrolidone)-stabilized water-soluble nickel(0) nanoclusters with total turnovers of 8700 [49], have been used as effective catalysts in the hydrolysis of sodium borohydride.

As it was mentioned earlier, there is no sufficient information about homogeneous catalysts for the hydrolysis of sodium borohydride and besides a research work performed by Schlesinger in 1953 with regard to testing a number of metal salts as homogeneous catalysts, another research work concerning using of ruthenium(III) acetylacetonate Figure (1.2) as a homogeneous catalyst in the hydrolysis of sodium borohydride was accomplished in 2008 [50]. On contrary to nickel(II) acetylacetonate or ruthenium(III) chloride which are reduced to Ni(0) and Ru(0) species in the presence of sodium borohydride as a reducing agent, ruthenium(III) acetylacetonate is not reduced by sodium borohydride under the experimental conditions and remains unchanged even for days. Although ruthenium(III) acetylacetonate could not be reduced by sodium borohydride, it was surprisingly observed that the hydrolysis of sodium borohydride is catalyzed by this solution, implying that ruthenium(III) acetylacetonate acts as homogeneous catalyst.

Ruthenium(III) acetylacetonate was found to be a highly active homogeneous catalyst providing 1200 turnovers over 3 h in hydrogen generation from the hydrolysis of sodium borohydride before it is deactivated [50].

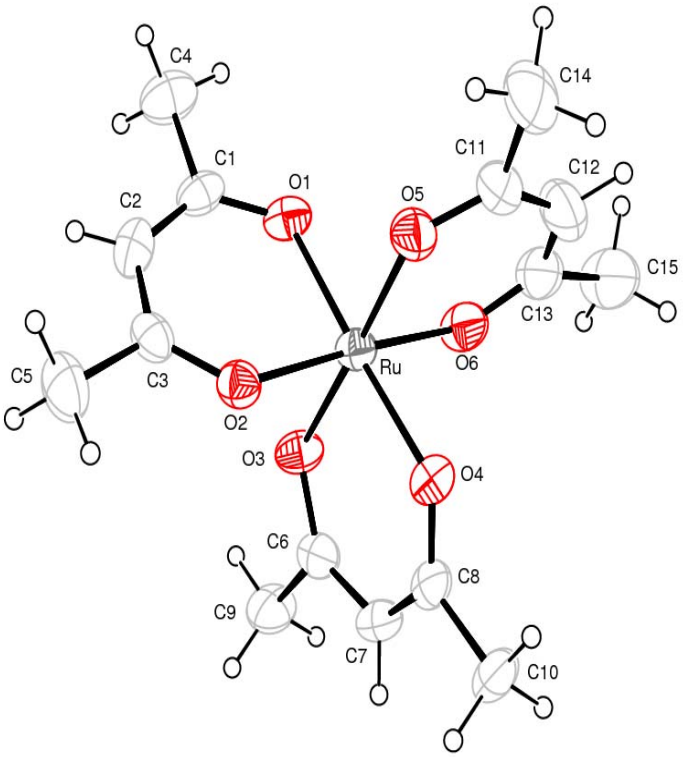

Figure 1.2. $Ru(acac)_3$ is acting as a homogeneous catalyst in the hydrolysis of sodium borohydride

Although there has been no indication of the formation of bulk ruthenium metal during the catalytic hydrolysis of $NaBH_4$ in the presence of $Ru(acac)_3$, the issue of homogeneous/heterogeneous catalysis has been addressed by performing poisoning experiments [51]. A poisoning experiment with trimethylphosphite, $P(OMe)_3$, has been used to prove that the hydrolysis of $NaBH_4$ catalyzed by $Ru(acac)_3$ is a homogeneous catalysis. Indeed, addition of one equivalent $P(OMe)_3$ per ruthenium into the system has been shown to inhibit the catalytic activity of $Ru(acac)_3$ in the hydrolysis of $NaBH_4$. On the other hand, the rate of catalytic reaction decreases almost linearly with the addition of trimethylphosphite and

ultimately stops when one equivalent of poison (trimethylphosphite) is added [50]. However, observation of the reaction for a longer time shows a sudden increase in the hydrogen generation rate after a certain period of time (induction time) [52]. When two equivalents of $P(OMe)_3$ per ruthenium are added to the reaction solution containing 450 mM $NaBH_4$ and 2 mM $Ru(acac)_3$ in 50 mL H_2O-THF solution, the hydrogen generation rate was practically stopped (or reduced to the level of self hydrolysis). However, the catalytic hydrolysis of $NaBH_4$ restarts at an unexpectedly high rate in a certain period of time (75 minutes in this case) after addition of $P(OMe)_3$. After 75 minutes, the hydrogen generation restarts and continues at a rate (83 mL H_2/minute) faster than that before the addition of $P(OMe)_3$ (11 mL H_2/minute). This observation indicates the formation of a new ruthenium species involving $P(OMe)_3$, which is obviously much more active than the $Ru(acac)_3$ catalyst itself in the hydrolysis of $NaBH_4$ [52].

Two questions needed to be addressed initially: The first question is whether this behavior is unique for $P(OMe)_3$ or other alkylphosphines show similar activities of enhancing the rate of catalytic hydrolysis of $NaBH_4$. The second issue concerns the effect of varying amount of phosphorus per ruthenium on this rate enhancement. Figure 1.3. shows that use of not only trimethylphosphite but also triphenylphosphite lead to formation of an active species yielding an acceleration in the hydrogen generation from the hydrolysis of sodium borohydride [52]. In the case of triphenylphosphite, the induction time for formation of active catalyst is about 30 minutes and after induction time, the rate of hydrogen generation is enhanced. The same effect of acceleration in the hydrogen generation from the hydrolysis of sodium borohydride was observed for $Ru(acac)_3$ in the presence of triphenylphosphine and 1,2-bis(diphenylphosphino)ethane compounds [52,53].

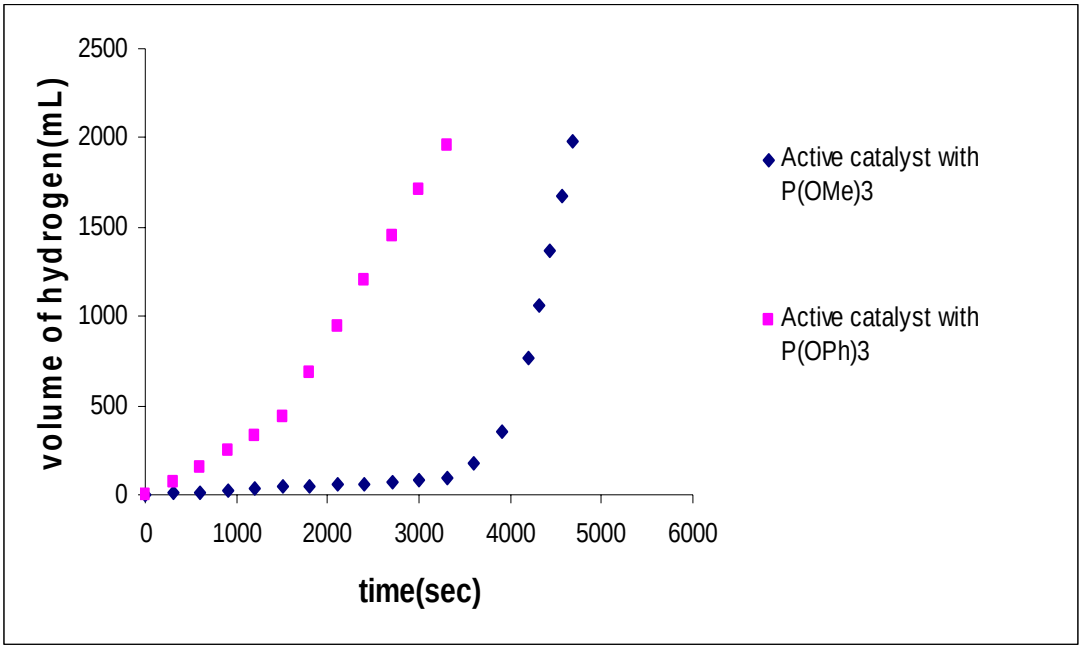

Figure 1.3. Plot of the volume of hydrogen generated versus time for the hydrolysis of $NaBH_4$ at 25 ºC in 50 mL THF/water (1/9) solution starting with [$NaBH_4$] = 450 mM, [$Ru(acac)_3$] = 3 mM, and (trimethylphosphite [$P(OMe)_3$] or triphenylphosphite [$P(OPh)_3$] = 6 mM) added at the beginning of catalytic reaction.

Accordingly, phosphorus compound, usually known as poison in catalysis, is involved in the formation of a species which has higher catalytic activity in comparison with $Ru(acac)_3$ alone. Observation of the unexpected catalytic activity of the ruthenium species involving a molecule known to be poison in catalysis prompted us to investigate the catalytic activity of $Ru(acac)_3$ in the presence of trimethylphosphite and triphenylphosphite compounds. The results of a kinetic study on the catalytic hydrolysis of $NaBH_4$ in the presence of ruthenium(III) acetylacetonate and a phosphorus compound (trimethylphosphite or triphenylphosphite) will be extensively discussed in chapter 3.

The second issue which needs to be addressed concerns the effect of varying amount of phosphine per ruthenium on the rate enhancement of hydrogen evolution. Figure 1.4. shows the rate of hydrogen generation obtained from the linear portion of curves against the mole ratio of phosphorus to ruthenium for all of phosphines [52].

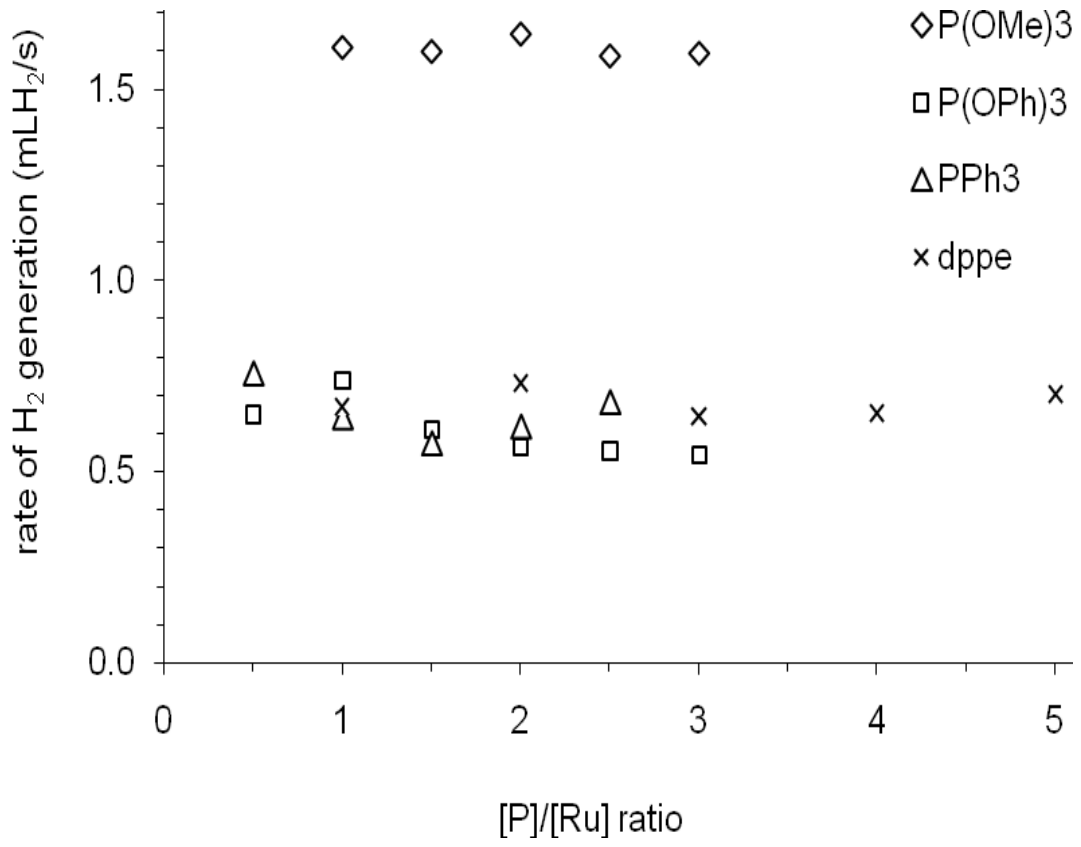

Figure 1.4. Plot of hydrogen generation rate versus mole ratio of phosphine to ruthenium in the hydrolysis of $NaBH_4$ catalyzed by $Ru(acac)_3$ plus a phosphine. $[NaBH_4]$ = 450 mM, [Ru] = 2.0 mM, T = 25 ºC.

Inspection of the diagrams given in Figure 1.4. reveals the following points: (i) All of the phosphorus compounds used lead to formation of an active species yielding an acceleration in the hydrogen generation from the hydrolysis of $NaBH_4$. (ii) However, using $P(OMe)_3$ yields the most active catalyst with ruthenium for the hydrolysis of $NaBH_4$. (iii) The rate of hydrolysis varies very slightly with the mol ratio of phosphorus to ruthenium for all of the phosphorus compounds. However, two equivalents of phosphorus per ruthenium were used for the further experiments with all of the phosphines. In chapter 3, results of the kinetic study on the hydrolysis of $NaBH_4$ catalyzed by $Ru(acac)_3$ and phosphine (2 equivalents of phosphorus per ruthenium) will be discussed.

The observation that the phosphorus to ruthenium molar ratio of 2 shows usually high activity prompted us to synthesize ruthenium acetylacetonato complexes containing two trimethylphosphite ligands and test them as homogeneous catalysts in the hydrolysis of sodium borohydride. Synthesis and characterization of trans- and cis-[$Ru(acac)_2\{P(OMe)_3\}_2$] by single crystal X-ray diffraction, Mass, UV-Visible, ^1H, ^{13}C and ^{31}PNMR spectroscopy plus testing their catalytic activity in hydrogen generation from the hydrolysis of sodium borohydride, will be extensively discussed in chapter 3. As a summary, none of the *trans*- and *cis*-[$Ru(acac)_2\{P(OMe)_3\}_2$] complexes was found to be efficient catalyst in the hydrolysis of sodium borohydride. However, the catalytic activity of *cis*-[$Ru(acac)_2\{P(OMe)_3\}_2$] in the hydrolysis of sodium borohydride is significantly enhanced by the addition of two equivalents of trimethylphosphite per ruthenium into the medium [54] indicating the formation of an active ruthenium species which involves more than two phosphorus ligands. That observation prompted us to isolate, stabilize and characterize the active catalyst forming in aqueous solution during hydrolysis of sodium borohydride starting with $Ru(acac)_3$ or *cis*-[$Ru(acac)_2\{P(OMe)_3\}_2$] plus $P(OMe)_3$.

A few reports are available regarding aqueous organometallic chemistry of ruthenium complexes. The first water-soluble ruthenium complex which was isolated and characterized by X-ray crystal structure, was chloro[(1-3-η:6-8-η)-2,7-dimethyl octadienediyl](semicarbazide)ruthenium(IV)chloride with a ruthenium ion at the center of a distorted trigonal bipyramid [55]. The complex fac-[$Ru(OCOCF_3)_2(CO)_3(H_2O)$] provides a new type of aqueous organometallic chemistry [56]. The substitution of trifluoroacetato ligands by H_2O, nucleophilic attack by the solvent and CO_2 elimination provide [fac-$RuH(CO)_2(H_2O)_3]^+$. Another H_2O-soluble ruthenium catalyst used in hydrogenation and hydroformylation, is [$RuH(Cl)(CO)(mtppms)_3$] (mtppms = meta-monosulfonated triphenylphosphine) that in aqueous solution reversibly dissociate to give [$RuH(CO)(H_2O)(mtppms)_3]^+$ [57].

Apart from the above examples, there are some reports about preparation of ruthenium complexes containing phosphorus ligands in non-aqueous solution that

most of them are applied as homogeneous catalysts in different catalytic reactions. $[Ru\{P(OMe)_3\}_4Cl_2]$ is an example of ruthenium complex with four trimethylphosphite ligands, produced by the reaction of $P(OMe)_3$ with $RuCl_3.3H_2O$ in non-aqueous solution [58,59]. $[Ru(PPh_3)_3Cl_2]$ is another example of ruthenium complexes with triphenylphosphine ligands used as homogeneous catalyst in aerobic oxidation of primary alcohols to aldehydes under atmospheric oxygen [60], transformation of $–CH_3$ into $=CHPHPh_3$ in Biacetylmonoximeacetyl-/Aroylhydrazones [61] and formation of β-cyanoalkylsilane by reaction of trichlorosilane with acrylonitrile [62]. In addition to $[Ru(PPh_3)_3Cl_2]$, some other ruthenium complexes containing triphenylphosphine ligands have been used as homogeneous catalysts in formation of β-cyanoalkylsilanes such as $Ru(CO)_3(PPh_3)_2$, $RuCl_2(PPh_3)_4$, $RuH_2(PPh_3)_4$ and $RuHCl(PPh_3)_3$ [62]. Ruthenium complexes containing triphenylphosphine ligands are used as homogeneous catalysts not only for the formation of β-cyanoalkylsilanes, but also for CO_2 hydrogenation into formic acid. Some ruthenium complexes with triphenylphosphine and trimethylphosphine ligands have been applied for catalytic formation of formic acid such as $RuH_2(PPh_3)_4$, $RuH_2(PMe_3)_4$, $RuCl_2(PMe_3)_4$, $RuCl(OAc)(PMe_3)_4$ [63,64,65,66] and $TpRu(PPh_3)(CH_3CN)H$ (Tp = hydrotris(pyrazolyl)borate [67]. $[RuH_2(H_2)_2(PCy_3)_2]$ is another example of ruthenium complex containing tricyclohexylphosphine ligands with a catalytic activity for arene hydrogenation under mild conditions [68].

For the above examples, ruthenium compound already contains a phosphine ligand. However, some catalytic reactions have been accomplished with ruthenium complexes in the presence of phosphines. For instance, ruthenium compounds such as ruthenium dodecacarbonyl, ruthenium chloride, dichlorotricarbonyl ruthenium(II) dimer or ruthenium(III) acetylacetonate in the presence of phosphines were applied to catalyze the formation of vinyl esters by addition of carboxylic acids to acetylenically unsaturated compounds [69]. As another example, one in-situ catalyst generated from $Ru(acac)_3$ and $MeC(CH_2PPh_2)_3$ in an alcoholic solvent, catalyzes hydrogenation of aromatic and aliphatic esters to the corresponding alcohols [70] or hydrogenation of dimethyl oxalate [71,72].

In chapter 3, for the first time, we will report the isolation of a ruthenium(I) complex from the reaction solution after the hydrogen generation of sodium borohydride in the form of hydridotetrakis(trimethylphosphite)ruthenium(I), [Ru{P(OMe)$_3$}$_4$H], [73] and its characterization by single crystal X-ray diffraction, Mass, UV-Visible, FTIR, ^{1}H, ^{13}C and ^{31}P NMR spectroscopy. Moreover, stabilization of catalytically very active in-situ Ru(II) species by 2,2′-bipyridine as [Ru(acac)(bipy){P(OMe)$_3$}H] complex will also be reported. Stabilized Ru(II) species was also characterized by Mass, UV-Visible, FTIR, ^{1}H, ^{13}C and ^{31}P NMR spectroscopy.

As it was mentioned earlier, the catalytic activity of ruthenium(III) acetylacetonate in the hydrolysis of sodium borohydride is improved in the presence of different phosphorus compounds such as 1,2-bis(diphenylphosphino)ethane, dppe. At the end of catalytic reaction, in addition to the unreacted dppe, unexpectedly we isolated a new species which contains two BH_3 molecules coordinated to dppe. Obviously, in this catalytic reaction, $NaBH_4$ acts not only as a substrate to produce hydrogen, but also as a BH_3 supplier in forming phosphanylborohydrides such as 1,2-bis(diphenylphosphinoborane)ethane, dppe$(BH_3)_2$ [74]. In literature, phosphanylborohydrides have been prepared by using other borane sources: dppe$(BH_3)_2$ by complexation of dppe with $BH_3{\cdot}S(CH_3)_2$ [75], rac/meso-$[HP(BH_3)(Ph)CH_2]_2$ from the reaction of BH_3.thf [76] or reaction of phosphine oxides with diborane [77], from the reaction of trialkylphosphines with bromoboranes or bromochloroboranes [78]. In addition, following phosphanylborohydrides have been reported: tertiary mono and diphosphine-borane complexes [79,80,81], cyclic phosphine-boranes [82], phosphine-carborane clusters [83], phosphinyl-borane radicals [84] and phosphine alkylene boranes [85]. It is noteworthy that the phosphanylborohydride $[P(BH_3)Ph_2]^-$ forms dative bonds of higher p character and establish more stable σ adducts towards the acceptor orbital of the Lewis acid in comparison with its neutral counterpart $P(CH_3)Ph_2$ [86]. A similar phenomenon was observed in the study of chalcogenated phosphanylborohydrides K[EP$(BH_3)R_2$] (E: O, S, Se, Te; R: Ph, *t*-Bu) with a certain degree of E=P multiple

bond character [87]. Despite the known examples given above, the chemistry of phosphanylborohydrides is still largely undeveloped [88,89,90,91,92,93].

In chapter 3, we will report a new and simple synthetic way using $NaBH_4$ in an homogeneous aqueous-organic solution to yield 1,2-bis(diphenylphosphinoborane)ethane, dppe$(BH_3)_2$, and its characterization by single crystal X-ray diffraction, ^{1}H, ^{13}C, ^{31}P and ^{11}B NMR spectroscopy.

Altogether, via this research work, we studied the effect of different phosphorus compounds on the catalytic activity of ruthenium(III) acetylacetonate in the hydrolysis of sodium borohydride and on the kinetics of the catalytic hydrolysis. In addition, synthesis and characterization of ruthenium(III) acetylacetonato complexes containing two trimethylphosphite ligands were studied. Finally, isolation, stabilization and characterization of new ruthenium species (active catalyst), formed during catalytic hydrolysis of sodium borohydride starting with $Ru(acac)_3$ and $P(OMe)_3$, were discussed.

CHAPTER 2

EXPERIMENTAL

2.1. Materials

Ruthenium(III) acetylacetonate, $Ru(acac)_3$, (97 %), sodium borohydride, $NaBH_4$, (98%), trimethylphosphite, $P(OCH_3)_3$, 2,2´-bipyridine, and 1,2-bis(diphenylphosphino)ethane, dppe, were purchased from Aldrich®. Cyclooctene, triphenylphosphite, $P(OPh)_3$, tetrahydrofuran, THF and dichloromethane, CH_2Cl_2 were purchased from Merck®. Liquid zinc amalgam (2-3% Zn) was prepared by the appropriate literature procedure [94]. Zinc dust was treated immediately before use with dilute H_2SO_4 and washed successively with water, alcohol and diethyl ether. All glassware and teflon-coated magnetic stirring bars were cleaned with acetone, followed by copious rinsing with distilled water before drying at 150 $^{\circ}$C in oven for a few hours.

2.2. Equipment

All reactions involving air sensitive compounds were performed under argon or nitrogen atmospheres. ^{1}H, ^{13}C and ^{31}P NMR spectra were taken on a Bruker Avance DPX 400 MHz spectrometer (400.1 MHz for ^{1}H; 100.6 MHz for ^{13}C; 161.3 MHz for ^{31}P). Chemical shifts are given in ppm (δ) relative to Me_4Si as internal

standard for ^{1}H, ^{13}C and H_3PO_4 (85% in glass capillary) for ^{31}P NMR. UV-visible electronic absorption spectra were recorded on a Varian Carry-100 double beam spectrometer. The infrared spectrum was recorded from a KBr pellet using a Bruker AXS Tensor-27 or Vertex 70 ATR/FTIR spectrometer. Positive ion mass spectrometry data was acquired on a Micro TOF-LC/ESI/Ms system or fast atom bombardment (FAB-Ms) on a VG AutoSpec (Fisons Instruments). The experimental setup [46] used for performing the hydrolysis of sodium borohydride and measuring the hydrogen gas generated from the reaction consists of a 75 mL jacketed reaction flask containing a teflon-coated stirring bar placed on a magnetic stirrer (Heidolph MR-301) and thermostated to 25.0 ± 0.1°C by circulating water through its jacket from a constant temperature bath (RL6 LAUDA water bath). A graduated glass tube (50 cm in height and 2.5 cm in diameter) filled with water was connected to the reaction flask to measure the volume of the hydrogen gas to be evolved from the reaction (Figure 2.1).

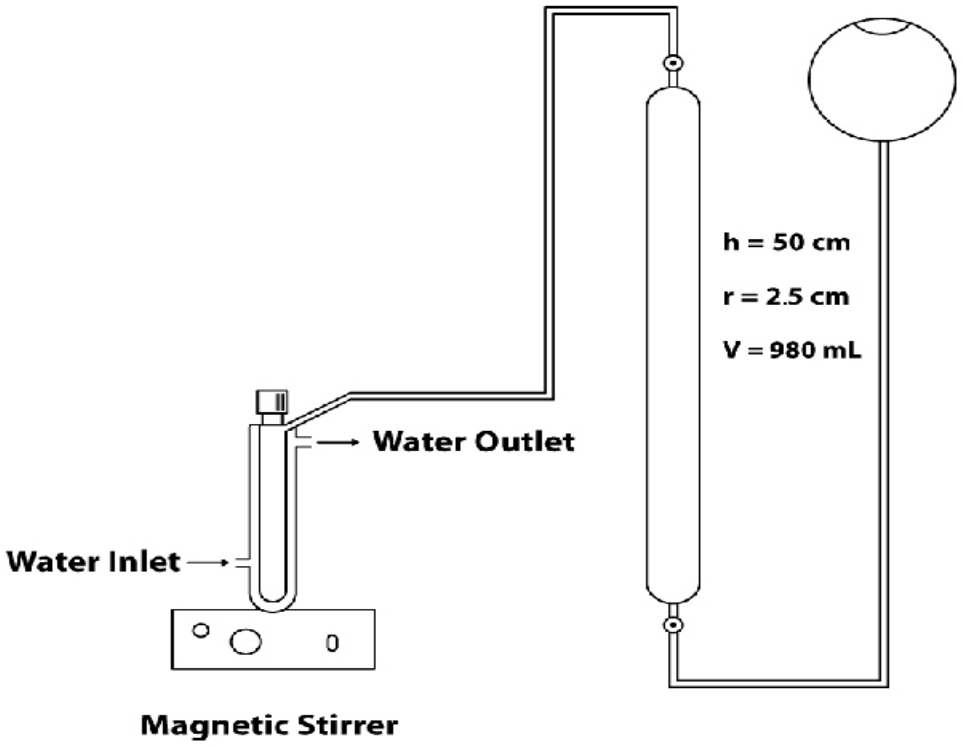

Figure 2.1. The experimental setup used in the measurement of the volume of hydrogen generated from the hydrolysis of sodium borohydride.

2.3. Self Hydrolysis of Sodium Borohydride

In order to measure the rate of hydrogen generation from the self hydrolysis of sodium borohydride, 852 mg (22.5 mmol) sodium borohydride was dissolved in 50 mL water and the solution was transferred into the reaction flask thermostated at 25.0 ± 0.1°C. The experiment was started by closing the reaction flask and turning on the stirrer at 1000 rpm simultaneously. The volume of hydrogen gas generated was recorded every 5 minutes.

2.4. Cataytic activity of ruthenium(III) acetylacetonate in the hydrolysis of sodium borohydride in the presence of trimethylphosphite

A stock solution of $P(OCH_3)_3$ (100 mM) in THF was prepared by dissolving 1.18 mL $P(OCH_3)_3$ (MW = 124.08 g/mol, d = 1.052 g/mL) to 100 mL THF. For the preparation of catalyst solution with $P(OCH_3)_3/Ru(acac)_3$ ratio of 1, 1.5, 2, 2.5 or 3, an aliquot of the stock solution (1, 1.5, 2, 2.5 or 3 mL, respectively) was diluted to 5 mL by adding THF and, then, 41 mg $Ru(acac)_3$ was added to this solution and dissolved completely by stirring the solution. Then, the solution was transferred into the reaction flask containing 852 mg (22.5 mmol) $NaBH_4$ dissolved in 45 mL water and thermostated at 25.0 ± 0.1 °C. The initial concentration of $Ru(acac)_3$ in the reaction solution was 2 mM and concentration of $P(OCH_3)_3$ was 2, 3, 4, 5 and 6 mM, respectively. The reaction was started by closing reaction flask and turning on the stirrer at 1000 rpm simultaneously. The volume of hydrogen gas generated was recorded every 5 minutes.

Kinetics of the hydrolysis of $NaBH_4$ catalyzed by $Ru(acac)_3$ and $P(OCH_3)_3$ system was studied depending on substrate concentration, catalyst concentration and the temperature. In a set of experiments, $NaBH_4$ concentration was held constant at 450 mM and $Ru(acac)_3$ concentration was varied in the range of 2, 2.5, 3, 3.5 and 4 mM, by holding $P(OCH_3)_3/Ru(acac)_3$ ratio at 2, at 25.0 ± 0.1 °C. The hydrogen

generation was measured for each set by recording the water level in graduated glass tube, which is connected to the reaction flask, in every 2 minutes. In the second set of experiments, $Ru(acac)_3$ concentration was held constant at 2 by keeping $P(OCH_3)_3/Ru(acac)_3$ ratio at 2, while $NaBH_4$ concentration was varied in the range of 300, 600, 900, 1200 and 1500 mM at 25.0 ± 0.1 °C. In the third set of experiments, the catalytic hydrolysis of $NaBH_4$ in the presence of $Ru(acac)_3/P(OCH_3)_3$ system with a $Ru(acac)_3$ concentration of 2 mM and a $P(OCH_3)_3/Ru(acac)_3$ ratio of 2 was performed by keeping $NaBH_4$ concentration constant at 450 mM at various temperatures in the range of 20, 25, 30, 35, and 40 °C in order to obtain the activation energy (E_a), enthalpy of activation ($\Delta H^{\neq}$) and entropy of activation ($\Delta S^{\neq}$).

2.5. Catalytic activity of ruthenium(III) acetylacetonate in the hydrolysis of sodium Borohydride in the presence of triphenylphosphite

A stock solution of $P(OPh)_3$ (100 mM) in THF was prepared by dissolving 2.6 mL $P(OPh)_3$ (MW = 310.29 g/mol, d = 1.19 g/mL) to 100 mL THF. For the preparation of catalyst solution with $P(OPh)_3/Ru(acac)_3$ ratio of 0.5, 1, 1.5, 2, 2.5 or 3, an aliquot of the stock solution (0.5, 1, 1.5, 2, 2.5, or 3 mL, respectively) was diluted to 5 mL by adding THF and, then, 41 mg $Ru(acac)_3$ was added to this solution and dissolved completely by stirring the solution. Then the solution was transferred into the reaction flask containing 852 mg (22.5 mmol) $NaBH_4$ dissolved in 45 mL water and thermostated at 25.0 ± 0.1 °C. The initial concentration of $Ru(acac)_3$ in the reaction solution was 2 mM and concentration of $P(OPh)_3$ was 1, 2, 3, 4, 5 and 6 mM, respectively. The reaction was started by closing reaction flask and turning on the stirrer at 1000 rpm simultaneously. The volume of hydrogen gas generated was recorded every 5 minutes.

Kinetics of the hydrolysis of $NaBH_4$ catalyzed by $Ru(acac)_3$ and $P(OPh)_3$ system was studied depending on substrate concentration, catalyst concentration and the temperature. In a set of experiments, $NaBH_4$ concentration was held constant at 450 mM and $Ru(acac)_3$ concentration was varied in the range of 2, 2.5, 3, 3.5 and 4

mM, by holding $P(OPh)_3$/ $Ru(acac)_3$ ratio at 2, at 25.0 ± 0.1 °C. The hydrogen generation was measured for each set by recording the water level in graduated glass tube, which is connected to the reaction flask, in every 2 minutes. In the second set of experiments, $Ru(acac)_3$ concentration was held constant at 2 by keeping $P(OPh)_3/Ru(acac)_3$ ratio at 2, while $NaBH_4$ concentration was varied in the range of 300, 600, 900, 1200 and 1500 mM at 25.0 ± 0.1 °C. In the third set of experiments, the catalytic hydrolysis of $NaBH_4$ in the presence of $Ru(acac)_3/P(OPh)_3$ system with a $Ru(acac)_3$ concentration of 2 mM and a $P(OPh)_3/Ru(acac)_3$ ratio of 2 was performed keeping $NaBH_4$ concentration constant at 450 mM at various temperatures in the range of 20, 25, 30, 35, and 40 °C in order to obtain the activation energy (E_a), enthalpy of activation ($\Delta H^{\neq}$) and entropy of activation ($\Delta S^{\neq}$).

2.6. Catalytic Lifetime of Ruthenium(III) Acetylacetonate in the Presence of Different Phosphorus Ligands

The catalytic lifetime of $Ru(acac)_3$ with different phosphorus ligands in the hydrolysis of sodium borohydride was determined by measuring the total turnover number (TTO). Such a lifetime experiment was started with a 50 mL solution containing 2 mM $Ru(acac)_3$, 450 mM $NaBH_4$ and keeping mole ratios constant as $P(OCH_3)_3$/ Ru = 2 or $P(OPh)_3$/ Ru = 2 at 25.0± 0.1 °C. When the conversion exceeded 75%, more $NaBH_4$ was added to the reaction solution and the reaction was continued in this way until hydrogen gas evolution was slowed down to the self hydrolysis level.

2.7. Poisoning Experiment

To determine whether the hydrolysis of sodium borohydride catalyzed by the $Ru(acac)_3$ and phosphine system is homogeneous or heterogeneous, a mercury poisoning experiment was performed [51]. To the reaction solution started with 450 mM $NaBH_4$ and 2 mM $Ru(acac)_3$ plus 4 mM $P(OMe)_3$ was added 1 equivalent of mercury per ruthenium after the 50% conversion. The hydrogen generation rate was

not changed at all after the addition of mercury, indicating that the reaction is indeed a homogeneous catalysis.

2.8. Preparation of cis-[Ru(acac)$_2$(η^2-C_8H_{14})$_2$] complex

Based on literature procedure [95], to a solution of [Ru(acac)$_3$] (167 mg, 0.42 mmol) in freshly distilled THF (35 cm^3) containing cyclooctene (5 cm^3) and water (1 cm^3) was added liquid zinc amalgam (16 cm^3) and the mixture heated under reflux with magnetic stirring in an nitrogen atmosphere for 3 h. The initially dark solution changed to orange within 30 minutes. The supernatant liquid was filtered through degassed celite into a flask and the orange-red filtrate evaporated under reduced pressure to about 25 cm^3 giving a solution assumed to contain 0.0168 mmol cm^{-3} of cis-[Ru(acac)$_2$(η^2-C_8H_{14})$_2$].

2.9. Preparation of trans and cis-[Ru(acac)$_2${P(OMe)$_3$}$_2$] complexes

Following the section 2.8, the prepared solution of cis-[Ru(acac)$_2$(η^2-C_8H_{14})$_2$] complex in THF (25 cm^3) was stirred with trimethylphosphite (0.5 cm^3, 4.3 mmol) overnight. The mixture was evaporated to about half its volume and filtered through degassed celite to remove a small amount of insoluble material. The filtrate was evaporated to dryness and the residue was dissolved in a mixture of hexane-dichloromethane solution giving red-brown crystals of trans-[Ru(acac)$_2${P(OMe)$_3$}$_2$] at 0°C after one day, which were separated by filtration and washed with hexane. trans-[Ru(acac)$_2${P(OMe)$_3$}$_2$] : ^{1}H NMR (C_6D_6, ppm): δ 1.95 (s, 12H, 4Me), 3.72 (t, 18H, 6OMe), 5.38 (s, 2H, 2CH). ^{13}C {^{1}H} NMR (C_6D_6, ppm): δ 27.01, 50.29, 99.64, 186.08.^{31}P {^{1}H} NMR (C_6D_6, ppm): δ 138.05. Mass: m/z 548 (M^+, 15%), 424 (100), 300 (14). UV: λ_{max} (THF, nm) (ε in dm^{3}mol^{-1}cm^{-1}) 280 (31900), 340 (15300), 510 (4200).

A sample of the trans isomer (150 mg, 0.27 mmol) was heated under reflux in toluene (25 cm^3) for 3 h, changing from orange to yellow-brown. Solvent was removed in vacuo and the residue dissolved in hexane. The solution was filtered

through degassed celite and the product eluted with THF-hexane; some unidentified material remained on the column. The filtrate was evaporated to dryness and the residue dissolved in a small amount of hexane giving Yellow-brown crystals of cis-[$Ru(acac)_2\{P(OMe)_3\}_2$] at 0 °C after one week. *cis*-[$Ru(acac)_2\{P(OMe)_3\}_2$] : ^1H NMR (C_6D_6, ppm) : δ 1.62 (s, 6H, 2Me), 1.82 (s, 6H, 2Me), 3.52 (t, 18H, 6OMe), 5.21 (s, 2H, 2CH). ^{13}C $\{^1H\}$ NMR (C_6D_6, ppm): δ 27.52, 27.86, 51.02, 99.12, 185.73, 186.51.^{31}P $\{^1H\}$ NMR (C_6D_6, ppm): δ 154.74. Mass: m/z 548 (M^+, 15%), 424 (100), 300 (14). UV: λ_{max} (THF, nm) (ε in $dm^3mol^{-1}cm^{-1}$) 240 (41600), 280 (40800), 530 (5100).

2.10. Crystal structure analysis of trans and cis-[$Ru(acac)_2\{P(OMe)_3\}_2$] complexes

To determine the crystal structures of the compounds, *trans* and *cis*-[$Ru(acac)_2\{P(OMe)_3\}_2$], X-ray diffraction data were collected at room temperature with graphite-monochromated CuK_α and MoK_α radiation, respectively on an Enraf-Nonius CAD4 diffractometer [96] operating in $\omega/2\theta$ scan mode. Cell refinement was carried out using CAD-4 EXPRESS. Data reduction was carried out using XCAD4 [97]. The *trans* structure was solved by SIR92 [98] and the *cis* structure solved by SHELXS-97 [99]. Both structures refinement were done by SHELXL-97. A full matrix least-squares refinement on F^2 was done. For all non-hydrogen atoms anisotropic displacement parameters were refined. All H atoms of the both compounds were placed in calculated positions and refined using a riding model. C-H(acac) = 0.93 Å / $U_{iso}(H)$ = $1.2U_{eq}$(C) and C-H(methyl) = 0.96 Å / $U_{iso}(H)$ = $1.5U_{eq}$(C). The graphical representations of the structure were made with ORTEP [100] and MERCURY [101].

2.11. Catalytic activity of trans and cis-[Ru(acac)$_2${P(OMe)$_3$}$_2$] in the hydrolysis of sodium borohydride

A solution of trans or cis-[Ru(acac)$_2${P(OMe)$_3$}$_2$] was prepared by dissolving 16.5 mg (0.03 mmol) ruthenium complex in a mixture of 5 mL THF and 5 mL water under vigorous stirring. In a separate glass vial, 852 mg (22.5 mmol) $NaBH_4$ was dissolved in 40 mL water and the solution was transferred into the reaction flask thermostated at 25.0 ± 0.1°C. Then, the ruthenium solution in 10 mL THF/water was transferred into the reaction flask, yielding a solution with ruthenium concentration of 0.6 mM and sodium borohydride concentration of 450 mM. The experiment was started by closing the reaction flask and turning on the stirring at 1000 rpm simultaneously. The volume of hydrogen gas evolved was measured by recording the displacement of water level in the graduated glass tube for every 5 minutes.

2.12. Catalytic activity of trans and cis-[Ru(acac)$_2${P(OMe)$_3$}$_2$] in the hydrolysis of sodium borohydride in the presence of trimethylphosphite

A stock solution of $P(OCH_3)_3$ (100 mM) in THF was prepared by dissolving 1.18 mL $P(OCH_3)_3$ (MW = 124.08 g/mol, d = 1.052 g/mL) to 100 ml THF. For the preparation of catalyst solutions with $P(OCH_3)_3$/Ru molar ratio of 2, an aliquot of the stock solution (0.6 mL) was diluted to 5 mL by adding THF and, then, 16.5 mg of ruthenium complex [Ru(acac)$_2${P(OMe)$_3$}$_2$] was added to this solution and dissolved completely by stirring the solution. Then, the solution was transferred into the reaction flask containing 852 mg (22.5 mmol) $NaBH_4$ dissolved in 45 mL water and thermostated at 25.0 ± 0.1°C. The initial concentrations in the reaction solution were 0.6 mM Ru, 1.2 mM $P(OCH_3)_3$, and 450 mM $NaBH_4$. The reaction was started by closing reaction flask and turning on the stirrer at 1000 rpm simultaneously. The volume of hydrogen gas generated was recorded every 5 minutes.

2.13. Catalytic activity of $Ru(acac)_3$ in the hydrolysis of sodium borohydride

Based on literature procedure [50], a solution of $Ru(acac)_3$ was prepared by dissolving 12 mg (0.03 mmol) Ruthenium complex in a mixture of 5 mL THF and 5 mL water under vigorous stirring. After the preparation of Ruthenium complex solution, 852 mg (22.5 mmol) $NaBH_4$ was dissolved in 40 mL water and the solution was transferred into the reaction flask thermostated at 25.0 ± 0.1°C. Then, the Ruthenium complex solution in 10 ml THF/water was transferred into the reaction flask, yielding a solution with Ru concentration of 0.6 mM and sodium borohydride concentration of 450 mM. The experiment was started by closing the reaction flask and turning on the stirring at 1000 rpm simultaneously. The volume of hydrogen gas evolved was measured by recording the displacement of water level in the graduated glass tube for every 5 minutes.

2.14. Isolation of hydridotetrakis(trimethylphosphite)ruthenium(I) complex, $[Ru\{P(OMe)_3\}_4H]$

A stock solution of $P(OCH_3)_3$ (100mM) in THF was prepared by dissolving 1.18 mL $P(OCH_3)_3$ (MW = 124.08 g/mol, d = 1.052 g/mL) to 100 mL THF. For the preparation of catalyst solution with $P(OCH_3)_3/Ru(acac)_3$ ratio of 4, an aliquot of the stock solution (4 mL) was diluted to 5 mL by adding THF and, then, 41 mg $Ru(acac)_3$ was added to this solution and dissolved completely by stirring the solution. Then, the solution was transferred into the reaction flask containing 1136 mg (30 mmol) $NaBH_4$ dissolved in 45 mL water and thermostated at 25°C. The initial concentration of $Ru(acac)_3$ in the reaction solution was 2 mM and concentration of $P(OCH_3)_3$ was 8 mM. The reaction was started by turning on the stirrer at 1000 rpm under inert atmosphere. After 6 h stirring, the mixture was extracted with dichloromethane and the combined organic extracts were cooled in order to be precipitated some traces of $NaBH_4$ or metaborates remaining in oganic extracts. Then, the solution was dried over magnesium sulfate, filtered and evaporated in vacuo giving a mixture of recycled $Ru(acac)_3$ and $[Ru\{P(OMe)_3\}_4H]$

complexes. The mixture, was solved in cold hexane and due to lower solubility of $Ru(acac)_3$ in hexane, it was precipitated and separated from $[Ru\{P(OMe)_3\}_4H]$ complex by filteration. Evaporation of hexane in vacuo gives pure $[Ru\{P(OMe)_3\}_4H]$ complex (19.2 mg). Colorless crystals of hydridotetrakis(trimethylphosphite)ruthenium(I) complex, were obtained by the crystallization from hexane at 0°C after 10 days.

$[Ru\{P(OMe)_3\}_4H]$: ^1H NMR ($CDCl_3$, ppm) : δ -5.71 (br s, 1H, 1Ru-H), 3.45 (s, 9H, 3OMe), 3.47 (d, J = 4.4 Hz, 27H, 9OMe). ^{13}C $\{^1H\}$ NMR (CDCl3, ppm): δ 49.32, 49.8. ^{31}P $\{^1H\}$ NMR ($CDCl_3$, ppm): δ 169.65, 172.4. Mass: m/z 597 (M^+, 100%), 473(38). UV: λ_{max} (THF, nm) (ε in $dm^3mol^{-1}cm^{-1}$) 295 (52500). FTIR (neat, cm^{-1}) : 2928 m, 1580-1720 m, 1445 w, 1375 w, 1066 s.

2.15. Single Crystal X-ray diffraction analysis of $[Ru\{P(OMe)_3\}_4H]$

A colorless, prismatic crystal of dimensions 0.3x0.2x0.2 mm^3 was glued to a thin quartz glass and mounted on the goniometry of an Enraf Nonious CAD4 difractometer at room temperature. A hemisphere of data was collected in ω/2θ scan mode with graphite monochromated MoK_α radiation, =0.71073 Å. Data collection and initial indexing were handled using XCAD4 [97]. Semi-empirical absorption corrections were performed using PSI-SCANS [102]. The structure was solved using direct methods and difference Fourier techniques. All hydrogen atoms were attached via the riding model. The final structural refinement included anisotropic temperature factors on all non-hydrogen atoms. Structure solution, refinement, graphics, and creation of publication material were performed using SHELX [99] and WinGX package [103]. The graphical representations of the structure was made with MERCURY [101].

2.16. Catalytic activity of [Ru{P(OMe)$_3$}$_4$H] in the hydrolysis of sodium borohydride

A solution of [Ru{P(OMe)$_3$}$_4$H] was prepared by dissolving 18 mg (0.03 mmol) ruthenium complex in a mixture of 5 mL THF and 5 mL water under vigorous stirring. In a separate glass vial, 852 mg (22.5 mmol) $NaBH_4$ was dissolved in 40 mL water and the solution was transferred into the reaction flask thermostated at 25.0 ± 0.1°C. Then, the reaction solution in 10 mL THF/water was transferred into the reaction flask, yielding a solution with ruthenium concentration of 0.6 mM and sodium borohydride concentration of 450 mM. The experiment was started by closing the reaction flask and turning on the stirring at 1000 rpm simultaneously. The volume of hydrogen gas evolved was measured by recording the displacement of water level in the graduated glass tube for every 5 minutes.

2.17. UV-Visible spectroscopic measurements during hydrolysis of sodium borohydride catalyzed by Ru(acac)$_3$ and P(OMe)$_3$

A stock solution of $P(OCH_3)_3$ (100mM) in THF was prepared by dissolving 1.18 mL $P(OCH_3)_3$ (MW = 124.08 g/mol, d = 1.052 g/mL) in 100 mL THF. For the preparation of catalyst solution with $P(OCH_3)_3$/Ru(acac)$_3$ ratio of 2-4, an aliquot of the stock solution (2-4 mL) was diluted to 5 mL by adding THF and, then, 41 mg Ru(acac)$_3$ was added to this solution and dissolved completely by stirring the solution. Then, the solution was transferred into the reaction flask containing 852 mg (22.5 mmol) $NaBH_4$ dissolved in 45 mL water and thermostated at 25°C. The initial concentration of Ru(acac)$_3$ in the reaction solution was 2 mM and concentration of $P(OCH_3)_3$ was in the range of 4-8 mM. The reaction was started by turning on the stirrer at 1000 rpm under inert atmosphere. The hydrolysis of sodium borohydride catalyzed by different ratio of $P(OCH_3)_3$/Ru(acac)$_3$, was followed by taking the UV-Visible absorption spectra on a Varian Carry-100 double beam spectrometer. Every 10 minutes, 50 μL sample was taken by using a micropipette and diluted to 3 mL with $NaBH_4$ solution (450 mM) in H_20-THF (9 : 1). The UV-Visible spectrum of the diluted solution was taken immediately.

2.18. Stabilization of catalytically very active in-situ Ru(II) species by 2,2´-bipyridine in the form of [Ru(acac)(bipy){P(OMe)$_3$}H]

A stock solution of $P(OCH_3)_3$ (100mM) in THF was prepared by dissolving 1.18 mL $P(OCH_3)_3$ (MW = 124.08 g/mol, d = 1.052 g/mL) in 100 mL THF. For the preparation of catalyst solution with $P(OCH_3)_3/Ru(acac)_3$ ratio of 3, an aliquot of the stock solution (3 mL) was diluted to 5 mL by adding THF and, then, 41 mg $Ru(acac)_3$ was added to this solution and dissolved completely by stirring the solution. Then, the solution was transferred into the reaction flask containing 852 mg (22.5 mmol) $NaBH_4$ dissolved in 45 mL water and thermostated at 25°C. The initial concentration of $Ru(acac)_3$ in the reaction solution was 2 mM and concentration of $P(OCH_3)_3$ was 6 mM. The reaction was started by turning on the stirrer at 1000 rpm under inert atmosphere. After about 1 h stirring (induction time), active catalyst was formed accompanied by a sudden increase in the hydrogen generation rate and at that time, formation of active catalyst was controlled by UV-Visible spectroscopic measurement. After formation of in-situ active catalyst, immediately, 20 mg (0.127 mmol) 2,2´-bipyridine was added to the reaction solution and it was stirred for additional 5 h at 25°C under inert atmosphere. During that time, the color of solution changed from red to red-brown and finally to dark-brown. Then, the mixture was extracted with dichloromethane and the combined organic extracts were cooled in order to be precipitated some traces of $NaBH_4$ or metaborates remaining in organic extracts. Then, the solution was dried over magnesium sulfate, filtered and evaporated in vacuo giving a mixture of stabilized active catalyst [Ru(acac)(bipy){P(OMe)$_3$}H] and some traces of 2,2´-bipyridine which were easily separated from stabilized active catalyst by washing in cold hexane. Recrystallization from a mixture of chloroform-hexane solution yields the complex (21.7 mg).

[Ru(acac)(bipy){P(OMe)$_3$}H] : ^{1}H NMR ($CDCl_3$, ppm) : δ -5.59 (s, 1H, 1Ru-H), 1.45 (br, 6H, 2Me), 3.42 (s, 9H, 3OMe), 6.45 (m, 4H, 4H-bipy), 6.99 (m, 4H, 4H-bipy). ^{13}C {^{1}H} NMR (CDCl3, ppm): δ 40.5, 50.91, 100.02, 125.6, 127.8, 145.18. ^{31}P {^{1}H} NMR ($CDCl_3$, ppm): δ 163.22. Mass: m/z 456 ([M-2C]$^+$, 100%).

UV: λ_{max} (THF/H_2O, nm) (ε in $dm^3mol^{-1}cm^{-1}$) 235 (12400), 285 (36500), 460 (4500). FTIR (neat, cm^{-1}) : 1490-1550 s.

2.19. Catalytic activity of stabilized active catalyst with 2,2´-bipyridine in the hydrolysis of sodium borohydride and UV-Visible spectroscopic measurements

A stock solution of $P(OCH_3)_3$ (100mM) in THF was prepared by dissolving 1.18 mL $P(OCH_3)_3$ (MW = 124.08 g/mol, d = 1.052 g/mL) in 100 mL THF. For the preparation of catalyst solution with $P(OCH_3)_3/Ru(acac)_3$ ratio of 3, an aliquot of the stock solution (3 mL) was diluted to 5 mL by adding THF and, then, 41 mg $Ru(acac)_3$ was added to this solution and dissolved completely by stirring the solution. Then, the solution was transferred into the reaction flask containing 852 mg (22.5 mmol) $NaBH_4$ dissolved in 45 mL water and thermostated at 25°C. The initial concentration of $Ru(acac)_3$ in the reaction solution was 2 mM and concentration of $P(OCH_3)_3$ was 6 mM. The experiment was started by closing the reaction flask and turning on the stirring at 1000 rpm simultaneously. The volume of hydrogen gas evolved was measured by recording the displacement of water level in the graduated glass tube for every 5 minutes. After about 1 h stirring (induction time), which was the time of active catalyst formation and a huge amount of hydrogen evolution was observed, 20 mg (0.127 mmol) 2,2´-bipyridine was added to reaction solution at 25°C under inert atmosphere. Then, the volume of hydrogen gas evolved was measured every 5 minutes (for additional 4 h) in order to realize the difference between catalytic activity of in-situ active catalyst without stabilization in hydrogen generation and in the case of stabilization with 2,2´-bipyridine.

The above experiment containing 41 mg $Ru(acac)_3$ (2mM), 852 mg $NaBH_4$ (450 mM), 20 mg 2,2´-bipyridine (2.5 mM) and a $P(OCH_3)_3/Ru(acac)_3$ ratio of 3 (6 mM of phosphine) in 50 mL H_2O-THF, was repeated in order to perform UV-Visible spectroscopic measurements during hydrolysis of sodium borohydride catalyzed by $Ru(acac)_3$ and $P(OMe)_3$ along with stabilization with 2,2´-bipyridine. The reaction was followed by taking the UV-Visible absorption spectra on a Varian Carry-100 double beam spectrometer. Every 10 minutes, 50 μL sample was taken by using a

micropipette and diluted to 3 mL with $NaBH_4$ solution (450 mM) in H_20-THF (9 : 1). Following the above catalytic reaction by taking the UV-Visible absorption spectra is very important to realize if the in-situ active catalyst is stabilized in the presence of 2,2′-bipyridine or it is recycled to ruthenium(III) acetylacetonate which is the starting material.

2.20. Preparation of 1,2-bis(diphenylphosphinoborane)ethane, dppe$(BH_3)_2$

For the preparation of 1,2-bis(diphenylphosphinoborane)ethane, dppe$(BH_3)_2$, 140 mg (0.35 mmol) of 1,2-bis(diphenylphospino)ethane, dppe, was completely dissolved in 10 mL of THF by rigorous stirring. Then, the solution was transferred into a 75 mL jacketed reaction flask containing 30 mg (0.79 mmol) $NaBH_4$ dissolved in 40 mL water and thermostated at 25.0 °C by circulating water through its jacket from a constant temperature bath (RL6 LAUDA water bath). The reaction was started by turning on the magnetic stirrer (Heidolph MR-301) at 1000 rpm under inert atmosphere (argon or nitrogen). Note that hydrogen liberated during hydrolysis of sodium borohydride was released from the flask through a bubbler. After 3 h stirring, the mixture was extracted with dichloromethane and the combined organic extracts were cooled in order to precipitate out traces of sodium borohydride or metaborate remaining in organic extracts. Then, the solution was dried over magnesium sulfate, filtered and evaporated in vacuum giving 144 mg of pure dppe$(BH_3)_2$ complex (96% yield). Colorless crystals of dppe$(BH_3)_2$ complex were obtained by crystallization from the hexane-dichloromethane solution at 0°C after one week, which were separated by filtration.

$[Ph_2P(BH_3)CH_2]_2$: ^{1}H NMR (CD_2Cl_2, ppm): δ 1.99 (t, 6H, J = 4.8 Hz, $2BH_3$), 2.15 (br d, 2H, J = 6.4 Hz, CH_2), 2.38 (br d, J = 2.8 Hz, 2H, CH_2), 7.38 (m, 12H, H-m,p), 7.54(m, 4H, H-o), 7.61 (m, 4H, H-o). ^{13}C {^{1}H} NMR (CD_2Cl_2, ppm): δ 22.93, 127.81, 129.87, 131.85, 137.59. ^{31}P {^{1}H} NMR (CD_2Cl_2, ppm): δ -12.5. ^{11}B {^{1}H} NMR (CD_2Cl_2, ppm): δ -40.06. MS, taken by a Micro TOF-LC/ESI/Ms system, does not show the molecular ion peak expected at m/z = 425. Instead, it shows peaks

at m/z = 429 or 431 due to oxidation of dppe$(BH_3)_2$ during the sampling/ionization whereby BH_3 groups are replaced by the oxo groups.

2.21. Single Crystal X-ray diffraction analysis of 1,2-bis(diphenylphosphinoborane)ethane, $[Ph_2P(BH_3)CH_2]_2$

X-ray diffraction measurements were performed with MoK_α radiation on an Enraf-Nonius CAD4 diffractometer [96] equipped with a graphite monochromator. Intensity data were collected by $\omega/2\theta$ scan technique in the θ range of 2.21–26.29°. Data reduction was carried out using XCAD4 [97]. The structures were solved by Patterson methods and refined using the program SHELX [99]. A full-matrix least-squares refinement on F^2 was done. For all non-hydrogen atoms anisotropic displacement parameters were refined. Borane (BH_3) and phenyl ring hydrogen's of the compound were placed geometrically and a riding model was used with $U_{iso}(H)=1.5\ U_{eq}(C)$ and $U_{iso}(H)=1.2\ U_{eq}(C)$, respectively. Methylene hydrogen's were taken from a difference Fourier map and refined. The graphical representations of the structure was made with ORTEP [100].

CHAPTER 3

RESULTS AND DISCUSSION

3.1. Self hydrolysis of sodium borohydride

The rate of hydrogen generation from self hydrolysis of sodium borohydride is slow. Whatever the amount of sodium borohydride as a substrate is increased, the volume of hydrogen generation is getting increased, too. However, as the reaction proceeds, the basic metaborate ion is formed which results in increasing the PH of solution and subsequentely, the initial rate of hydrolysis is decreased. For that reason, applying a suitable catalyst for the hydrolysis of sodium borohydride is required. Figure 3.1 shows the hydrogen volume versus time for the self hydrolysis of sodium borohydride (starting with 450 mM) in 50 mL water at 25°C. When the conversion exeeds 80%, another 450 mM of $NaBH_4$ was added to the reaction solution and the reaction was continued for 3 days with a regular addition of sodium borohydride (each time 450 mM of substrate was added). Based of Figure 3.1 the total volume of hydrogen liberated during self hydrolysis of sodium borohydride (starting with 450 mM), is about 4000 mL after 3 days. Although, the total volume of hydrogen for that period of time (3 days) is not so high, it is not negligible, either. Accordingly, in all of experiments concerning catalytic hydrolysis of sodium borohydride which follows, the volume of hydrogen generation is corrected by subtracting the volume of hydrogen liberated from self hydrolysis of sodium borohydride at the same period of time.

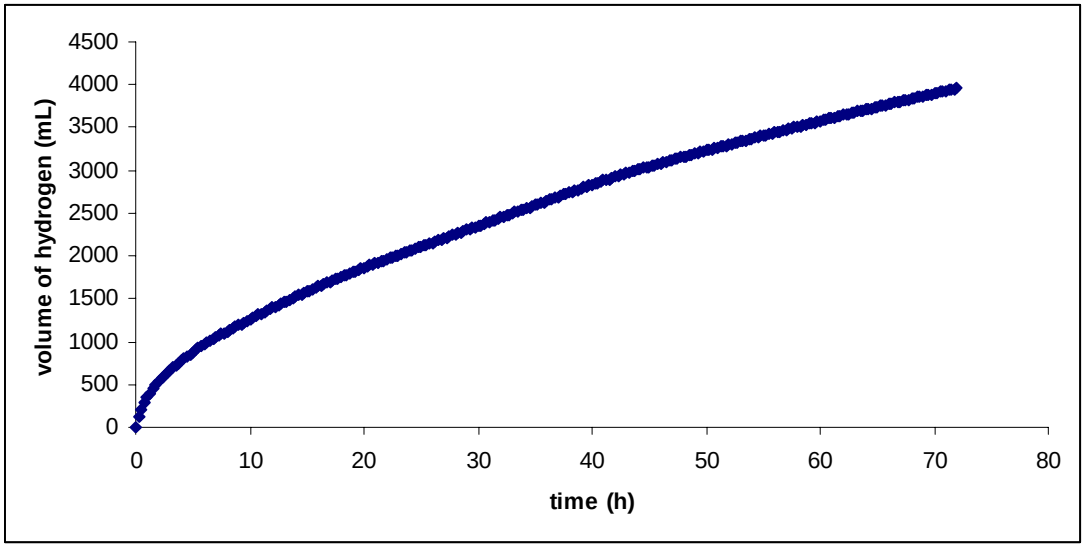

Figure 3.1. plot of hydrogen volume versus time in the self hydrolysis of sodium borohydride starting with 450 mM $NaBH_4$ in 50 mL H_2O at 25°C.

3.2. Ruthenium(III) Acetylacetonate: a homogeneous catalyst in the hydrolysis of sodium borohydride

It has been reported that ruthenium(III) acetylacetonate, $Ru(acac)_3$, acts as a catalyst in the hydrolysis of sodium borohydride with a total turnover number of 1200 before its deactivation [50]. Figure 3.2. shows the volume of hydrogen generation versus time for the hydrolysis of sodium borohydride (450 mM) in the presence of $Ru(acac)_3$ (2 mM) as a catalyst in 50 mL H_2O-THF (9:1) along with hydrogen generation volume for self hydrolysis of sodium borohydride (450 mL) in 50 mL H_2O. According to Figure 3.2, volume of hydrogen generation for self hydrolysis of sodium borohydride is about 900 mL over 6 hours, while at the same period of time, about 3500 mL of H_2 is evolved during hydrolysis of sodium borohydride catalyzed by $Ru(acac)_3$ showing the effective role of catalyst for the hydrolysis of sodium borohydride.

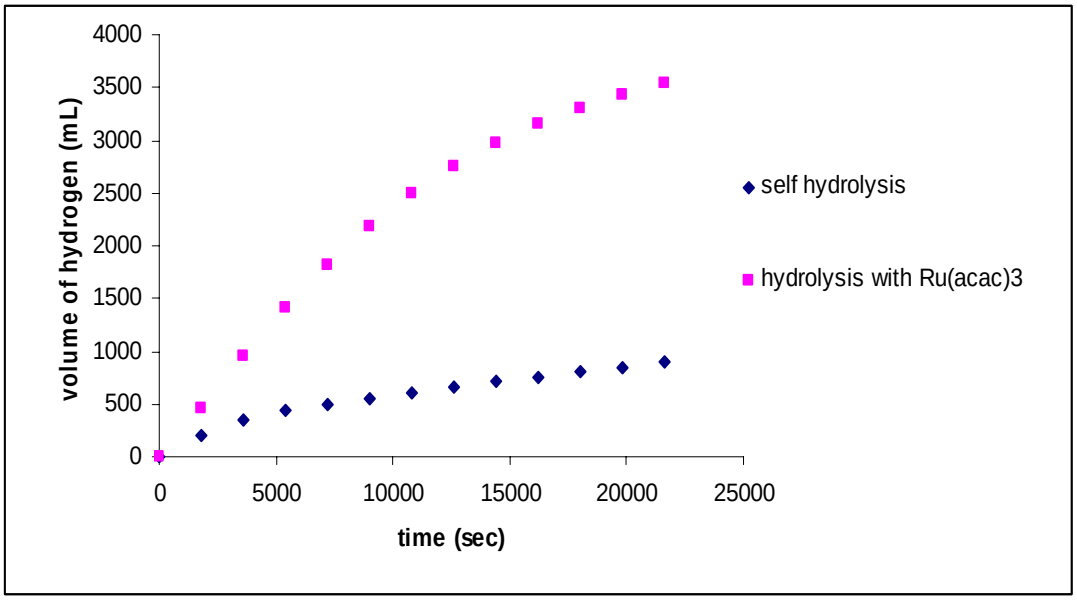

Figure 3.2. Plots of hydrogen volume versus time for the self hydrolysis of sodium borohydride and hydrolysis of sodium borohydride catalyzed by $Ru(acac)_3$. $[NaBH_4]$ = 450 mM, $[Ru(acac)_3]$ = 2 mM, T = 25°C.

A poisoning experiment with trimethylphosphite was performed to realize if $Ru(acac)_3$ is homogeneous or heterogeneous catalyst [51]. Based on Figure 3.3, by increasing the mole ratio of $P(OMe)_3$ to $Ru(acac)_3$ up to 1, the relative rate of hydrogen generation is linearly getting decreased and when the catalytic hydrolysis of sodium borohydride is performed in the presence of $Ru(acac)_3$ and 1 equivalent of $P(OMe)_3$, the relative rate of hydrogen generation is nearly zero. Accordingly, applying 1 equivalent $P(OMe)_3$ per ruthenium results in poisoning the $Ru(acac)_3$ catalyst and this is a satisfactory evidence that $Ru(acac)_3$ is a homogeneous catalyst.

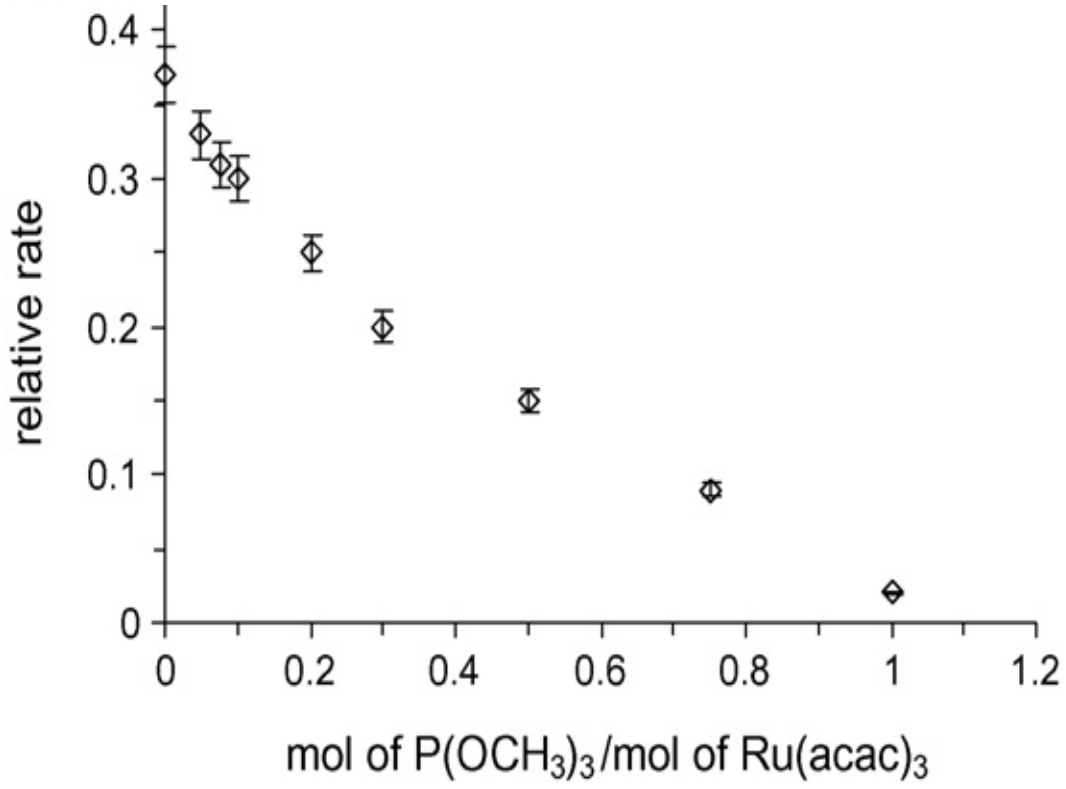

Figure 3.3. Plot of the relative rate versus the moles of $P(OCH_3)_3$/the moles of $Ru(acac)_3$ in the hydrolysis of sodium borohydride.

3.3. Catalytic activity of $Ru(acac)_3$ for the hydrolysis of $NaBH_4$ in the presence of trimethylphosphite

Although the catalytic activity of $Ru(acac)_3$ in the hydrolysis of sodium borohydride is negatively affected by the addition of 1 equivalent of $P(OMe)_3$ per ruthenium into the medium, following the catalytic reaction for a longer time shows that the rate of hydrogen generation is highly increased after a certain period of time (induction time). Figure 3.4 shows the hydrogen volume versus time plot during the catalytic hydrolysis of sodium borohydride (450 mM) performed starting with 2 mM $Ru(acac)_3$ and 2 equivalents of $P(OMe)_3$ per ruthenium in 50 mL H_2O-THF solution. As catalytic reaction proceeds, the rate of hydrogen generation is very low and it is comparable to value of self hydrolysis, but after an inducton period of about 75 minutes the rate of hydrogen generation is suddenly increased (rate = 83 mL H_2/minute) and in a short period of time, a huge volume of hydrogen is liberated.

Therefore, 2 equivalents of $P(OMe)_3$ per ruthenium not only acts as non-poison in the catalytic hydrolysis of sodium borohydride but also highly accelerates the rate of hydrogen generation showing formation of a new ruthenium species with high catalytic activity.

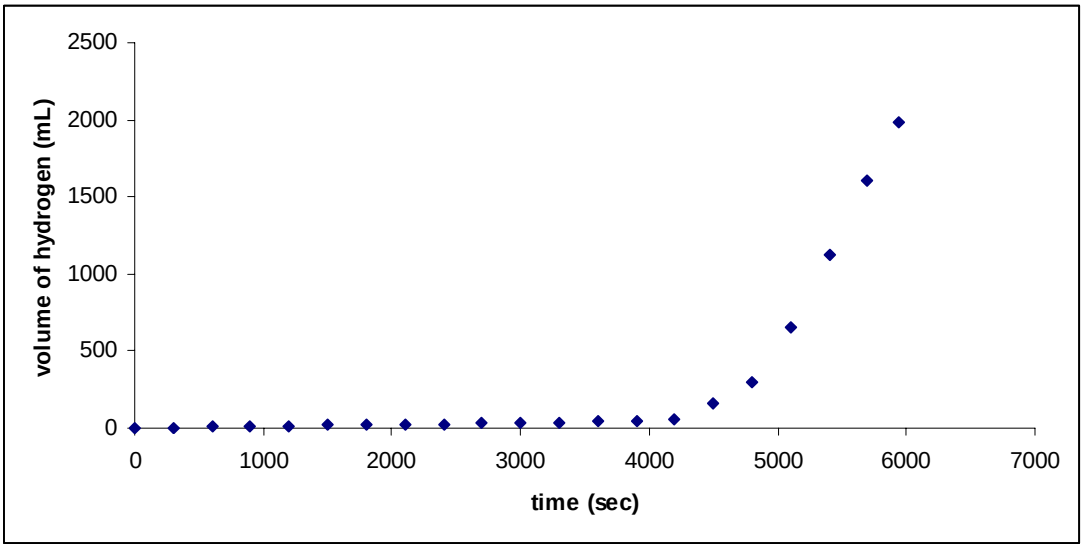

Figure 3.4. Plot of the volume of hydrogen generated versus time for the hydrolysis of $NaBH_4$ at 25 ºC in 50 mL THF/water (1/9) solution starting with $[NaBH_4]$ = 450 mM, $[Ru(acac)_3]$ = 2 mM and $[P(OMe)_3]$ = 4 mM added at the beginning of catalytic reaction.

Another catalytic experiment was performed in order to make a comparison between catalytic activity of new ruthenium species formed after induction time (active catalyst) and sole $Ru(acac)_3$. That experiment encompasses hydrolysis of sodium borohydride (450 mM) starting with 2 mM $Ru(acac)_3$ in 50 mL H_2O-THF and after 80 minutes, 4 mM $P(OMe)_3$ was added into reaction solution. Based on Figure 3.5, the rate of hydrogen generation before addition of $P(OMe)_3$ is about 11 mL H_2/minute showing the catalytic activity of $Ru(acac)_3$ alone. However, after addition of 2 equivalents of trimethylphosphite, hydrogen generation rate is decreased to self hydrolysis level and after 75 minutes a new ruthenium species

(active catalyst) is formed accompanied by a rapid hydrogen evolution with a rate of 83 mL H_2/minute. So, this experiment shows that addition of $P(OMe)_3$ to catalytic solution containing $Ru(acac)_3$ leads to the formation of a new ruthenium species which is much more active than sole $Ru(acac)_3$.

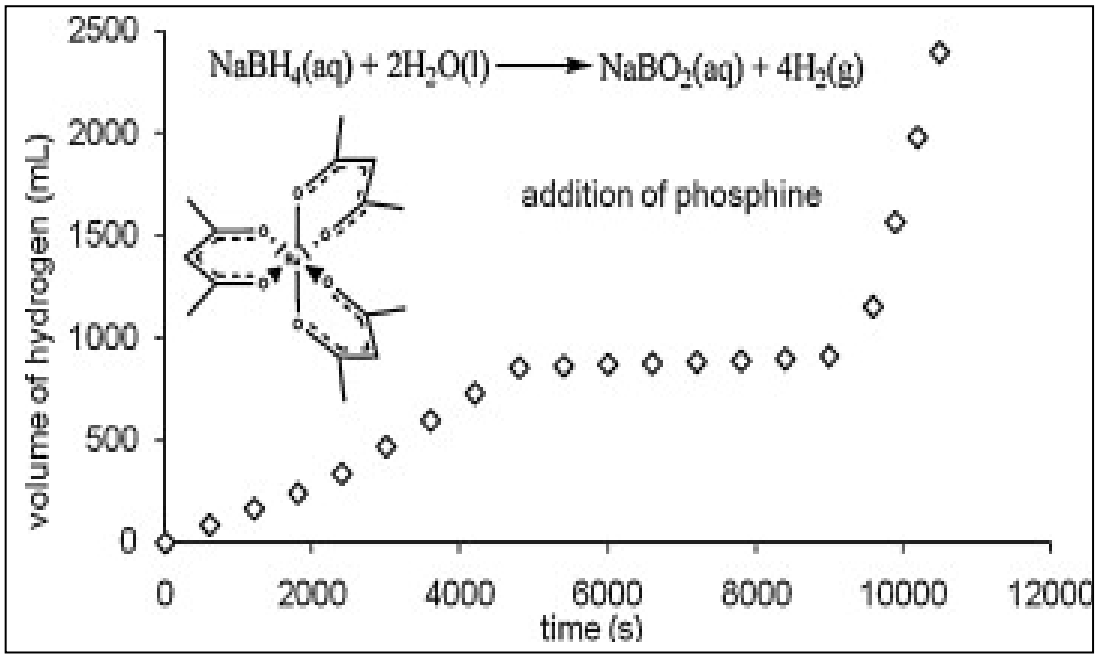

Figure 3.5. Plot of the volume of hydrogen generated versus time for the hydrolysis of $NaBH_4$ at 25 ºC in 50 mL THF/water (1/9) solution starting with [$NaBH_4$] = 450 mM, [$Ru(acac)_3$] = 2 mM, and trimethylphosphite ([$P(OMe)_3$] = 4 mM) added in 80 minutes after the start of reaction. The addition of trimethylphosphite first stops the reaction completely. The reaction restarts at a faster rate in 75 minutes after the addition of $P(OMe)_3$.

Two questions need to be addressed: the first one concerns if the enhancement of hydrogen generation rate in the hydrolysis of sodium borohydride starting with $Ru(acac)_3$ can be observed in the presence of other phosphorus compounds such as triphenylphosphite. The second issue concerns whether concentration of phosphorus compounds or varying the mole ratio of phosphorus per ruthenium affects the rate of hydrogen evolution or not.

3.4. Catalytic activity of $Ru(acac)_3$ for the hydrolysis of $NaBH_4$ in the presence of triphenylphosphite

To reply the first question, another catalytic experiment concerning hydrolysis of sodium borohydride (450 mM) was performed starting with 2 mM $Ru(acac)_3$ and 2 equivalents of $P(OPh)_3$ in 50 mL H_2O-THF solution at 25 ºC. According to Figure 3.6, after about 25 minutes the rate of hydrogen generation is increased showing the formation of a new ruthenium species with triphenylphosphite compound. The active catalyst with triphenylphosphite has a hydrogen generation rate of 34 mL H_2/minute which is about three times as much as the rate of hydrogen generation for $Ru(acac)_3$ alone. However, catalytic activity of active catalyst with trimethylphosphite (rate = 83 mL H_2/minute) is much higher than the active catalyst containing triphenylphosphite compound. Altogether, catalytic activity of $Ru(acac)_3$ in the hydrolysis of sodium borohydride is improved in the presence of different phosphorus compounds such as trimethylphosphite, triphenylphosphite, triphenylphosphine or 1,2-bis (diphenylphosphino)ethane [52,53].

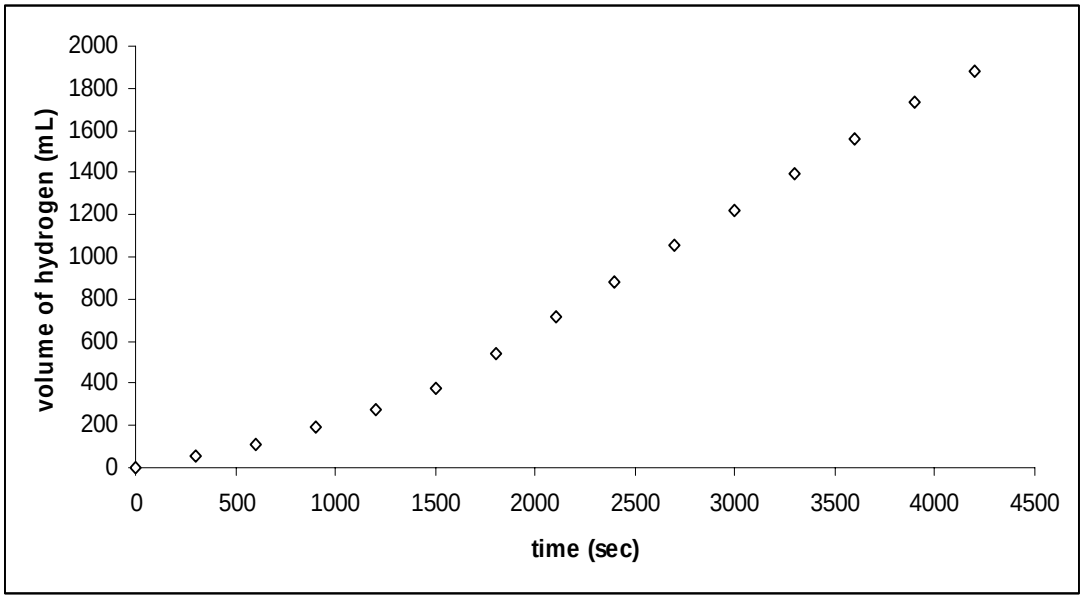

Figure 3.6. Plot of the volume of hydrogen generated versus time for the hydrolysis of $NaBH_4$ at 25 ºC in 50 mL THF/water (1/9) solution starting with $[NaBH_4]$ = 450 mM, $[Ru(acac)_3]$ = 2 mM and $[P(OPh)_3]$ = 4 mM.

3.5. The effect of phosphorus concentration on catalytic activity of $Ru(acac)_3$ for the hydrolysis of $NaBH_4$

Another issue which needs to be addressed is related to the effect of different phosphorus concentration on the rate of hydrogen generation or in other words, whether varying the mole ratio of phosphorus per ruthenium leads to change in hydrogen generation rate or not. To answer this question, a set of experiments were performed using 50 mL H_2O-THF solution, with 450 mM $NaBH_4$ and 2 mM $Ru(acac)_3$, and different ratios of $P(OMe)_3$ to $Ru(acac)_3$ (in the range of 1-3).

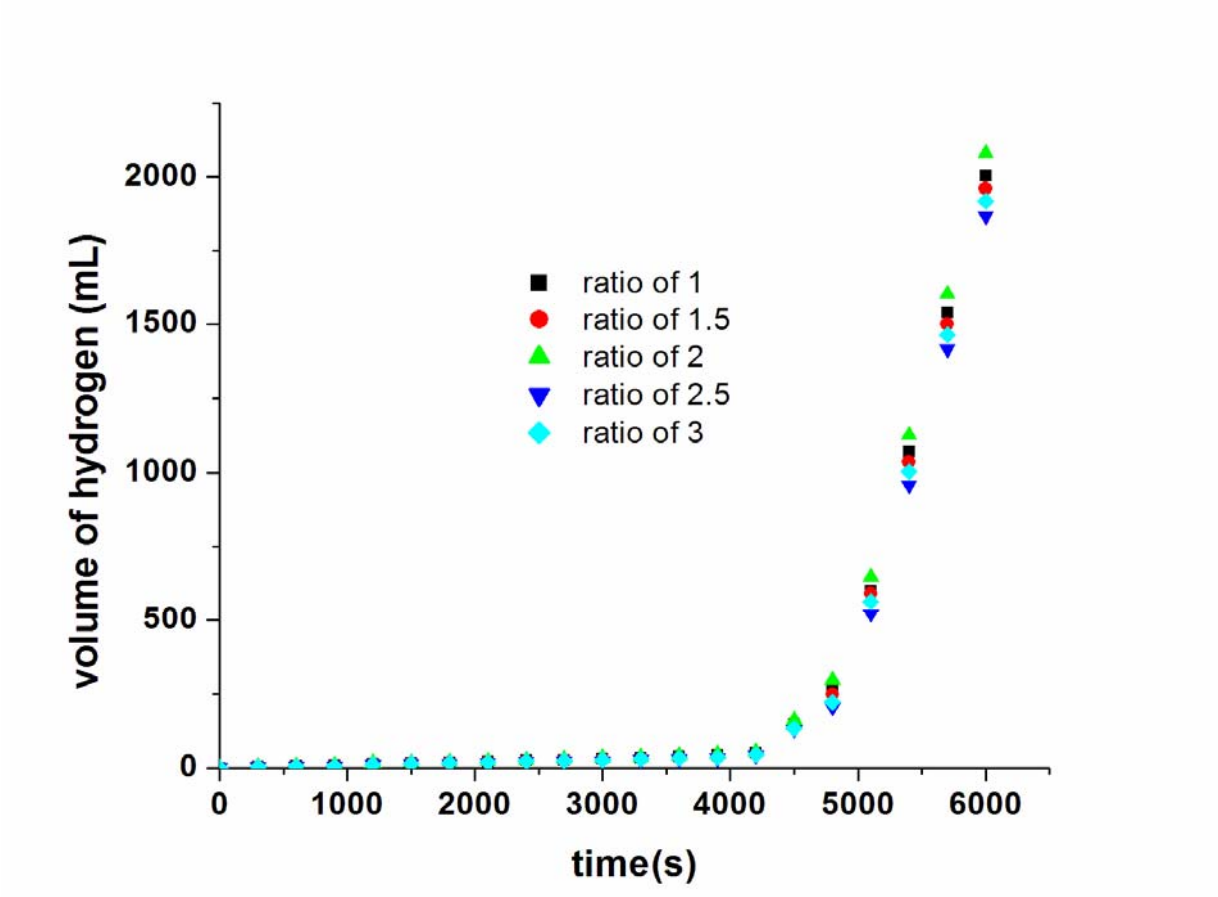

Figure 3.7. Plot of hydrogen volume versus time in the hydrolysis of sodium borohydride starting with a solution containing 450 mM $NaBH_4$ and 2 mM $Ru(acac)_3$ plus different equivalents of $P(OCH_3)_3$ per ruthenium at 25°C.

As seen in Figure 3.7, varying the mole ratios of $P(OMe)_3$ to ruthenium does not affect the rate of hydrogen generation or in other words, the rate of sodium borohydride hydrolysis is independent of trimethylphosphite concentration.

Another set of experiments containing 450 mM $NaBH_4$, 2 mM $Ru(acac)_3$ and different ratios of $P(OPh)_3$ to $Ru(acac)_3$ (in the range of 0.5-3) in 50 mL H_2O-THF solution was performed. As seen in Figure 3.8, changing the concentration of triphenylphosphite compound affects the rate of hydrogen generation slightly. Essentially, the hydrolysis rate of sodium borohydride is nearly independent of the ratio of triphenylphosphite to ruthenium.

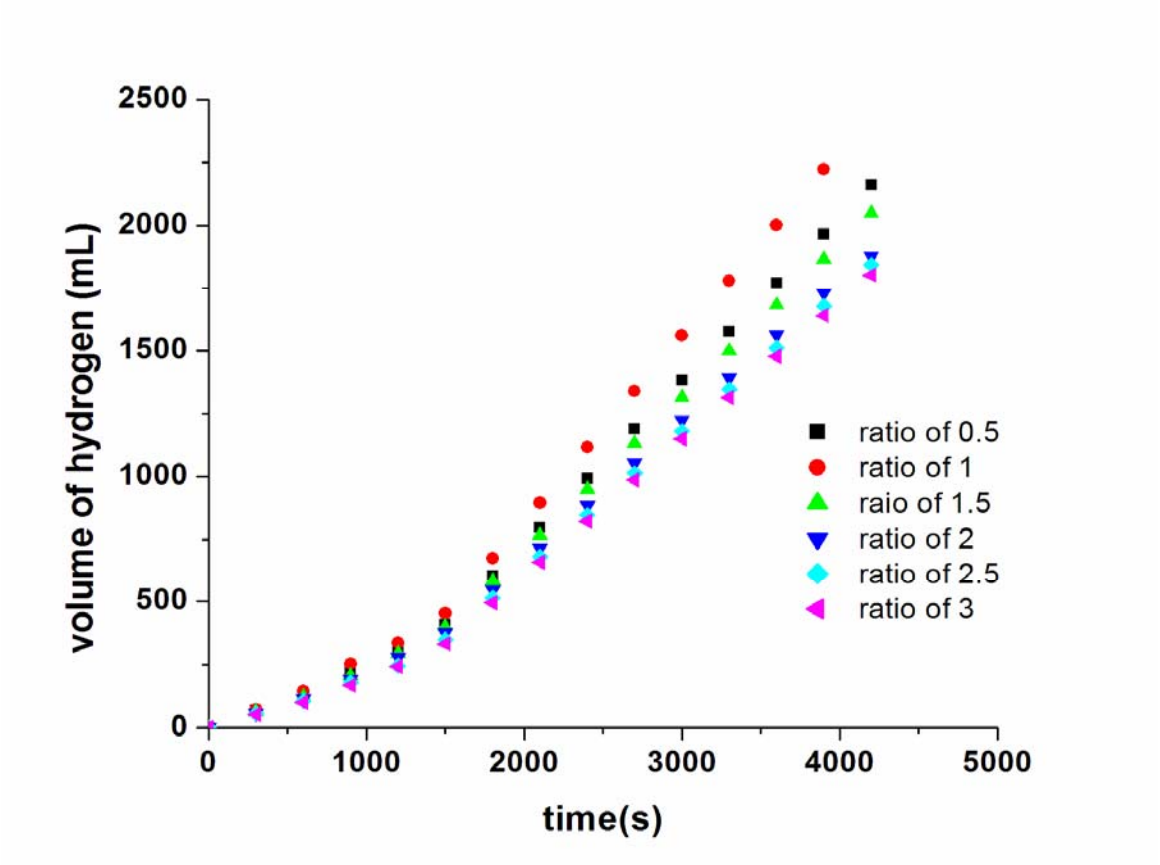

Figure 3.8. Plot of hydrogen volume versus time in the hydrolysis of sodium borohydride starting with a solution containing 450 mM $NaBH_4$ and 2 mM $Ru(acac)_3$ plus different equivalents of $P(OPh)_3$ per ruthenium at 25°C.

As seen in Figures 3.7 and 3.8, after the induction time, a linear hydrogen evolution is observed from which the rate of hydrogen generation is acquired. Figure 3.9 shows the rate of hydrogen generation versus the mole ratio of phosphorus to ruthenium for trimethylphosphite and triphenylphosphite compounds.

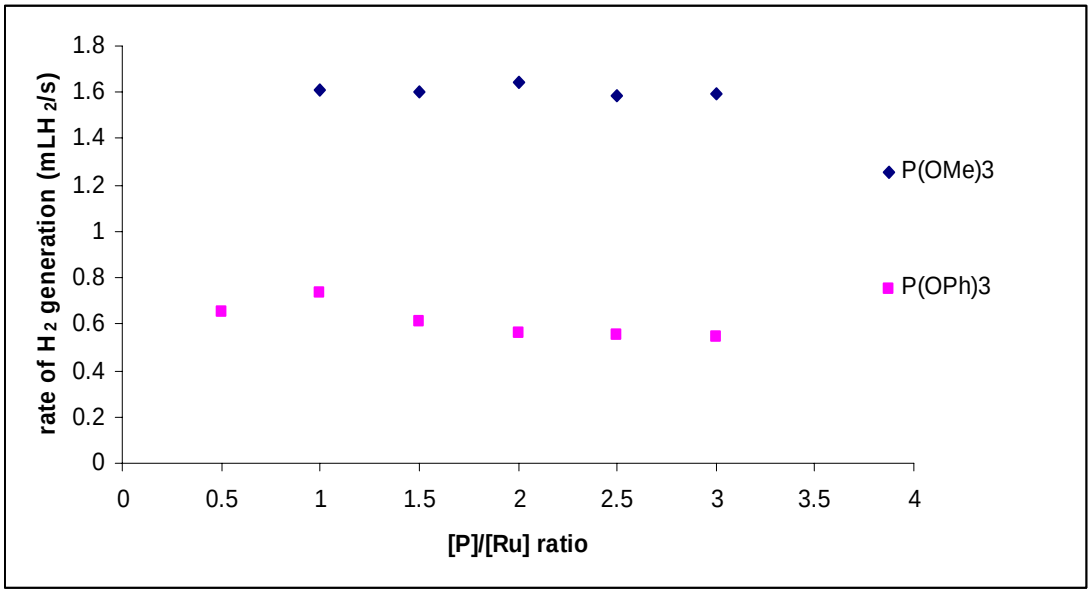

Figure 3.9. Plot of hydrogen generation rate versus mole ratio of phosphine to ruthenium in the hydrolysis of $NaBH_4$ catalyzed by $Ru(acac)_3$ plus a phosphine. $[NaBH_4]$ = 450 mM, [Ru] = 2.0 mM, T = 25 ºC.

According to the plots given in Figure 3.9, catalytic activity of $Ru(acac)_3$ in hydrogen generation from the hydrolysis of $NaBH_4$ is enhanced in the presence of different phosphorus compounds such as $P(OMe)_3$ or $P(OPh)_3$ after a certain period of time (induction time). However, the rate of hydrogen generation for the active catalyst containing $P(OMe)_3$ is higher than that with $P(OPh)_3$ compound. Moreover, for both of $P(OMe)_3$ and $P(OPh)_3$ compounds, changing the mole ratio of phosphine to ruthenium does not affect the rate of hydrogen generation significantly. At the beginning, we expected that one acetylacetonato group is replaced by two phosphorus ligands during the induction time. For that reseaon, in what follows, the results of kinetic study concerning hydrolysis of sodium borohydride catalyzed by $Ru(acac)_3$ and 2 equivalents of phosphorus compound, will be discussed.

3.6. Kinetic study of the hydrolysis of sodium borohydride catalyzed by $Ru(acac)_3$ plus 2 equivalents of $P(OMe)_3$

Kinetics of the hydrolysis of sodium borohydride in the presence of $Ru(acac)_3$ plus 2 equivalents of $P(OMe)_3$ were accomplished by monitoring the hydrogen generation depending on catalyst concentration, substrate concentration and temperature.

$$NaBH_4 + 2H_2O \xrightarrow[\text{Water / THF (9:1)}]{\text{Ru(acac)}_3 \text{ / P(OMe)}_3} NaBO_2 + 4H_2 \qquad (3.1)$$

3.6.1. The rate law for the hydrolysis of sodium borohydride catalyzed by Ruthenium(III) acetylacetonate plus 2 equivalents of $P(OMe)_3$

Ruthenium(III) acetylacetonate plus 2 equivalents of trimethylphosphite per ruthenium was employed as a homogeneous catalyst in the hydrolysis of sodium borohydride. Figure 3.10 shows the hydrogen volume versus time plots during the hydrolysis of $NaBH_4$ (450 mM) catalyzed by different concentrations of $Ru(acac)_3$ (in the range of 2-4 mM) and 2 equivalents of $P(OMe)_3$ per ruthenium at 25 ºC . Depending on the catalyst concentration, a linear hydrogen generation at different rates is observed after the induction time. As the catalyst concentration is increased, the induction time decreases and formation of active catalyst is getting faster. After the induction time, the hydrogen generation starts at a measurable rate. A sharp start up is not observed because the hydrogen evolution increases gradually at the beginning as the active catalyst is formed. As seen in Figure 3.10, catalytic activity during induction time is very low and comparable to level of self hydrolysis. However, after the induction time, catalytic activity is highly increased which is indicative of the formation of active catalyst from the reaction of $Ru(acac)_3$ and $P(OMe)_3$ during the induction time.

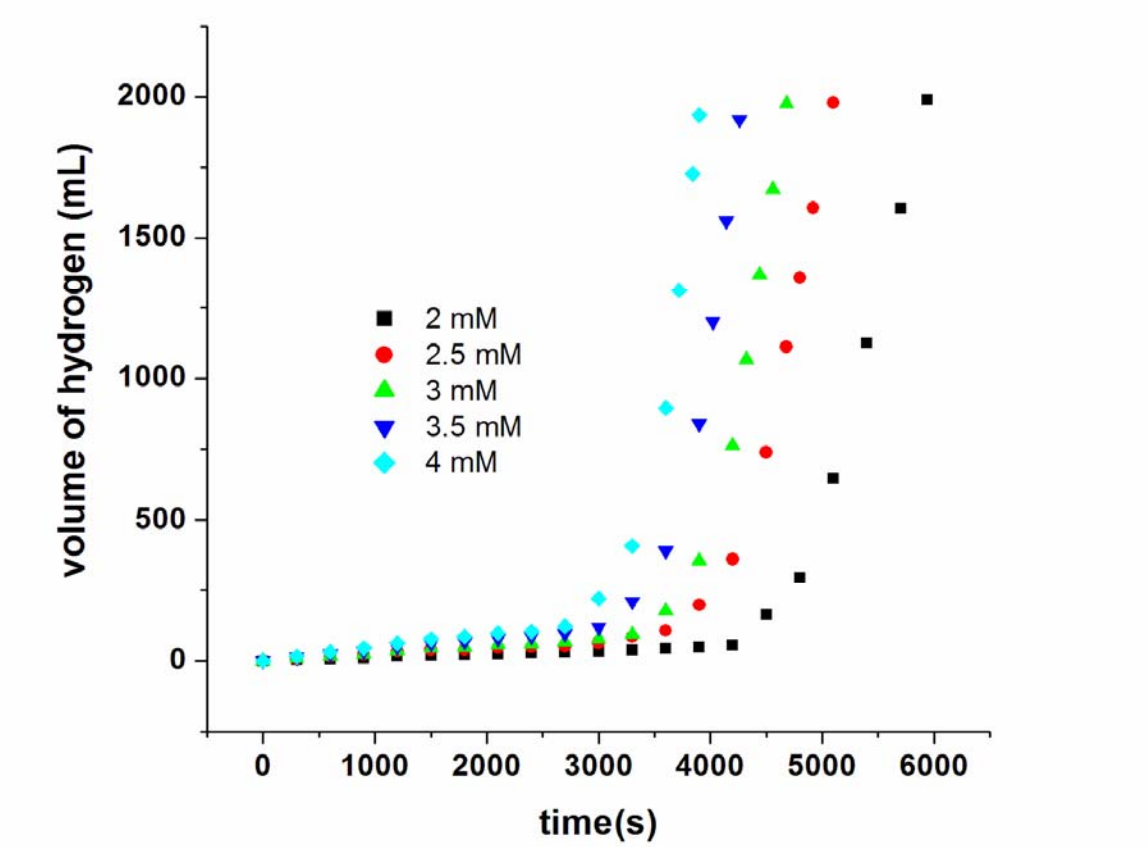

Figure 3.10. The volume of H_2 versus time plots during the hydrolysis of $NaBH_4$ solution (450 mM) catalyzed by $Ru(acac)_3$ and 2 equivalents of $P(OMe)_3$ in different ruthenium concentration at 25°C.

From the slope of the linear portion of plots, hydrogen generation rate is acquired and as the concentration of catalyst is increased, the rate of hydrogen generation increases. Figure 3.11 shows the plot of hydrogen generation rate versus ruthenium concentrations, both in logarithmic scale. Based on Figure 3.11, a straight line with a slope of about 1 is obtained showing that hydrolysis of sodium borohydride is first order with respect to catalyst concentration or in other words, the rate of hydrogen generation shows first order dependency on the concentration of ruthenium.

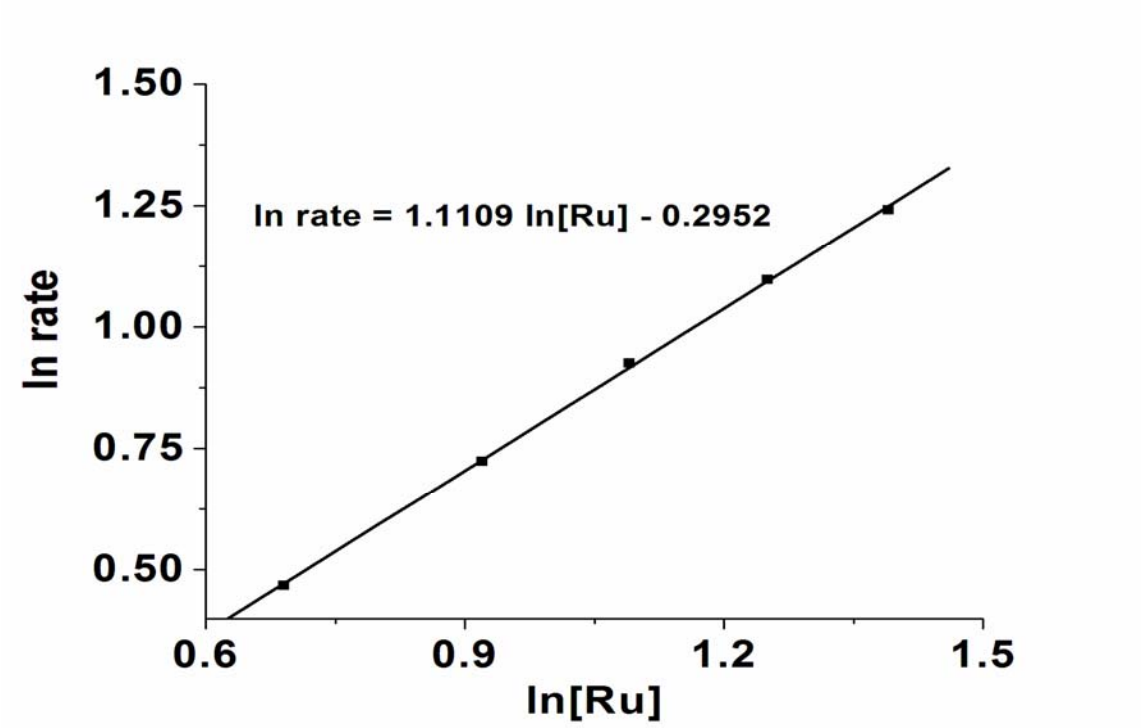

Figure 3.11. The graph of ln (rate) versus ln [Ru] for the hydrolysis of sodium borohydride catalyzed by different concentrations of $Ru(acac)_3$ and 2 equivalents of $P(OMe)_3$ per ruthenium at 25°C.

In the second set of experiments, $NaBH_4$ concentration was varied in the hydrolysis of $NaBH_4$ catalyzed by a constant concentration of $Ru(acac)_3$ and 2 equivalents of $P(OMe)_3$ per ruthenium at 25°C. Figure 3.12 shows hydrogen volume versus time plots during the hydrolysis of $NaBH_4$ with different concentrations (in the range of 300-1500 mM) catalyzed by a constant concentration of $Ru(acac)_3$ (2 mM) and 2 equivalents of $P(OMe)_3$ per ruthenium at 25ºC. As the concentration of $NaBH_4$ is increased, the induction time decreases and formation of active catalyst becomes faster.

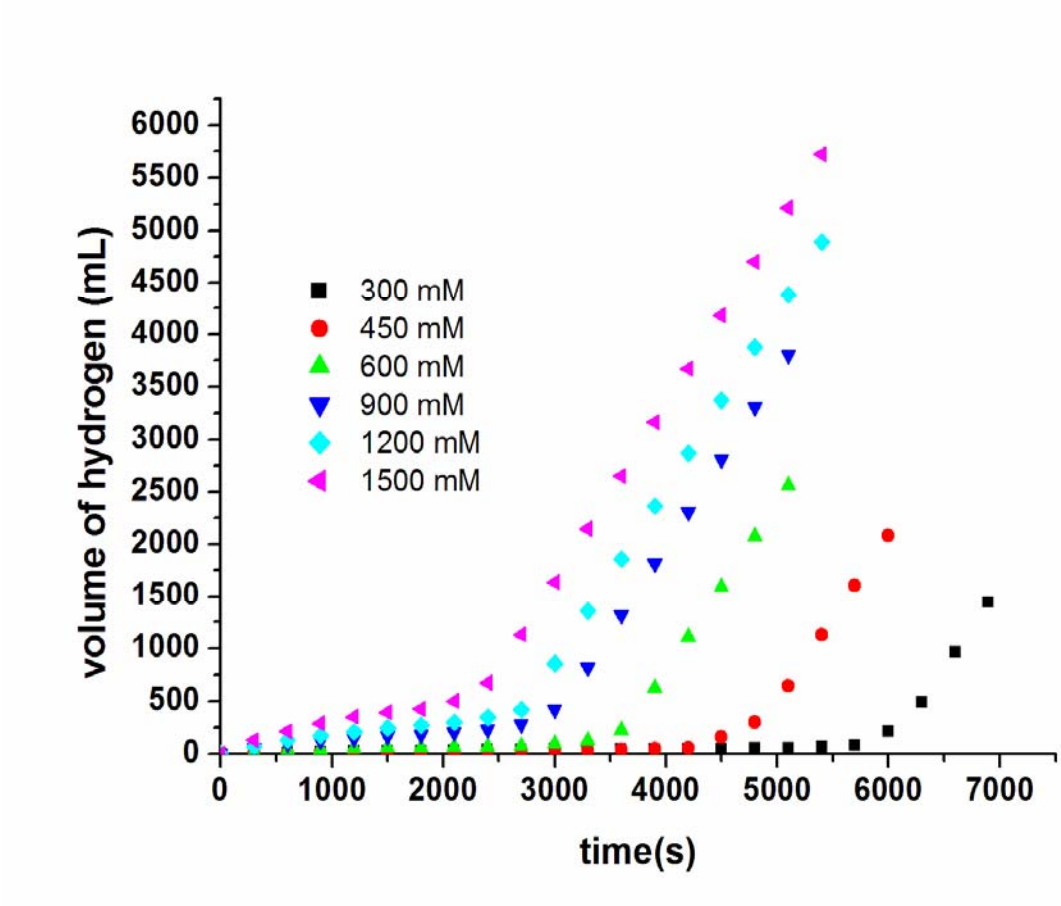

Figure 3.12. The volume of H_2 versus time plot during the hydrolysis of sodium borohydride solution catalyzed by 2 mM $Ru(acac)_3$ and 2 equivalents of $P(OMe)_3$ in different sodium borohydride concentrations at 25°C.

In the range of 0.30-1.5 M $NaBH_4$, the rate of hydrogen generation was found to be almost independent of the $NaBH_4$ concentration. Figure 3.13 shows the plot of hydrogen generation rate versus $NaBH_4$ concentrations, both in logarithmic scale, which gives a straight line with a slope of about zero. This indicates that hydrolysis of sodium borohydride is zero order with respect to substrate concentration or in other words, the rate of hydrogen generation shows no dependency on the concentration of $NaBH_4$.

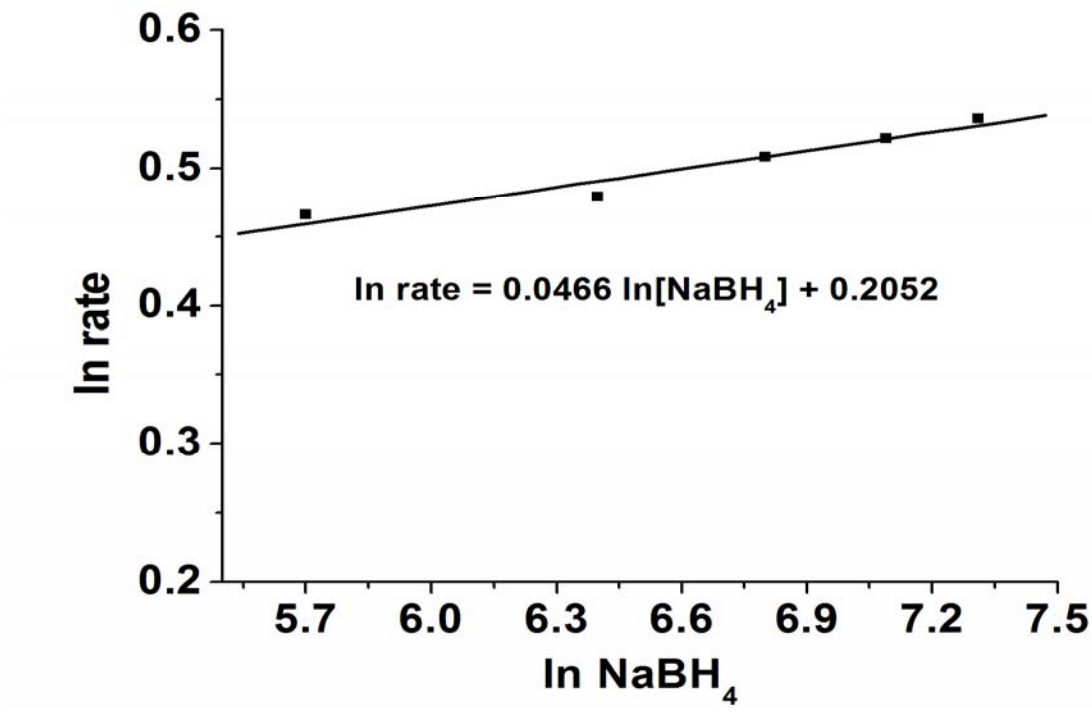

Figure 3.13. The graph of ln (rate) versus ln [$NaBH_4$] for the hydrolysis of sodium borohydride with different concentrations (in the range of 300-1500 mM) catalyzed by a constant concentration of $Ru(acac)_3$ (2 mM) and 2 equivalents of $P(OMe)_3$ at 25.0°C.

Thus the rate law for the hydrolysis of sodium borohydride catalyzed by $Ru(acac)_3$ and 2 equivalents of $P(OMe)_3$ per ruthenium can be given as :

$$- 4d\,[NaBH_4]/dt = d[H_2]/dt = k\,[Ru] \qquad (3.2)$$

3.6.2. Activation parameters for the hydrolysis of $NaBH_4$ catalyzed by $Ru(acac)_3$ plus 2 equivalents of $P(OMe)_3$

In order to find the activation parameters, the hydrolysis of $NaBH_4$ was performed at five different temperatures, 20, 25, 30, 35 and 40°C in the presence of $Ru(acac)_3$ (2 mM) and 2 equivalents of $P(OMe)_3$. Figure 3.14 shows hydrogen

volume versus time plots during the hydrolysis of $NaBH_4$ (450 mM) catalyzed by 2 mM $Ru(acac)_3$ and 2 equivalents of $P(OMe)_3$ per ruthenium at various temperatures.

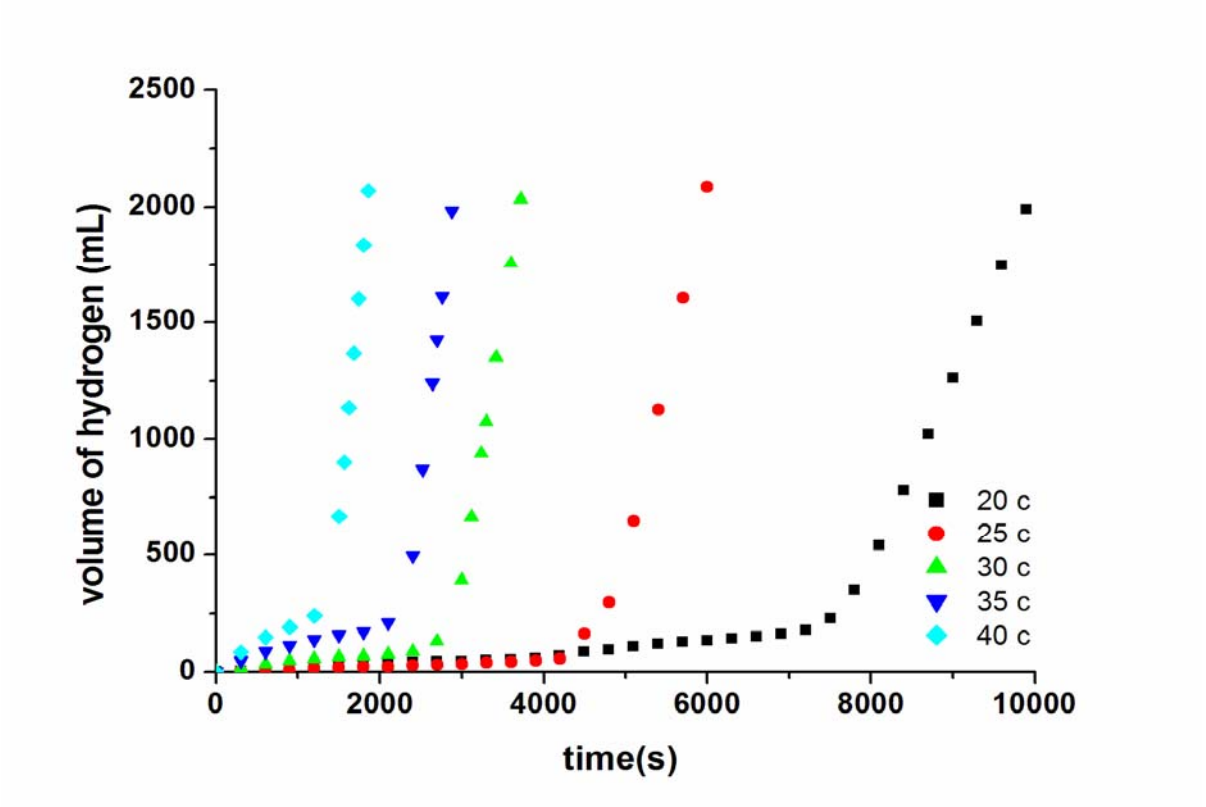

Figure 3.14. Plot of hydrogen volume generated versus time for the hydrolysis of sodium borohydride (450 mM) catalyzed by 2 mM $Ru(acac)_3$ and 2 equivalents of $P(OMe)_3$ per ruthenium at various temperatures.

Based on Figure 3.14, as the temperature is increased, the induction time becomes shorter or formation of active catalyst is getting faster. Moreover, at high temperatures, the activity during induction time and rate of hydrogen generation after induction time are getting increased. Rate constant values for the hydrogen generation obtained from the linear part of the plots in Figure 3.14, are listed in Table 3.1.

Table 3.1. Rate constant valuse for the hydrolysis of sodium borohydride (450 mM) catalyzed by 2 mM $Ru(acac)_3$ and 2 equivalents of $P(OMe)_3$ per ruthenium at various temperatures.

Temperature (°C)	**Rate Constant, *k*** **(mmol H_2). (mmol Ru)$^{-1}$. s^{-1}**
20	0.329 ± 0.0066
25	0.468 ± 0.013
30	0.918 ± 0.0183
35	1.25 ± 0.025
40	1.60 ± 0.032

Rate constant valuses for the hydrogen generation were used to acquire the activation parameters by considering either Arrhenius or Eyring plots. The activation energy was determined by using of Arrhenius Equation:

$$\mathbf{k = A.e^{-Ea/RT}} \qquad (3.3)$$

Where Ea is the Arrehenius activation energy, A is the preexponential factor as a characteristic contant and R is the gas constant. The Equation (3.3) is changed to Equation (3.4) by taking natural logarithm of both sides:

$$\mathbf{\ln k = \ln A - [Ea/RT]} \qquad (3.4)$$

According to Figure 3.15, a straight line with a slope of [-Ea/R] is obtained by the plot of ln k versus 1/T.

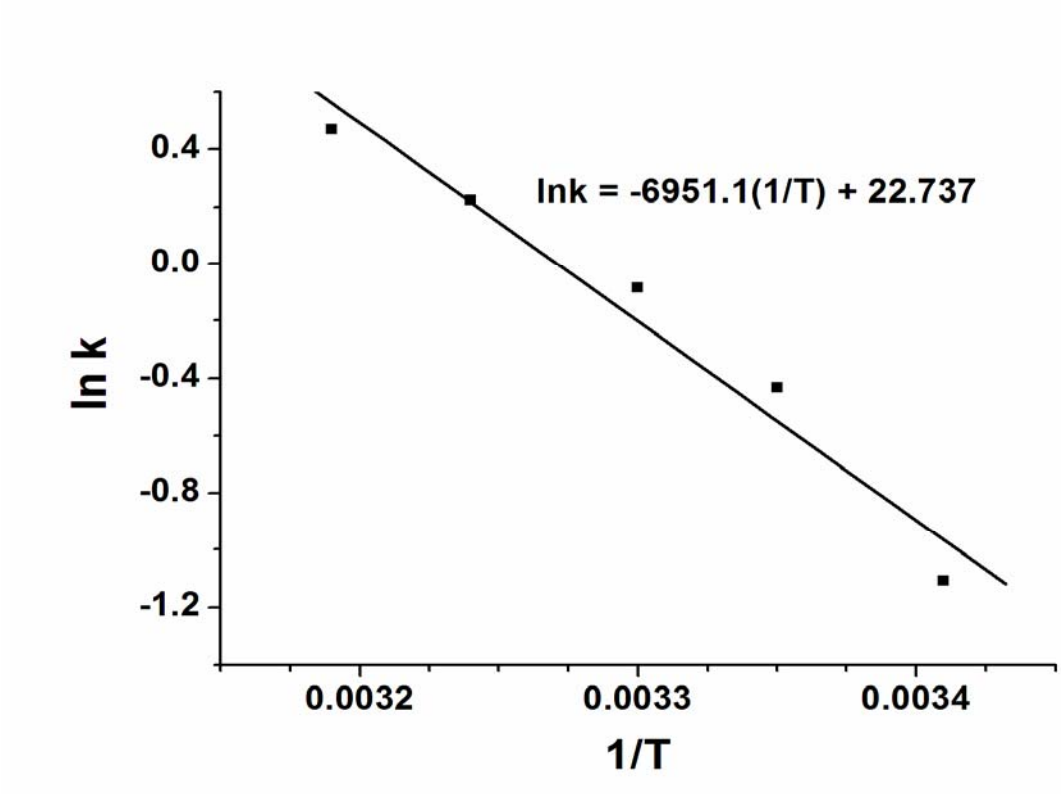

Figure 3.15. Arrhenius plot for the hydrolysis of sodium borohydride (450 mM) catalyzed by 2 mM $Ru(acac)_3$ and 2 equivalents of $P(OMe)_3$ per ruthenium at various temperatures.

The activation energy, Ea, for the hydrolysis of sodium borohydride catalyzed by $Ru(acac)_3$ and 2 equivalents of $P(OMe)_3$ is 58 ± 2 kJ/mol which was calculated by using the slope of Arrhenius plot.

The enthalpy of activation, $\Delta H^{\#}$ and the enthropy of activation, $\Delta S^{\#}$ were calculated by using of Eyring Equation:

$$\mathbf{\ln k/T = 1/T\ [\Delta H^{\#}/R] + \ln k_b/h + \Delta S^{\#}/R} \qquad (3.5)$$

According to Figure 3.16, a straight line with a slope of $[\Delta H^{\#}/R]$ and an intercept of $[\ln k_b/h + \Delta S^{\#}/R]$ is obtained by the plot of ln k/T versus 1/T.

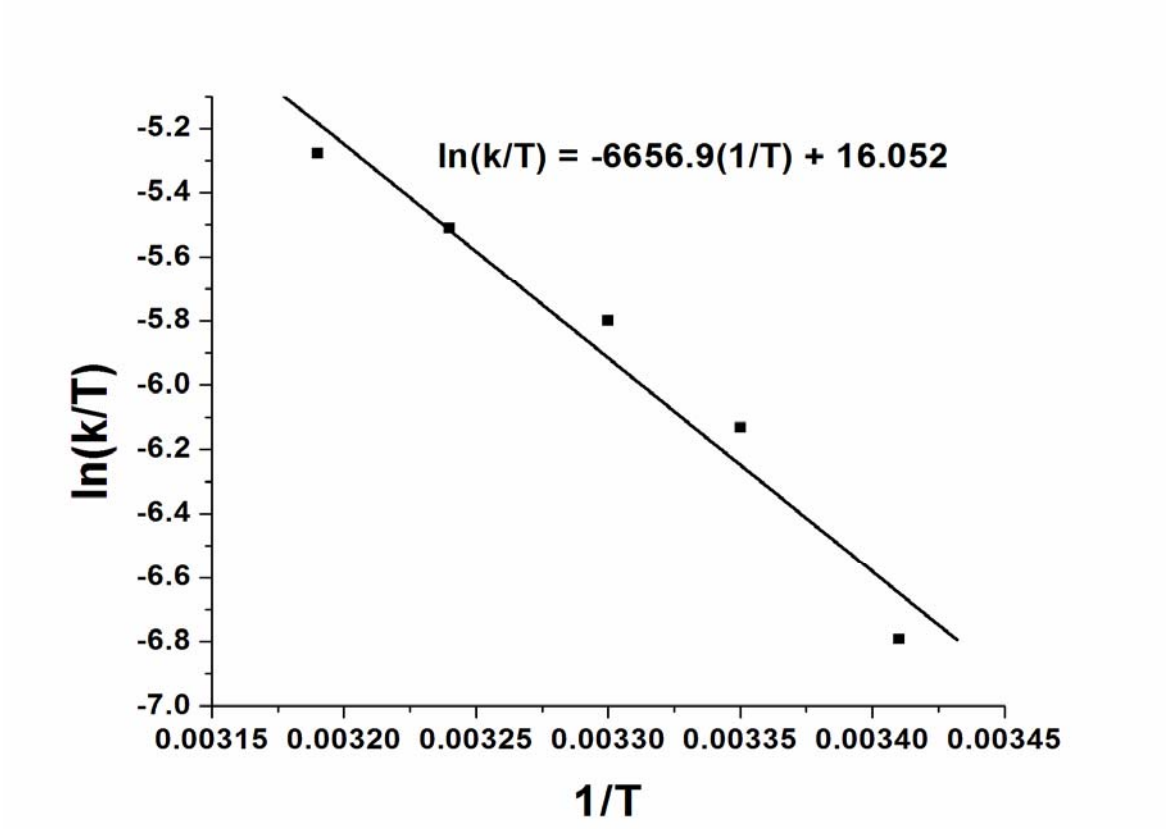

Figure 3.16. Eyring plot for the hydrolysis of sodium borohydride (450 mM) catalyzed by 2 mM $Ru(acac)_3$ and 2 equivalents of $P(OMe)_3$ per ruthenium at various temperatures.

The enthalpy of activation, $\Delta H^{\#}$, for the hydrolysis of sodium borohydride catalyzed by $Ru(acac)_3$ and 2 equivalents of $P(OMe)_3$ is 56 ± 2 kJ/mol which was calculated by using the slope of Eyring plot while the enthropy of activation obtained by using the intercept of Eyring plot was calculated as -64 ± 4 J/mol.K.

3.7. The catalytic life time of ruthenium(III) acetylacetonate and 2 equivalents of $P(OMe)_3$ per ruthenium

Lifetime of the catalyst involving $Ru(acac)_3$ and 2 equivalents of $P(OMe)_3$ was measured by determining the total turnover number (TTON) in hydrogen generation from the hydrolysis of sodium borohydride. The system containing

$Ru(acac)_3$ and 2 equivalents of $P(OMe)_3$ per ruthenium is stable and long-live catalyst in the hydrolysis of sodium borohydride. The TTON value for the catalyst containing $Ru(acac)_3$ and $P(OMe)_3$ is 20700 over 72 hours and the highest value of turnover frequency is 38.4 (mol H_2).(mol Ru)$^{-1}$.(min)$^{-1}$. Figure 3.17 shows the plot of total turnover number versus time for hydrogen generation from the catalytic hydrolysis of sodium borohydride starting with 2 mM $Ru(acac)_3$, 2 equivalents of $P(OMe)_3$ per ruthenium and 450 mM $NaBH_4$ at 25.0 °C.

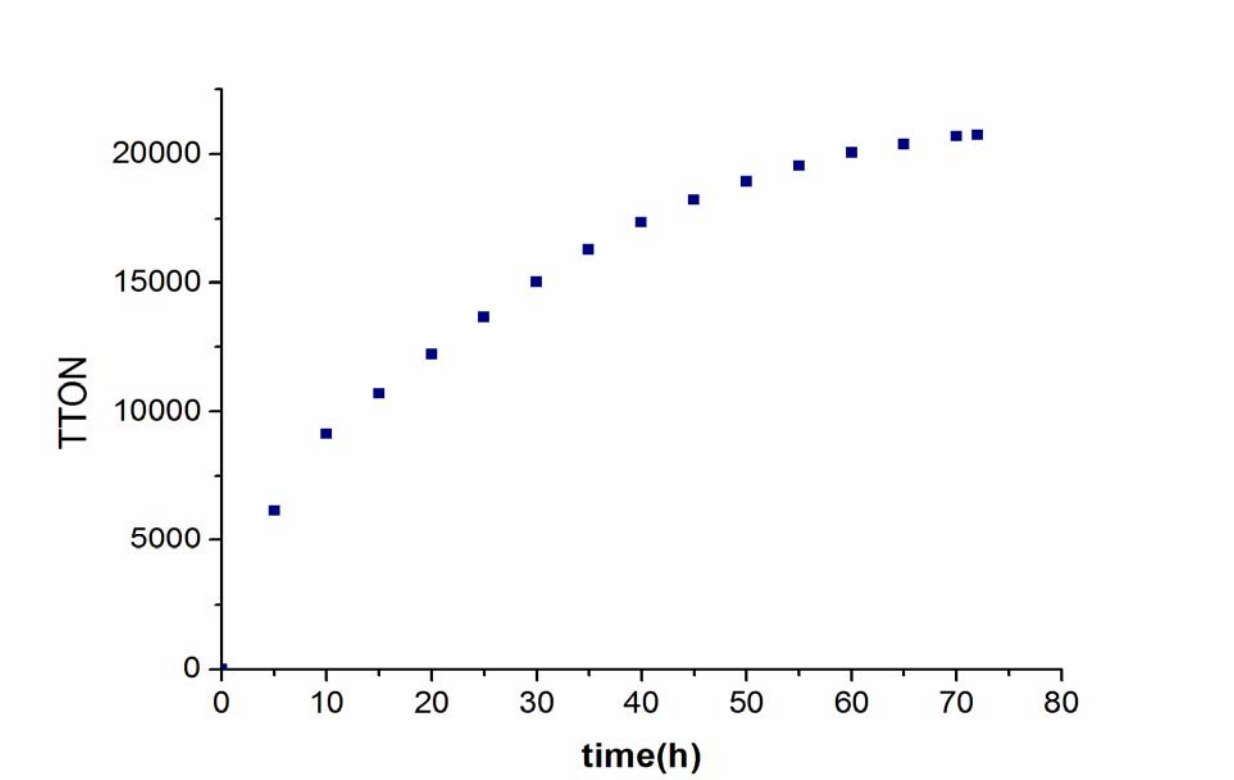

3.17. Plot of total turnover number versus time for hydrogen generation from the catalytic hydrolysis of sodium borohydride starting with 2 mM $Ru(acac)_3$, 2 equivalents of $P(OMe)_3$ per ruthenium and 450 mM $NaBH_4$ in 50 mL H_2O-THF solution at 25.0°C.

3.8. Kinetic study of the hydrolysis of sodium borohydride catalyzed by $Ru(acac)_3$ plus 2 equivalents of $P(OPh)_3$

Kinetics of the sodium borohydride hydrolysis in the presence of $Ru(acac)_3$ plus 2 equivalents of $P(OPh)_3$ were accomplished by monitoring the hydrogen generation depending on catalyst concentration, substrate concentration and temperature.

$$NaBH_4 + 2H_2O \xrightarrow[\text{Water / THF (9:1)}]{Ru(acac)_3 \,/\, P(OPh)_3} NaBO_2 + 4H_2 \qquad (3.6)$$

3.8.1. The rate law for the hydrolysis of sodium borohydride catalyzed by Ruthenium(III) acetylacetonate plus 2 equivalents of $P(OPh)_3$

Ruthenium(III) acetylacetonate plus 2 equivalents of triphenylphosphite per ruthenium was applied as a homogeneous catalyst in the hydrolysis of sodium borohydride. Figure 3.18 shows hydrogen volume versus time plots during the hydrolysis of $NaBH_4$ (450 mM) catalyzed by different concentrations of $Ru(acac)_3$ (in the range of 2-4 mM) and 2 equivalents of $P(OPh)_3$ per ruthenium at 25 ºC . Depending on the catalyst concentration, a linear hydrogen generation is observed after finishing the induction time. By increasing the concentration of $Ru(acac)_3$, the induction time decreases and formation of active catalyst is getting faster. When the induction time ends, the hydrogen generation starts at a measurable rate and a sharp end point is difficult to distinguigh because the hydrogen evolution increases gradually at the beginning of active catalyst formation. Based on Figure 3.18, catalytic activity during induction time is low and slightly higher than level of self hydrolysis. However, after finishing the induction time, catalytic activity is highly increased which is indicative of the formation of active catalyst from the reaction of $Ru(acac)_3$ and $P(OPh)_3$ during the induction time.

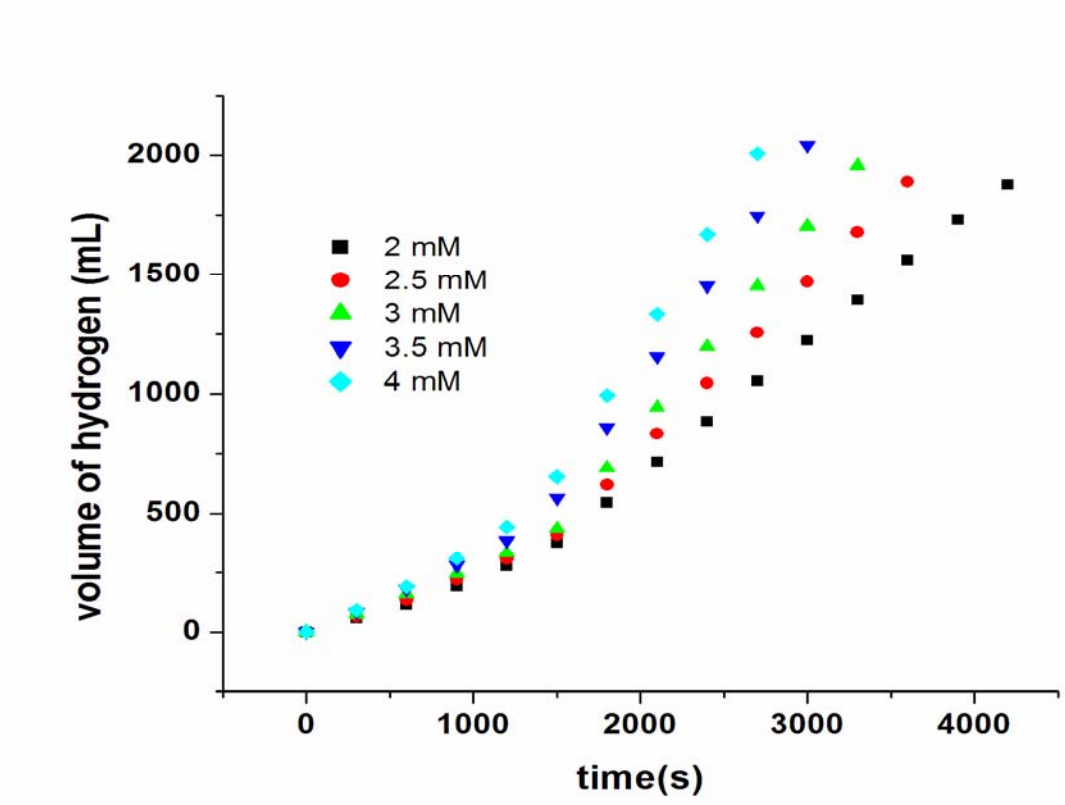

Figure 3.18. The volume of hydrogen versus time plots during the hydrolysis of $NaBH_4$ solution (450 mM) catalyzed by $Ru(acac)_3$ and 2 equivalents of $P(OPh)_3$ in different ruthenium concentration at 25°C.

From the slope of the linear portion of plots, hydrogen generation rate is obtained and as the concentration of catalyst is increased, the rate of hydrogen generation increases. Figure 3.19 shows the plot of hydrogen generation rate versus ruthenium concentrations, both in logarithmic scale. Based on Figure 3.19, a straight line with a slope of about 1 is obtained showing that hydrolysis of sodium borohydride is first order with regard to catalyst concentration or in other words, the rate of hydrogen generation shows first order dependency on the concentration of ruthenium.

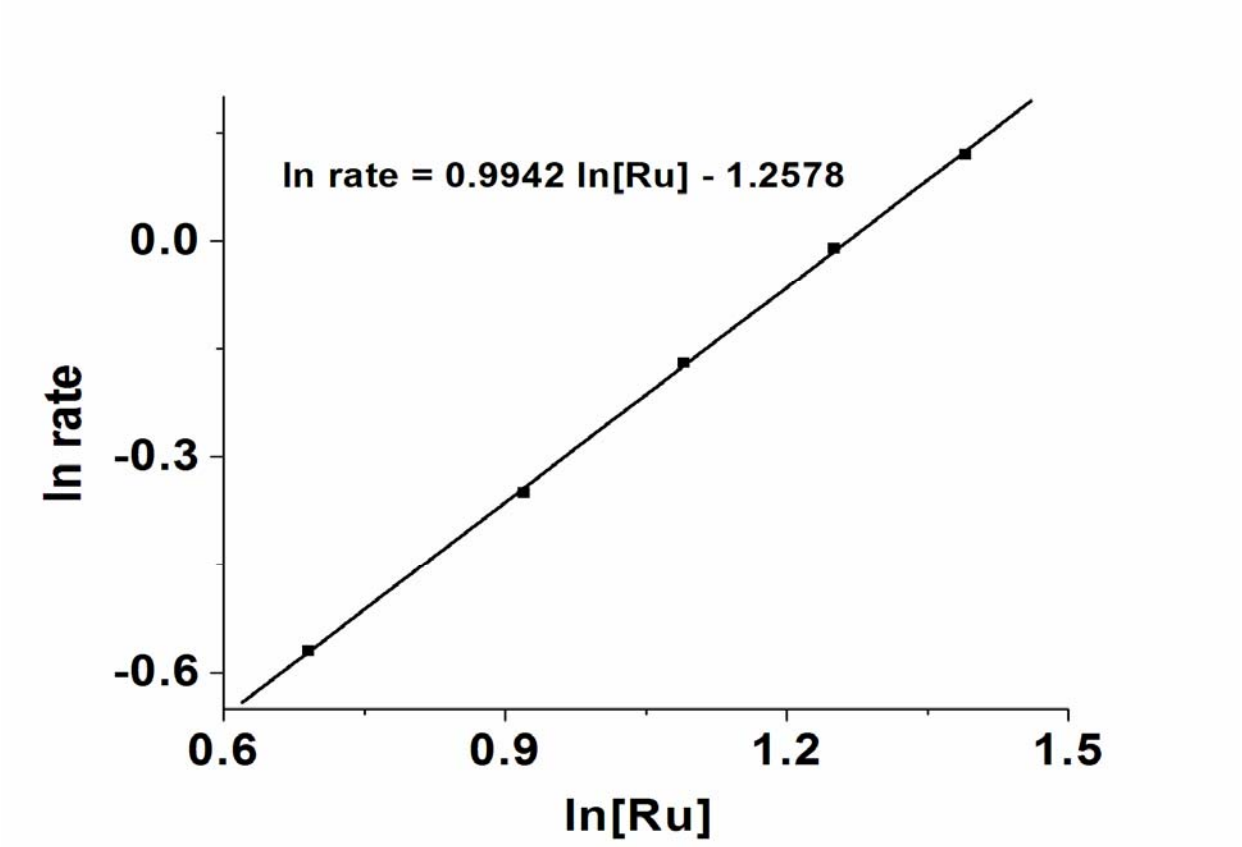

Figure 3.19. The graph of ln (rate) versus ln [Ru] for the hydrolysis of sodium borohydride catalyzed by different concentrations of $Ru(acac)_3$ and 2 equivalents of $P(OPh)_3$ per ruthenium at 25°C.

In the second set of experiments, $NaBH_4$ concentration was varied in the hydrolysis of $NaBH_4$ catalyzed by a constant concentration of $Ru(acac)_3$ and 2 equivalents of $P(OPh)_3$ per ruthenium at 25°C. Figure 3.20 shows hydrogen volume versus time plots during the hydrolysis of $NaBH_4$ with different concentrations (in the range of 300-1500 mM) catalyzed by a constant concentration of $Ru(acac)_3$ (2 mM) and 2 equivalents of $P(OPh)_3$ per ruthenium at 25ºC. By increasing the concentration of sodium borohydride, the induction time decreases and formation of active catalyst is getting faster.

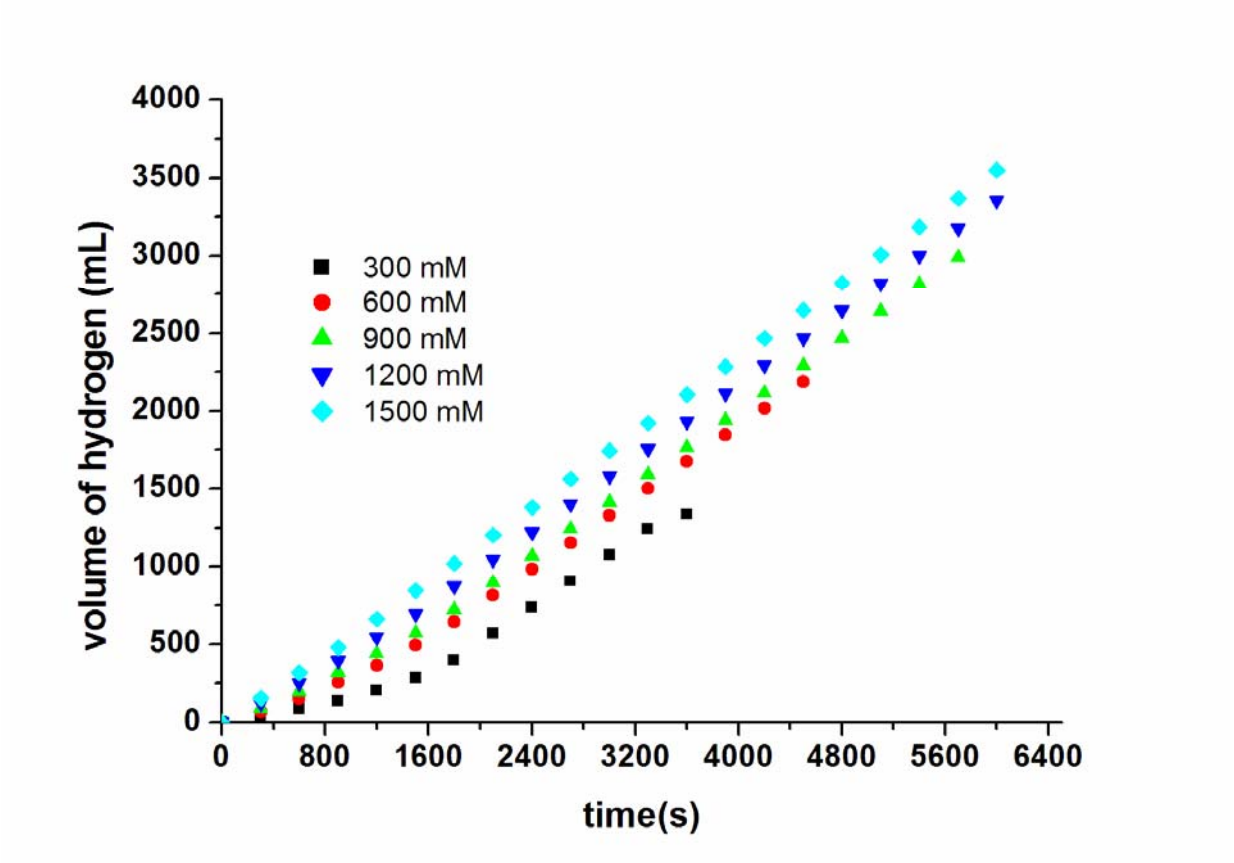

Figure 3.20. The volume of H_2 versus time plot during the hydrolysis of sodium borohydride solution catalyzed by 2 mM $Ru(acac)_3$ and 2 equivalents of $P(OPh)_3$ in different sodium borohydride concentrations at 25°C.

In the range of 0.30-1.5 M $NaBH_4$, the hydrogen evolution rate was found to be almost independent of the sodium borohydride concentration. Figure 3.21 shows the plot of hydrogen generation rate versus $NaBH_4$ concentrations, both in logarithmic scale. Based on Figure 3.21, a straight line with a slope of about zero is acquired showing that hydrolysis of sodium borohydride is zero order with regard to sodium borohydride concentration or in other words, the rate of hydrogen generation shows no dependency on the concentration of $NaBH_4$.

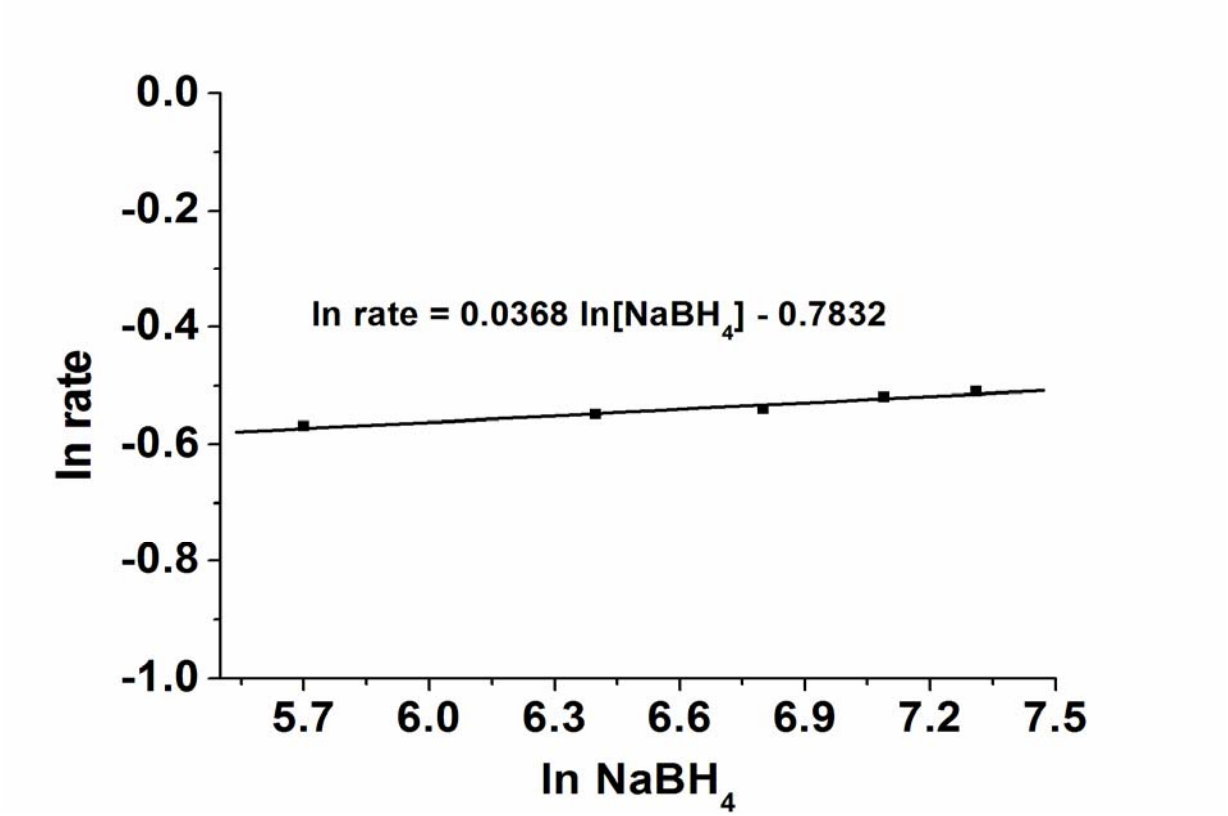

Figure 3.21. The graph of ln (rate) versus ln [$NaBH_4$] for the hydrolysis of sodium borohydride with different concentrations (in the range of 300-1500 mM) catalyzed by a constant concentration of $Ru(acac)_3$ (2 mM) and 2 equivalents of $P(OPh)_3$ at 25.0°C.

Thus the rate law for the hydrolysis of sodium borohydride catalyzed by $Ru(acac)_3$ and 2 equivalents of $P(OPh)_3$ per ruthenium is given as :

$$- 4d\,[NaBH_4]/dt = d[H_2]/dt = k\,[Ru] \qquad (3.7)$$

3.8.2. Activation parameters for the hydrolysis of $NaBH_4$ catalyzed by $Ru(acac)_3$ plus 2 equivalents of $P(OPh)_3$

In order to find the activation parameters, the hydrolysis of sodium borohydride was performed at five different temperatures, 20, 25, 30, 35 and 40°C in the presence of $Ru(acac)_3$ (2 mM) and 2 equivalents of $P(OPh)_3$. Figure 3.22 shows

volume of hydrogen versus time plots during the hydrolysis of $NaBH_4$ (450 mM) catalyzed by 2 mM $Ru(acac)_3$ and 2 equivalents of $P(OPh)_3$ per ruthenium at various temperatures.

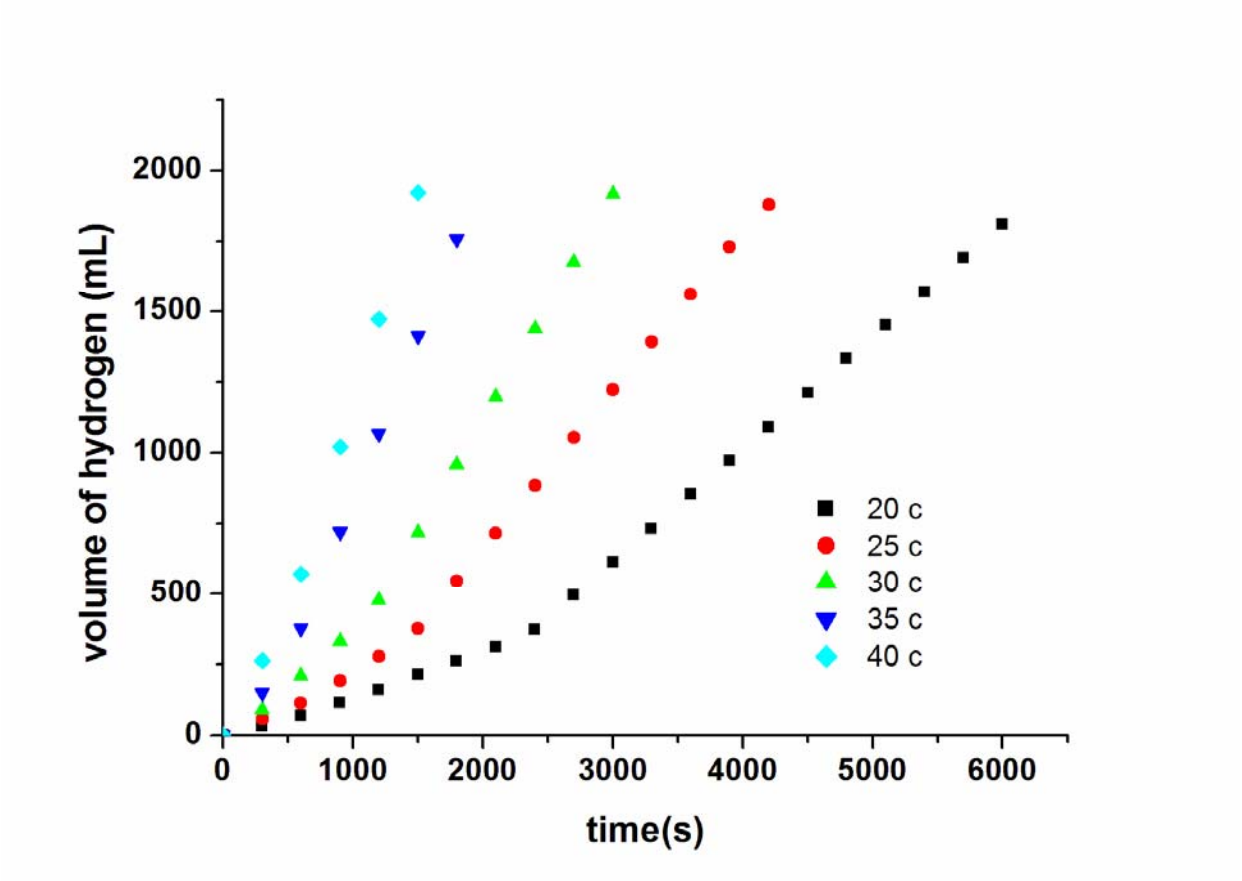

Figure 3.22. Plot of hydrogen volume generated versus time for the hydrolysis of sodium borohydride (450 mM) catalyzed by 2 mM $Ru(acac)_3$ and 2 equivalents of $P(OPh)_3$ per ruthenium at various temperatures.

Based on Figure 3.22, by increasing the temperature, the induction time becomes shorter or formation of active catalyst is getting faster. Moreover, at high temperatures, the activity during induction time and rate of hydrogen generation after induction time are getting increased. Rate constant values for the hydrogen generation obtained from the linear part of the plots in Figure 3.22, are listed in Table 3.2.

Table 3.2. Rate constant valuse for the hydrolysis of sodium borohydride (450 mM) catalyzed by 2 mM $Ru(acac)_3$ and 2 equivalents of $P(OPh)_3$ per ruthenium at various temperatures.

Temperature (°C)	**Rate Constant, *k*** **(mmol H_2). (mmol Ru)$^{-1}$. s^{-1}**
20	0.162 ± 0.0032
25	0.228 ± 0.0046
30	0.324 ± 0.0065
35	0.467 ± 0.0093
40	0.610 ± 0.0122

Rate constant valuses for the hydrogen generation were used to obtain the activation parameters by considering either Arrhenius (Equations 3.3 and 3.4) or Eyring (Equation 3.5) plots.

The activation energy was determined by using of Arrhenius Equation. According to Figure 3.23, a straight line with a slope of [-Ea/R] is obtained by the plot of ln k versus 1/T.

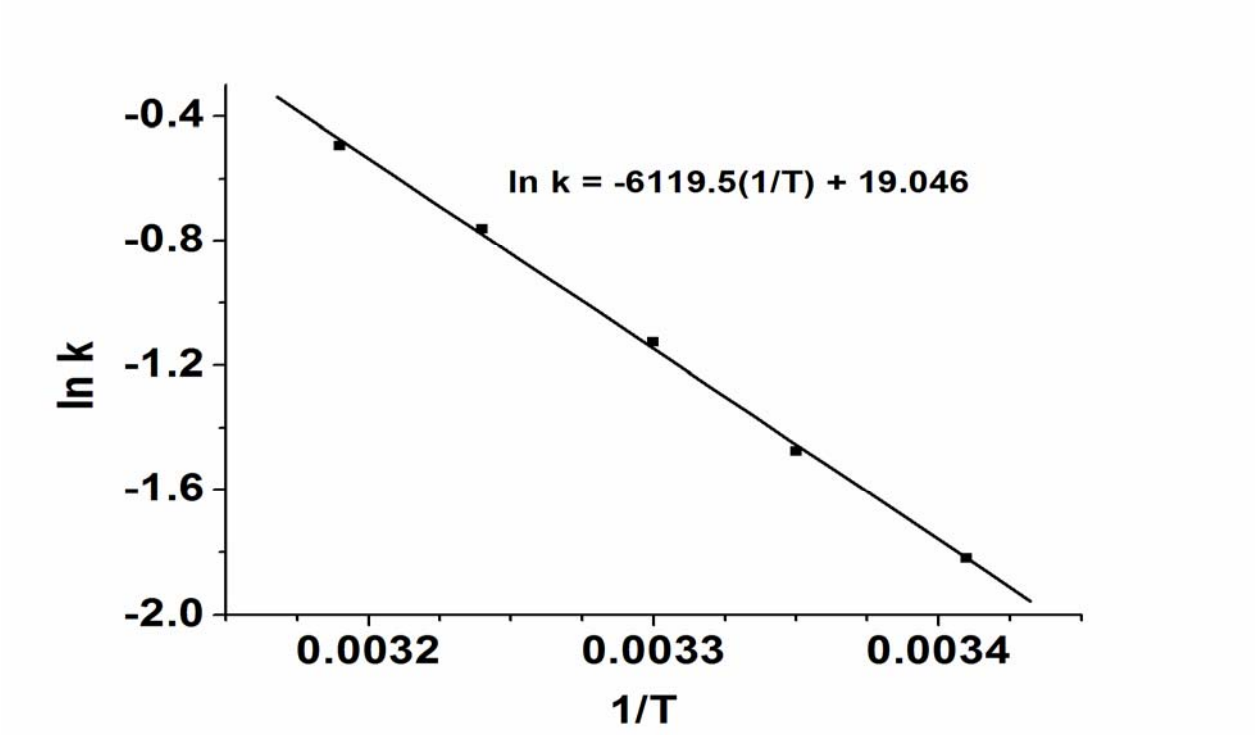

Figure 3.23. Arrhenius plot for the hydrolysis of sodium borohydride (450 mM) catalyzed by 2 mM $Ru(acac)_3$ and 2 equivalents of $P(OPh)_3$ per ruthenium at various temperatures.

The activation energy, Ea, for the hydrolysis of sodium borohydride catalyzed by $Ru(acac)_3$ and 2 equivalents of $P(OPh)_3$ is 52 ± 2 kJ/mol which was calculated by using the slope of Arrhenius plot.

The enthalpy of activation, $\Delta H^{\#}$ and the enthropy of activation, $\Delta S^{\#}$ were calculated by using of Eyring Equation (Equation 3.5). According to Figure 3.24, a straight line with a slope of $[\Delta H^{\#}/R]$ and an intercept of $[\ln k_b/h + \Delta S^{\#}/R]$ is obtained by the plot of ln k/T versus 1/T.

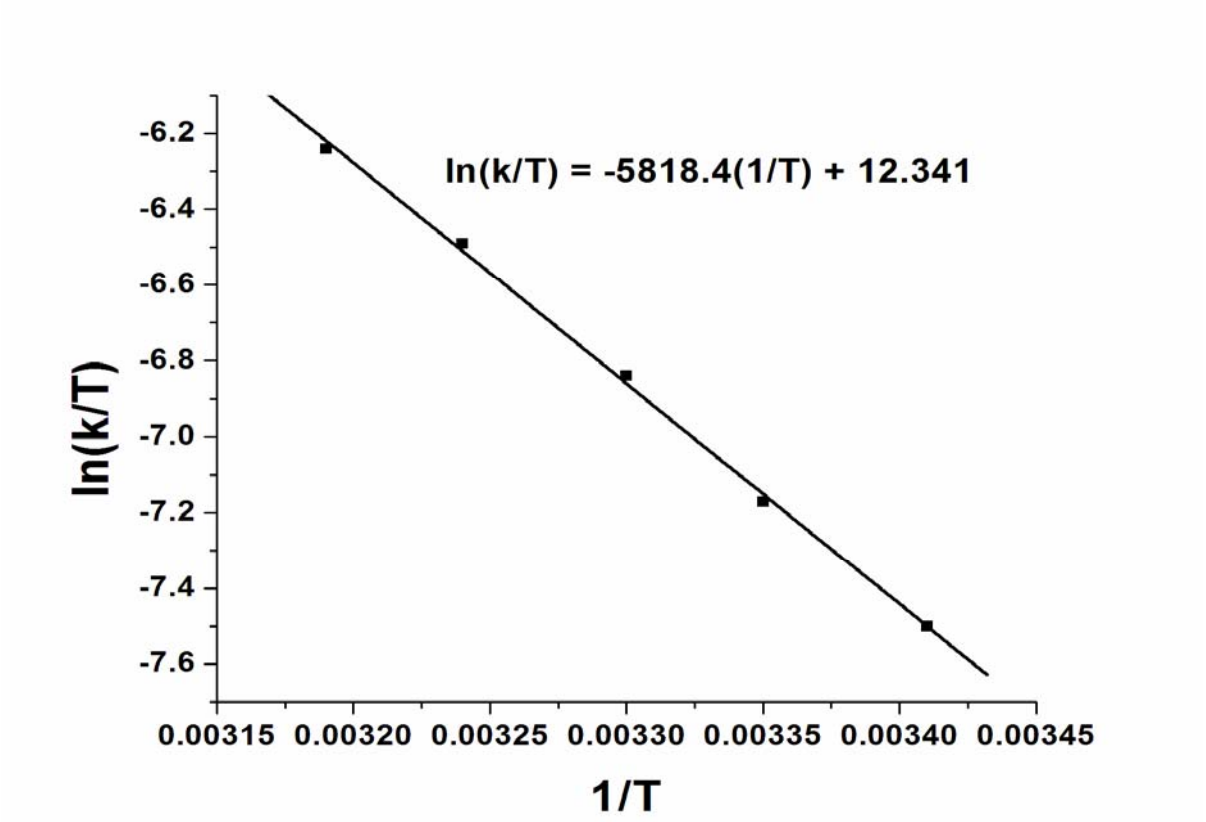

Figure 3.24. Eyring plot for the hydrolysis of sodium borohydride (450 mM) catalyzed by 2 mM $Ru(acac)_3$ and 2 equivalents of $P(OPh)_3$ per ruthenium at various temperatures.

The enthalpy of activation, $\Delta H^{\#}$, for the hydrolysis of sodium borohydride catalyzed by $Ru(acac)_3$ and 2 equivalents of $P(OPh)_3$ is 48 ± 2 kJ/mol which was calculated by using the slope of Eyring plot while the enthropy of activation obtained by using the intercept of Eyring plot was calculated as -95 ± 5 J/mol.K.

3.9. The catalytic life time of ruthenium(III) acetylacetonate and 2 equivalents of $P(OPh)_3$ per ruthenium

Lifetime of the catalyst involving $Ru(acac)_3$ and 2 equivalents of $P(OPh)_3$ was measured by determining the total turnover number (TTON) in hydrogen generation from the hydrolysis of sodium borohydride. The system containing

$Ru(acac)_3$ and 2 equivalents of $P(OPh)_3$ per ruthenium is nearly stable and long-live catalyst in the hydrolysis of sodium borohydride. The TTON value for the catalyst containing $Ru(acac)_3$ and $P(OPh)_3$ is 2850 over 17 hours and the highest value of turnover frequency is 17.8 (mol H_2).(mol Ru)$^{-1}$.(min)$^{-1}$. Figure 3.25 shows the plot of total turnover number versus time for hydrogen generation from the catalytic hydrolysis of sodium borohydride starting with 2 mM $Ru(acac)_3$, 2 equivalents of $P(OPh)_3$ per ruthenium and 450 mM $NaBH_4$ at 25.0 °C.

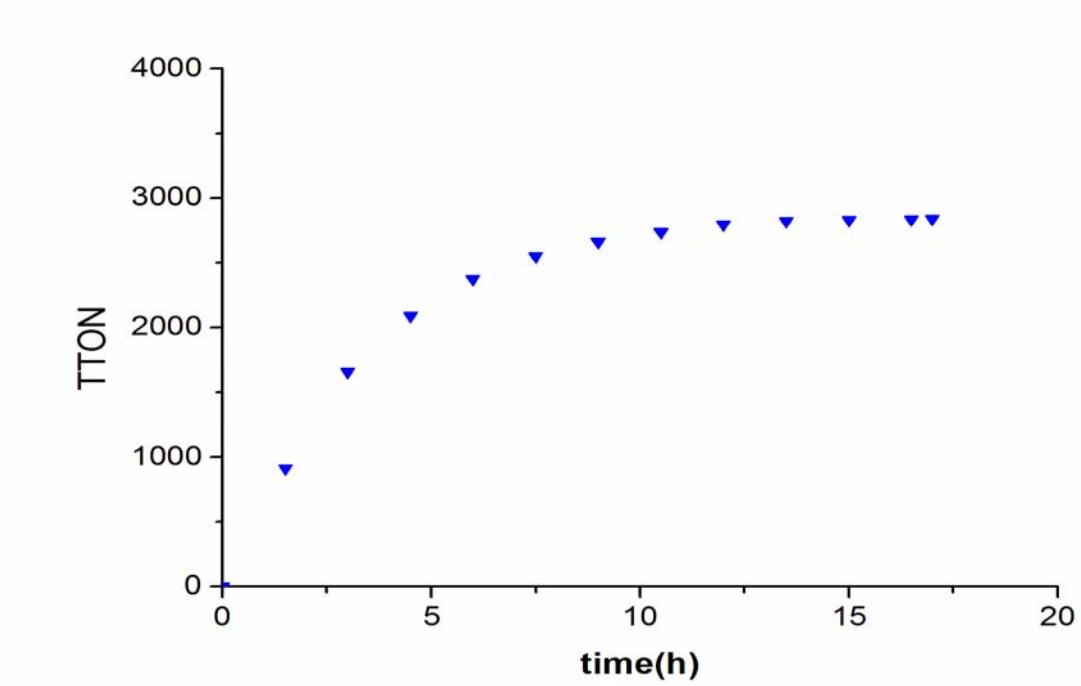

3.25. Plot of total turnover number versus time for hydrogen generation from the catalytic hydrolysis of sodium borohydride starting with 2 mM $Ru(acac)_3$, 2 equivalents of $P(OPh)_3$ per ruthenium and 450 mM $NaBH_4$ in 50 mL H_2O-THF solution at 25.0°C.

3.10. Activation parameters for the hydrolysis of $NaBH_4$ catalyzed by $Ru(acac)_3$ in the presence of different phosphorus compounds

In addition to $P(OMe)_3$ and $P(OPh)_3$ compounds, catalytic activity of $Ru(acac)_3$ in hydrogen generation from the hydrolysis of sodium borohydride in the presence of triphenylphosphine (PPh_3) and 1,2-bis(diphenylphosphino)ethane (dppe) has been

investigated [52,53]. Table 3.3 lists the overall results containing the rate constant values k in (mmol H_2). (mmol Ru)$^{-1}$. s^{-1} at verious temperatures, Arrhenius activation energy Ea in kJ.mol^{-1}, activation enthalpy $\Delta H^{\#}$ in kJ.mol^{-1}, and activation entropy $\Delta S^{\#}$ in J.mol^{-1}.K^{-1} for the hydrolysis of sodium borohydride catalyzed by $Ru(acac)_3$ plus 2 equivalents of phosphine per ruthenium starting with 450 mM $NaBH_4$ and 2 mM $Ru(acac)_3$ in 50 mL H_2O-THF solution for all of the four phosphorus compounds.

Table 3.3. The rate constant values k in (mmol H_2). (mmol Ru)$^{-1}$. s^{-1} at various temperatures and the activation parameters (Ea in kJ.mol^{-1}, A, $\Delta H^{\#}$ in kJ.mol^{-1}, and $\Delta S^{\#}$ in J.mol^{-1}.K^{-1}) for the hydrolysis of sodium borohydride catalyzed by $Ru(acac)_3$ plus 2 equivalents of phosphine per ruthenium starting with a solution of 450 mM $NaBH_4$ and 2 mM $Ru(acac)_3$**.**

	T (°K)	**$P(OMe)_3$**	**$P(OPh)_3$**	**PPh_3**	**dppe**
k	293	0.329 ± 0.0066	0.162 ± 0.0032	0.214 ± 0.0032	0.326 ± 0.0007
	298	0.468 ± 0.0130	0.228 ± 0.0046	0.309 ± 0.0049	0.502 ± 0.008
	303	0.918 ± 0.0183	0.324 ± 0.0065	0.421 ± 0.0064	0.722 ± 0.011
	308	1.25 ± 0.025	0.467 ± 0.0093	0.521 ± 0.0170	1.28 ± 0.044
	313	1.60 ± 0.032	0.610 ± 0.0122	0.742 ± 0.0280	1.604 ± 0.062
Ea		58 ± 2	52 ± 2	46 ± 2	59 ± 2
A		7.49×10^9	1.87×10^8	3.43×10^7	2.48×10^{10}
$\Delta H^{\#}$		56 ± 2	48 ± 2	43 ± 1	60 ± 2
$\Delta S^{\#}$		-64 ± 4	-95 ± 5	-109 ± 6	-50 ± 3

According to Table 3.3, both the activation energy (58 ± 2 kJ.mol^{-1}) and the enthalpy of activation (56 ± 2 kJ.mol^{-1}) for the active catalyst containing trimethylphosphite are very similar to the values reported for the sole $Ru(acac)_3$ (58.2 and 55.7 kJ·mol^{-1}), respectively. In comparison to the values of ruthenium(III) acetylacetonate [50], the ruthenium catalysts with triphenylphosphite or triphenylphosphine compounds have lower activation energy and enthalpy values, while the catalyst containing dppe compound has slightly higher values for both

activation energy and enthalpy. Additional stability of ruthenium catalyst containing dppe in ground state arisen from chelate effect lead to higher activation energy and enthalpy for the ruthenium-dppe catalyst [104]. It is noteworthy that the activation entropy has large negative value for all of the phosphorus compounds, showing an associative nature in the transition state for the catalytic hydrolysis of sodium borohydride [105,106]. In particular, the largest negative value observed for dppe might be due to the chelate effect leading to a decrease in the disorder in transition state [107].

3.11. The catalytic life time of ruthenium(III) acetylacetonate in the presence of different phosphorus compounds

In addition to $P(OMe)_3$ and $P(OPh)_3$ compounds, lifetime of the catalysts involving $Ru(acac)_3$ plus 2 equivalents of PPh_3 or 1 equivalent of dppe were measured by determining the total turnover number (TTON) in hydrogen generation from the hydrolysis of sodium borohydride [52,53]. The overall results related to lifetime of $Ru(acac)_3$ in the presence of different phosphorus compounds in hydrogen generation from the hydrolysis of sodium borohydride are shown in Figure 3.26. Based on Figure 3.26, the systems containing $Ru(acac)_3$ in the presence of different phosphorus compounds are stable and long-lived catalysts in the hydrolysis of sodium borohydride starting with 2 mM $Ru(acac)_3$, 2 equivalents of phosphines per ruthenium and 450 mM $NaBH_4$ in 50 mL H_2O-THF solution at 25.0 °C. The total turnover number (TTON) values for the ruthenium catalyst containing $P(OMe)_3$, $P(OPh)_3$, PPh_3, or dppe are 20700 (over 72 hours), 2850 (over 17 hours), 6080 (over 12 hours), and 12250 (over 28 hours), respectively, at 25.0°C. The highest values of turnover frequency (TOF) for the ruthenium catalyst containing $P(OMe)_3$, $P(OPh)_3$, PPh_3, or dppe are 38.4, 17.8, 13.2 and 16.4 $(mol\ H_2)\cdot(mol\ Ru)^{-1}\cdot(min)^{-1}$, respectively, at 25.0°C. In comparison with total turnover number (TTON) value of 1200 for the ruthenium(III) acetylacetonate alone [50], all the phosphorus compounds show noticable improvements for the lifetime of ruthenium catalyst. Especially, the catalyst system involving $Ru(acac)_3$ plus 2 equivalents of $P(OMe)_3$ provides the highest total turnover number (TTON) and turnover frequency (TOF) values. The

stability of ruthenium-dppe complex due to the chelate effect lead to higher values of TTON and TOF for the ruthenium catalyst with dppe in comparison with those of ruthenium catalyst containing triphenylphosphine compound [108].

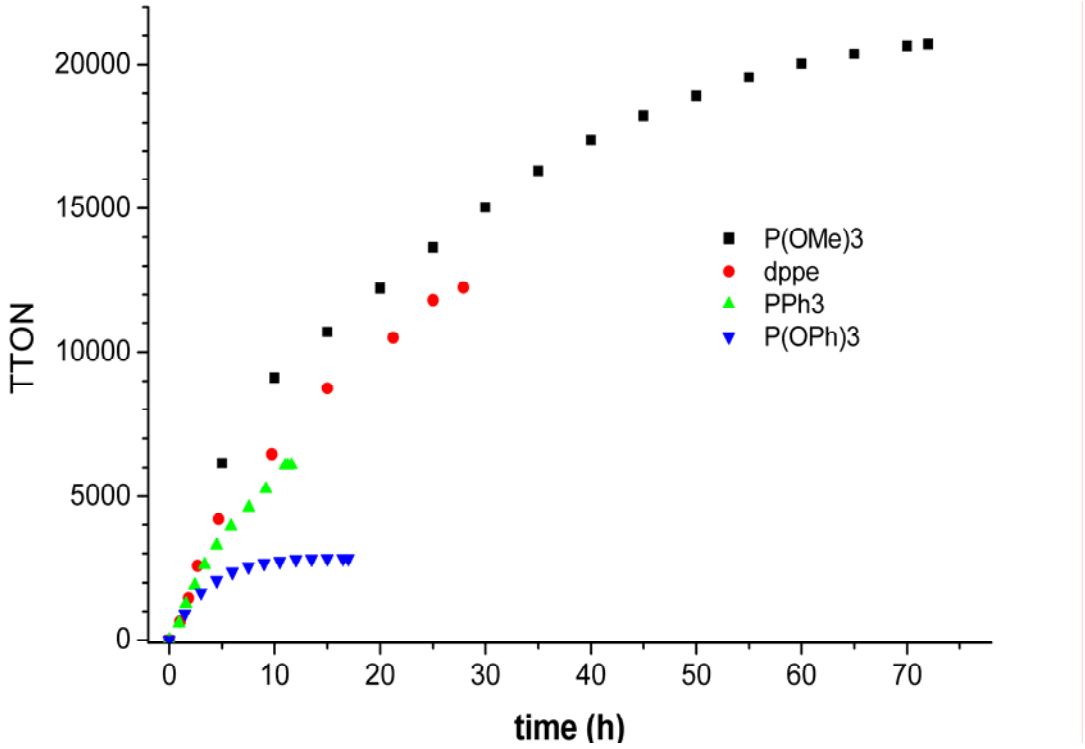

Figure 3.26. Plots of total turnover number versus time for hydrogen generation from the catalytic hydrolysis of sodium borohydride starting with 2 mM $Ru(acac)_3$, 2 equivalents of phosphine per ruthenium and 450 mM $NaBH_4$ in 50 mL H_2O-THF solution at 25.0 °C for all of the phosphines.

3.12. Synthesis of trans- and cis-$[Ru(acac)_2\{P(OMe)_3\}_2]$ complexes

As we discussed at the beginning of this chapter, when two equivalents of $P(OMe)_3$ per ruthenium is added to the reaction solution containing 450 mM $NaBH_4$ and 2 mM $Ru(acac)_3$ in 50 mL H_2O-THF solution, the hydrogen generation rate was practically stopped (or reduced to the level of self hydrolysis). However, the catalytic hydrolysis of sodium borohydride restarts at an unexpectedly high rate in a certain period of time (induction time) after addition of trimethylphosphite. Therefore,

phosphorus ligand, known to be a poison in the hydrolysis, is involved in the formation of a new ruthenium species containing trimethylphosphite which has higher catalytic activity in comparison with sole $Ru(acac)_3$. The rate of hydrolysis varies very slightly with the mole ratio of phosphorus to ruthenium or in other words, mechanism or structure of active catalyst formed during hydrolysis of sodium borohydride is independent of varying the mole ratio of $P(OMe)_3$ to $Ru(acac)_3$. However, the phosphine to ruthenium molar ratio of 2 shows usually high catalytic activity in hydrogen generation of sodium borohydride. This observation prompted us to synthesize ruthenium acetylacetonato complexes containing two trimethylphosphite ligands and test them as homogeneous catalysts in the hydrolysis of sodium borohydride.

For the preparation of ruthenium acetylacetonato complexes containing two trimethylphosphite ligands, at first $Ru(acac)_3$ is reduced by zinc amalgam in the presence of cyclooctene to form cis-$[Ru(acac)_2(\eta^2\text{-}C_8H_{14})_2]$. Then, the ready displacement of cyclooctene from cis-$[Ru(acac)_2(\eta^2\text{-}C_8H_{14})_2]$ by trimethylphosphite yields trans-$[Ru(acac)_2\{P(OMe)_3\}_2]$ which isomerizes on heating to its cis counterpart [95]. Both isomers of $[Ru(acac)_2\{P(OMe)_3\}_2]$ were isolated as single crystals and characterized by single crystal X-ray diffraction, UV-visible, Mass, ^1H, ^{13}C and ^{31}P NMR spectroscopy. Moreover, the isolated trans and cis isomers were tested as homogeneous catalysts in hydrogen generation of sodium borohydride.

The cyclooctene complex $[Ru(acac)_2(\eta^2\text{-}C_8H_{14})_2]$, which is easily accesible from $Ru(acac)_3$, provides a convenient entry into a wide range of trans- and cis-$[Ru(acac)_2L_2]$ complexes (L = Py, bipy, $CNBu^t$, NMe_3, PMe_3, $P(OMe)_3$, $P(OPh)_3$, PEt_3, PMe_2Ph or $SbPh_3$) [95]. Reduction of $Ru(acac)_3$ with zinc amalgam or zinc dust in hot THF containing some water in the presence of an excess of cyclooctene generates in solution cis-$[Ru(acac)_2(C_8H_{14})_2]$. The presence of a small amount of water is necessary for the formation of the cyclooctene complex, possibly because it increases the reducing power of the zinc by salvation of Zn^{2+}.

$$[Ru(acac)_3]^- + 2C_8H_{14} \longrightarrow [Ru(acac)_2(C_8H_{14})_2] + acac^- \qquad (1.2)$$

It has been reported that the alkene ligands of cis-[$Ru(acac)_2(\eta^2$-alkene$)_2$] [alkene = ethylene or cyclooctene) are easily displaced by ligands (L) such as tertiary phosphines, phosphites, pyridine or tert-butyl isocyanide, to yield trans-[$Ru(acac)_2L_2$] as the kinetic products, which then usually isomerize to the thermodynamically more stable cis-products on heating [95,109]. All of these complexes undergo reversible one-electron oxidations, without trans-cis interconversion; the resulting Ruthenium(III) cationic complexes can either be isolated or generated electrochemically and detected by UV-Vis and ESR spectroscopy [110,111,112]. The formation of trans-[$Ru(acac)_2L_2$] from cis-[$Ru(acac)_2(\eta^2$-$C_8H_{14})_2$] represents an unusual example of a well defined stereochemical course of ligand substitution at an octahedral metal center [113]. Detailed kinetic studies have not yet been carried out, but the isolation in two cases of monosubstitution products cis-[$Ru(acac)_2(\eta^2$-$C_8H_{14})L'$] (L′ = MeCN or $SbPh_3$) supports the idea that the olefins are replaced stepwise, most likely by a dissociative process. In the case of the group 15 donors, the second olefin must be replaced more rapidly than the first. The five coordinate intermediate [$Ru(acac)_2L$] generated at this step is assumed to be square pyramidal; preferential attack by the entering ligand L at the vacant site gives trans-[$Ru(acac)_2L_2$] (Scheme 3.1). The square pyramidal geometry for a five coordinate d^6-metal complex is expected on the basis of theoretical considerations [114,115] and is observed in complexes such as [$RuCl_2(PPh_3)_3$] [116]. At higher temperatures a trigonal bipyramidal geometry for [$Ru(acac)_2L$] may become accessible, hence reversible dissociation of L from trans-[$Ru(acac)_2L_2$] gives finally the cis isomer.

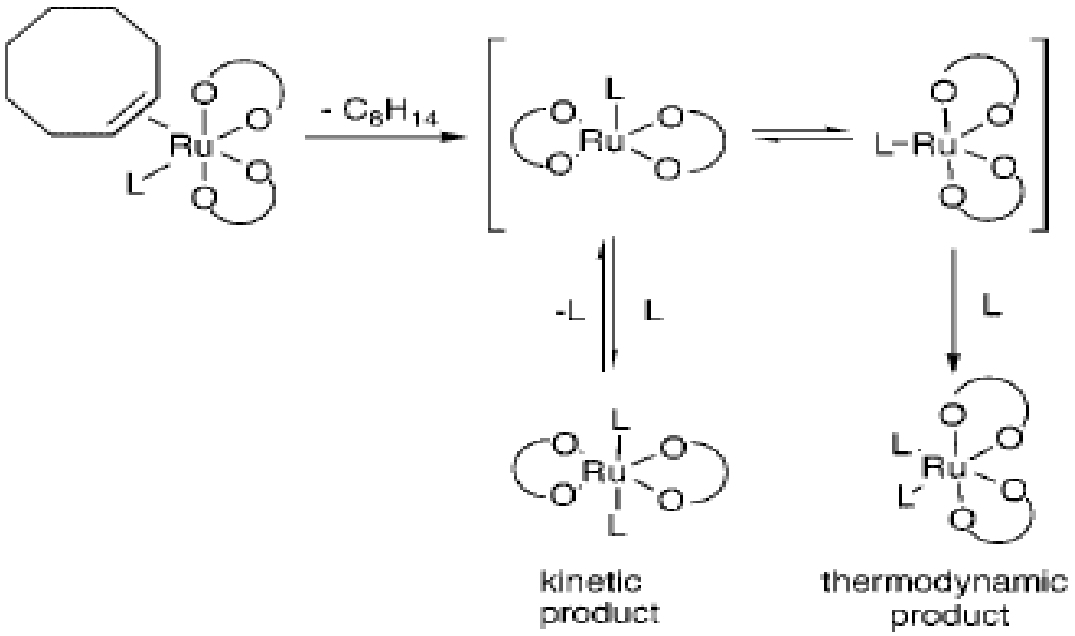

Scheme 3.1. Suggested pathway for fomation of trans- and cis-$[Ru(acac)_2L_2]$ from cis-$[Ru(acac)_2(\eta^2\text{-}C_8H_{14})L]$.

This trans to cis isomerisation of $[Ru(acac)_2L_2]$ occurs most readily for L = PPh_3, $PMePh_2$, $P(OPh)_3$, $P(OMe)_3$ and $AsPh_3$, presumably reflecting in part the trans-bond weakening influences of these ligands [117,118]. The greater thermodynamic stability of the cis isomers reflects the tendency of even the most weakly π-acceptor ligands to avoid competition for the same d orbital on ruthenium (II) species.

3.12.1. Characterization of trans- and cis-$[Ru(acac)_2\{P(OMe)_3\}_2]$ complexes by UV-visible, Mass, ^1H, ^{13}C and ^{31}P NMR spectroscopy

Trans- and cis- bis(acetylacetonato)bis(trimethylphosphite)ruthenium(II), $[Ru(acac)_2\{P(OMe)_3\}_2]$, complexes are readily identified by their ^1H, ^{13}C and ^{31}P NMR spectra. Based on Figure 3.27 trans isomer show just one acac methyl singlet [δ (^1H) 1.95] while the cis isomer shows two [δ (^1H) 1.62, 1.82] (Figure 3.28). The spectra of both trans and cis isomers show only one acac γ-CH resonance in the region of [δ (^1H) 5.38] for the trans isomer and [δ (^1H) 5.21] for the cis isomer. Peaks

in the region of [δ (^{1}H) 3.72] and [δ (^{1}H) 3.52] for the trans and cis isomers, are attributed to the methyl groups of trimethylphosphite which are more unshielded (close to electronegative oxygen atoms) in comparison with methyl groups of acac.

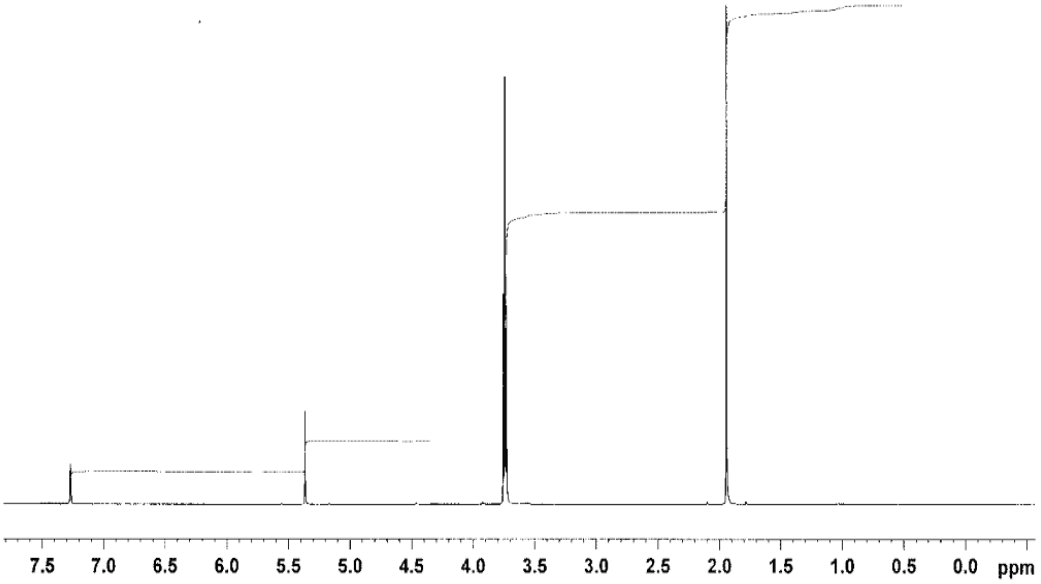

Figure 3.27. ^{1}H NMR of trans-[Ru(acac)$_2${P(OMe)$_3$}$_2$] complex taken in C_6D_6

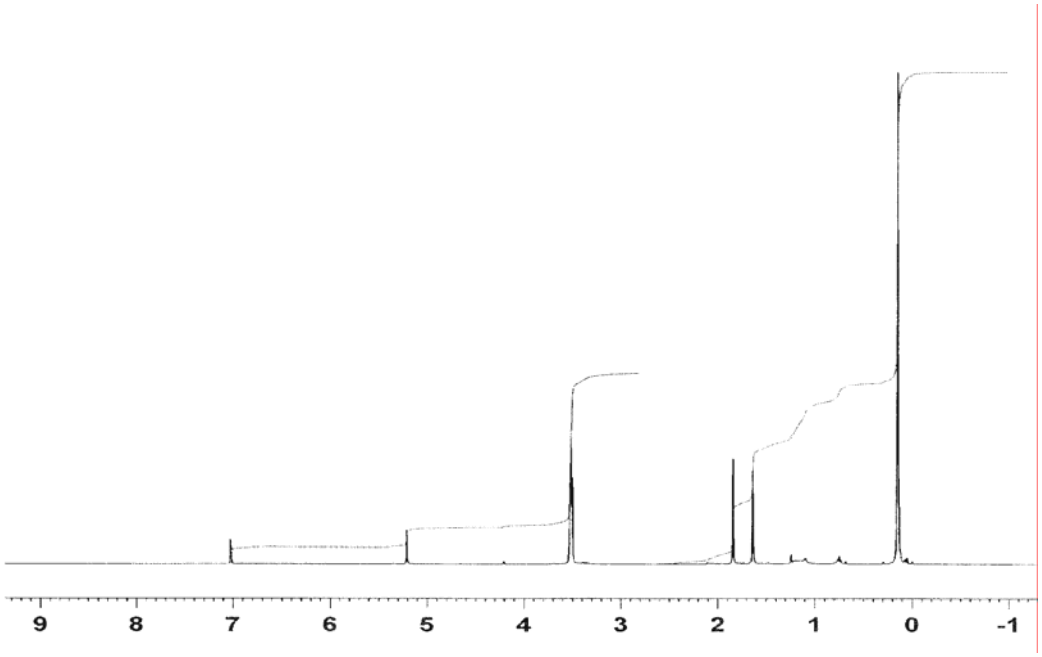

Figure 3.28. ^{1}H NMR of cis-[Ru(acac)$_2${P(OMe)$_3$}$_2$] complex taken in C_6D_6

Based of Figures 3.29 and 3.30 and similar to ^{1}H NMR of trans- and cis-$[Ru(acac)_2\{P(OMe)_3\}_2]$, ^{13}C NMR of trans isomer show just one acac methyl singlet [δ (^{13}C) 27.01] while the cis isomer shows two [δ(^{13}C) 27.52, 27.86]. In addition, the trans isomer show just one C=O resonance in its ^{13}C NMR spectrum in the region of δ 186.08, while the cis isomer shows two at 185.73 and 186.51. The spectra of both trans and cis isomers show only one acac γ-CH resonance in the region of [δ (^{13}C) 99.64] for the trans isomer and [δ (^{13}C) 99.12] for the cis isomer. Peaks in the region of [δ (^{13}C) 50.29] and [δ (^{13}C) 51.02] for the trans and cis isomers, are attributed to the methyl groups of trimethylphosphite which are more unshielded (close to electronegative oxygen atoms) in comparison with methyl groups of acac.

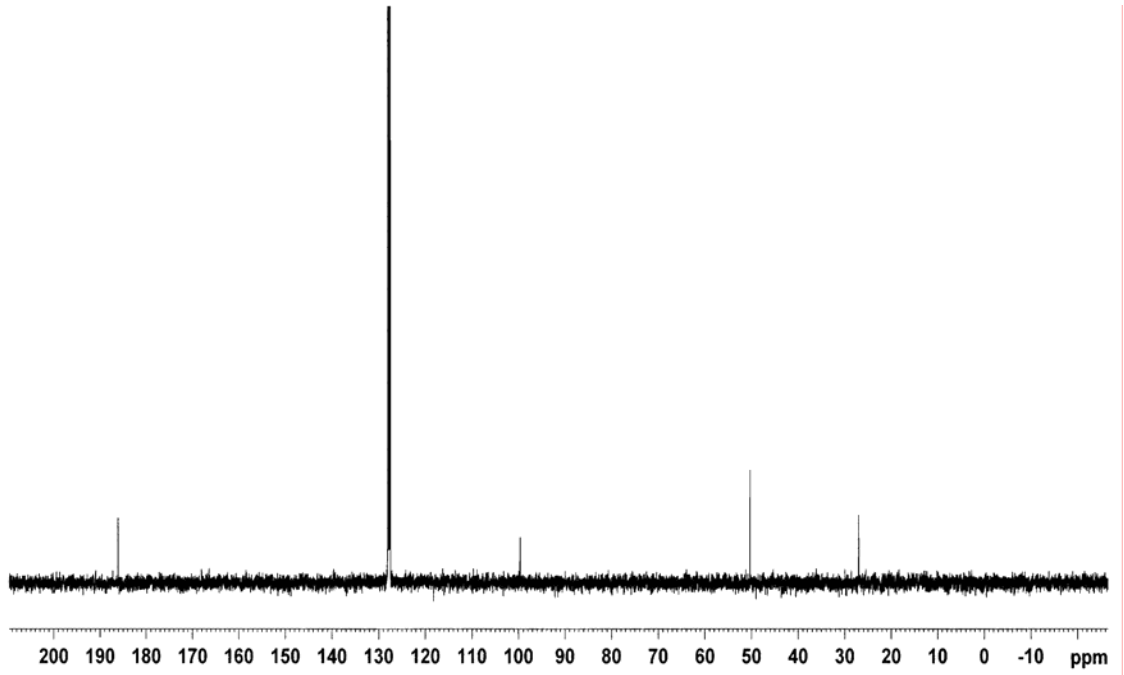

Figure 3.29. ^{13}C NMR of trans-$[Ru(acac)_2\{P(OMe)_3\}_2]$ complex taken in C_6D_6

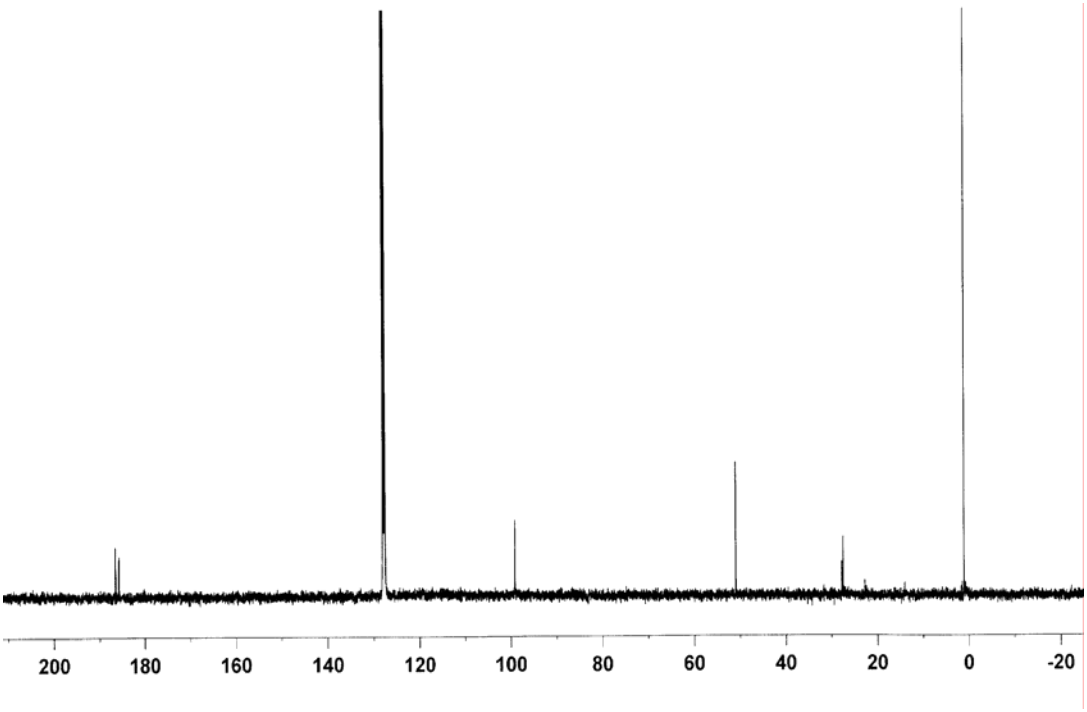

Figure 3.30. ^{13}C NMR of cis-$[Ru(acac)_2\{P(OMe)_3\}_2]$ complex taken in C_6D_6

Based on Figure 3.31, ^{31}P NMR spectrum of the trans isomer shows one singlet at 138 ppm which is about 16 ppm more shielded than that of the corresponding cis isomer (Figure 3.32). In the case of trans isomer, two trimethylphosphite ligands at the trans position, intract with the same d orbital of ruthenium which lead to a π-competition and for that reason, ruthenium-phosphorus bond in the trans isomer is getting weaker and electron density around phosphorus atoms of both trimethylphosphite ligands becomes higher. On the contrary of trans isomer, there is no π-competition in the cis isomer which results in a stronger ruthenium-phosphorus bond and a lower electron density around phosphorus atoms. That is why ^{31}P NMR of the cis isomer shows a peak at 154 ppm which is 16 ppm more unshielded than that of the corresponding trans isomer.

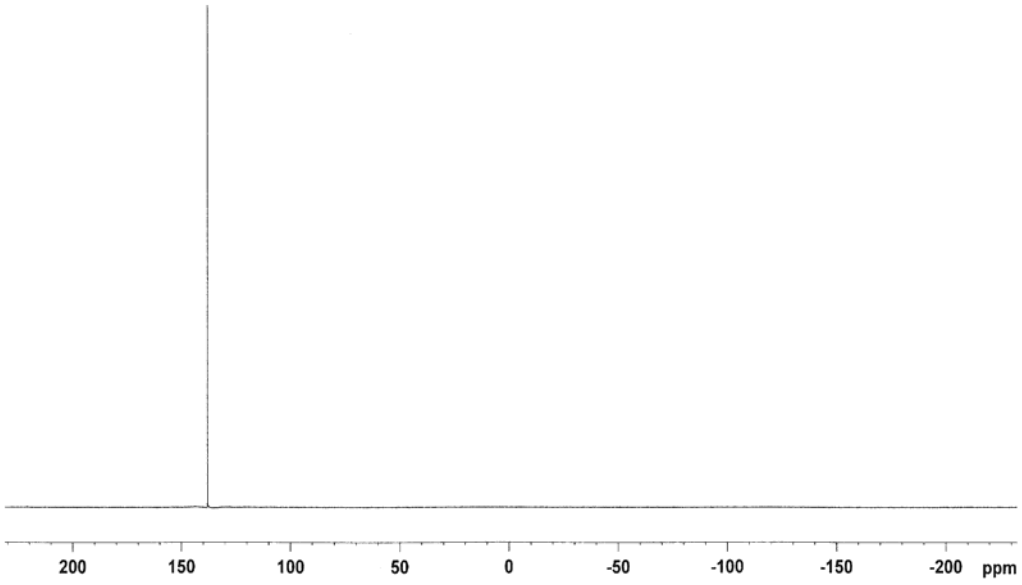

Figure 3.31. ^{31}P NMR of trans-[Ru(acac)$_2${P(OMe)$_3$}$_2$] complex taken in C_6D_6

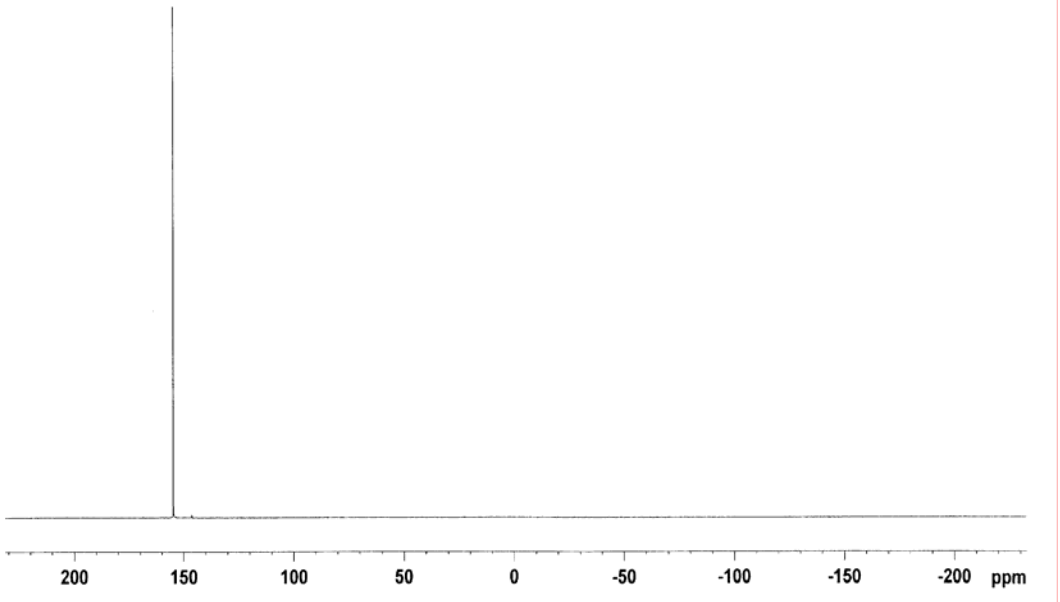

Figure 3.32. ^{31}P NMR of cis-[Ru(acac)$_2${P(OMe)$_3$}$_2$] complex taken in C_6D_6

Based on Figure 3.33, the FAB-Mass spectra of both *trans*-$[Ru(acac)_2\{P(OMe)_3\}_2]$ and *cis*-$[Ru(acac)_2\{P(OMe)_3\}_2]$ complexes show M^+ molecular ion peak at m/z = 548 plus two intense peaks at m/z = 424 and m/z = 300 related to $[M - P(OMe)_3]^+$ and $[M - 2P(OMe)_3]^+$ fragments, respectively.

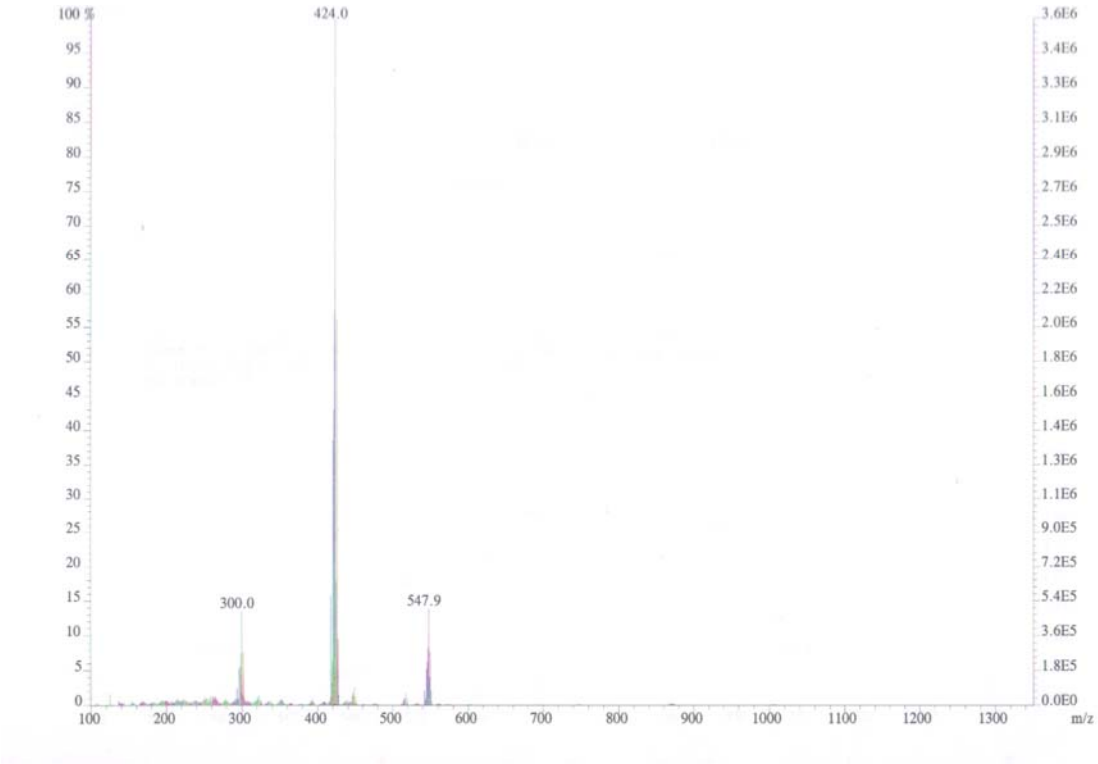

Figure 3.33. FAB-Mass spectrum of trans- or cis-$[Ru(acac)_2\{P(OMe)_3\}_2]$ complexes

According to Figure 3.34, UV-Vis spectrum of the trans-$[Ru(acac)_2\{P(OMe)_3\}_2]$ complex shows one broad band located at 510 nm along with two sharp absorption bands at 340 and 280 nm which are similar to those of $Ru(acac)_3$ [119]. In the case of cis -$[Ru(acac)_2\{P(OMe)_3\}_2]$ complex, UV-Vis spectrum (Figure 3.35) shows one broad absorption located at 530 nm plus two sharp bands at 280 and 240 nm.

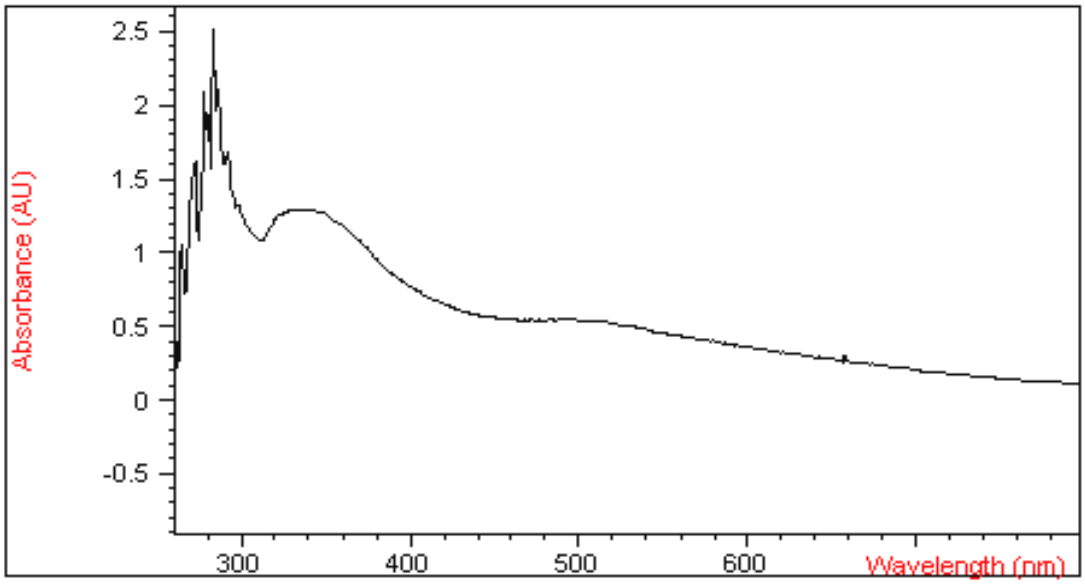

Figure 3.34. UV-Vis spectrum of trans-[Ru(acac)$_2${P(OMe)$_3$}$_2$] complex in THF

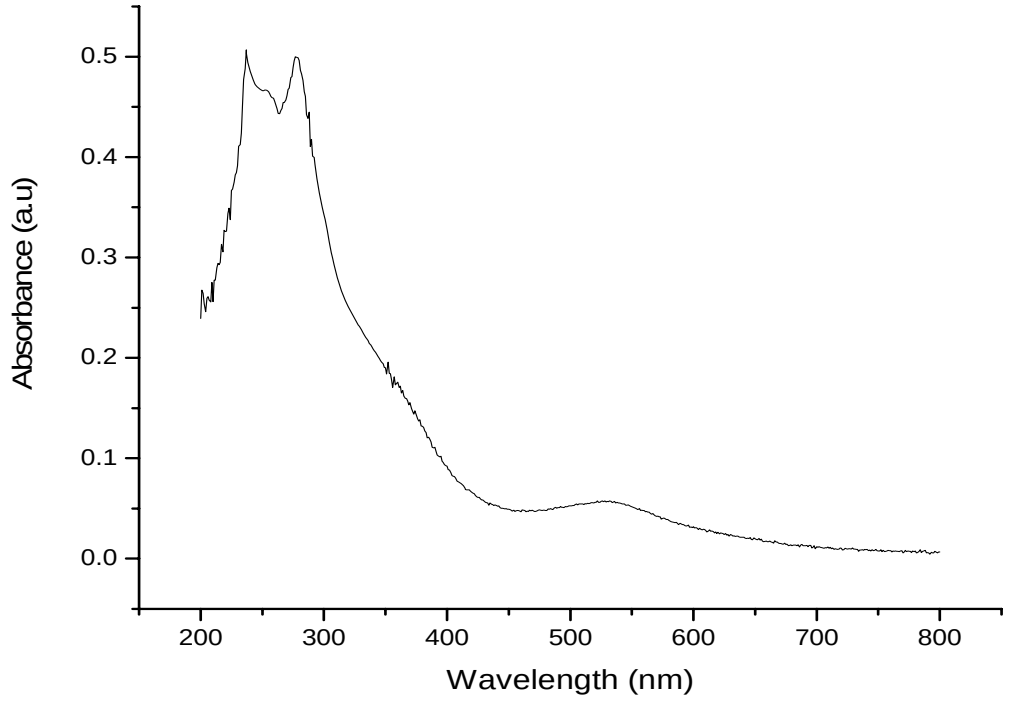

Figure 3.35. UV-Vis spectrum of cis-[Ru(acac)$_2${P(OMe)$_3$}$_2$] complex in THF

3.12.2. Crystal structure of trans- and cis-[Ru(acac)$_2${P(OMe)$_3$}$_2$]

The *trans*-[Ru(acac)$_2${P(OMe)$_3$}$_2$] complex was crystallized from hexane-dichloromethane solution. The *cis*-[Ru(acac)$_2${P(OMe)$_3$}$_2$] complex formed from the thermal conversion of the *trans*-isomer was crystallized from hexane solution. Single crystals of the compounds were used for the XRD structure determination. ORTEP drawing of the title compounds with the atomic numbering scheme displacement ellipsoids are drawn at the 30% probability level for *trans*- and *cis*-[Ru(acac)$_2${P(OMe)$_3$}$_2$] in Figure 3.36 and 3.37, respectively. Crystal data and results of structure refinement for *trans*- and *cis*-[Ru(acac)$_2${P(OMe)$_3$}$_2$] are summarized in Table 3.4. Both complexes crystallize in the triclinic $P\bar{1}$ space group. The *trans*-complex contains two half molecule in asymmetric unit without symmetry related and two formula units of $C_{16}H_{32}O_{10}P_2Ru$ in the unit cell. The *cis*-complex contains two molecules in asymmetric unit without symmetry related as well and four formula units of $C_{16}H_{32}O_{10}P_2Ru$ in the cell.

In both complexes, the coordination geometry around the Ru(II) ion is a slightly distorted octahedron involving four O atoms of two acac ligands and two P atoms of trimethylphosphites. Coordination environment of ruthenium(II) ion of the *trans*-[Ru(acac)$_2${P(OMe)$_3$}$_2$] structure involves four O atoms of two symmetry related acac ligands in the basal plane with the average Ru-O coordination bond length of 2.066 Å. The axial positions are occupied by the P atoms of two symmetry related trimethylphosphites with the Ru-P bond range of 2.3089(15) - 2.3175(14) and the average $P1\cdots P1^{i}$ (i: -x, -y, -z) distance of 4.6264 Å for two asymmetric units. The bond angles within the coordination sphere are close to the ideal value of 90° as shown in Figure 3.38 (a).

Coordination environment of ruthenium(II) ion of the *cis*-[Ru(acac)$_2${P(OMe)$_3$}$_2$] structure can be defined with two different basal plane each involving two O atoms from an acac ligand and one O atom of the other acac ligand and one P atom of a trimethylphosphite. Two basal planes of cis structure are almost

perpendicular to each other and dihedral angel between them is 86.08°. The axial positions are occupied by one O atom of the acac ligand with the chelate ring out of the basal plane and the P atom of other trimethylphosphites as shown in Figure 3.38 (b).

Table 3.4. Crystal data and results of structure refinement for trans- and cis-$[Ru(acac)_2\{P(OMe)_3\}_2]$ complexes

	trans	**cis**
Chemical Formula	**$C_{16}H_{32}O_{10}P_2Ru$**	**$C_{16}H_{32}O_{10}P_2Ru$**
F(000)	564	1128
M_r	547.43	547.43
D_x (Mg .m^{-3})	1.528	1.532
μ (mm^{-1})	7.018	0.841
Crystal system, space group	triclinic, $P\bar{1}$	triclinic, $P\bar{1}$
Radiation	CuK_α 1.54184 Å	MoK_α 0.71073 Å
Unit cell determination: Number of reflections used, theta range (°)	25, 19.13 - 42.50	15, 9.88 – 11.10
A (Å)	8.4916(10)	10.9781(16)
B (Å)	8.744(2)	12.709(2)
C (Å)	16.186(3)	17.896(2)
α (°)	97.897(15)	89.074(14)
β (°)	90.936(10)	73.279(10)
γ (°)	91.125(18)	83.039(13)
Cell volume (Å^3)	1190.0(4)	2373.2(6)
Z	2	4
Crystal shape, red	prism, red-brown	prism, light-red
Crystal size (mm)	0.40 x 0.10 x 0.10	0.40 x 0.35 x 0.15
Absorption correction (psi-scan)	T_{min} = 0.422, T_{max} = 0.493	T_{min} = 0.712, T_{max} = 0.844
θ-range for data collection [º]	2.76 to 74.21	2.89 to 26.29
Dataset	-10≤h≤10, -10≤k≤0, -20≤k≤20	-13≤h≤13, 0≤k≤15, -22≤k≤22
Reflections collected / Unique	4640 / 4365 (R_{int} = 0.0376)	10063 / 9612 (R_{int} = 0.0196)
Unique reflections [I>2σ(I)]	3428	6182
No. of data / parameters / restraints	4365 / 270 / 0	9612 / 543 / 0
R [I>2σ(I)]	R_1 =0.0506, [a]wR_2 = 0.1259	R_1 =0.0482, [b]wR_2 = 0.1173
R (all data)	R_1 =0.0730, wR_2 = 0.1381	R_1 =0.0985, wR_2 = 0.1376
S	1.055	1.026
$(\Delta/\sigma)_{max}$	0.001	0.002
ρ_{max} and ρ_{min} [e/Å^3]	1.118 and -1.616	1.448 and -0.591
Extinction correction and coefficient	SHELXL, 0.0021(3)	None

[a]w=1/[σ^2(F_o^2)+(0.0788P)^2^+0.9482P] and [b]w=1/[σ^2(F_o^2)+(0.0659P)^2^+2.4157P] where $P = (F_o^2 + 2F_c^2)/3$

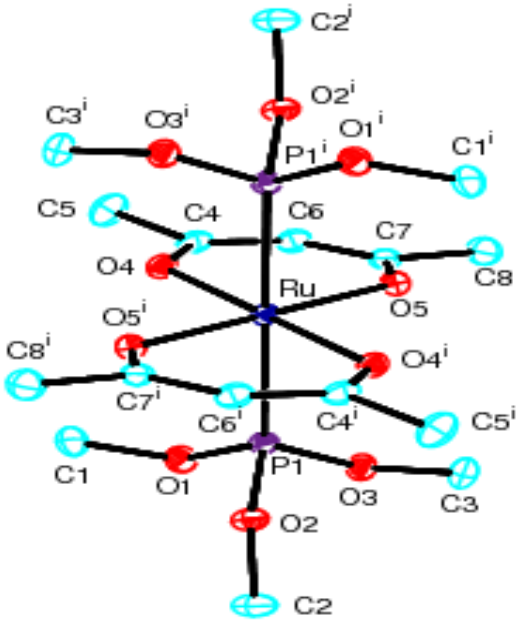

Figure 3.36. ORTEP drawing of the title compounds with the atomic numbering scheme Displacement ellipsoids are drawn at the 30% probability level for trans - $[Ru(acac)_2\{P(OMe)_3\}_2]$, where (i: -x, -y, -z).

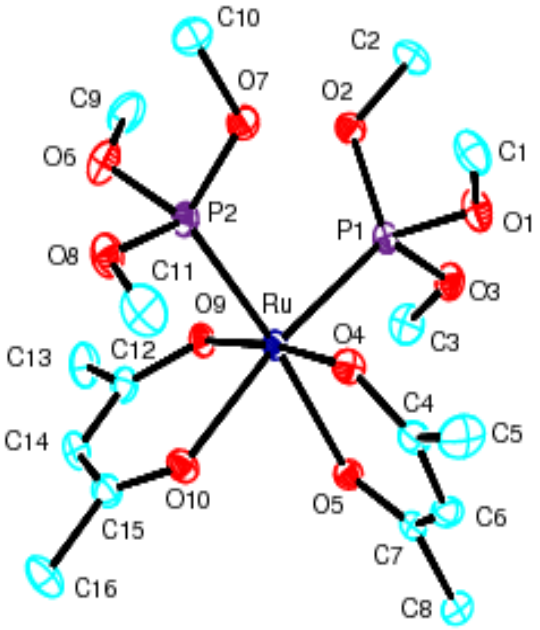

Figure 3.37. ORTEP drawing of the title compounds with the atomic numbering scheme Displacement ellipsoids are drawn at the 30% probability level for cis - $[Ru(acac)_2\{P(OMe)_3\}_2]$, where (i: -x, -y, -z).

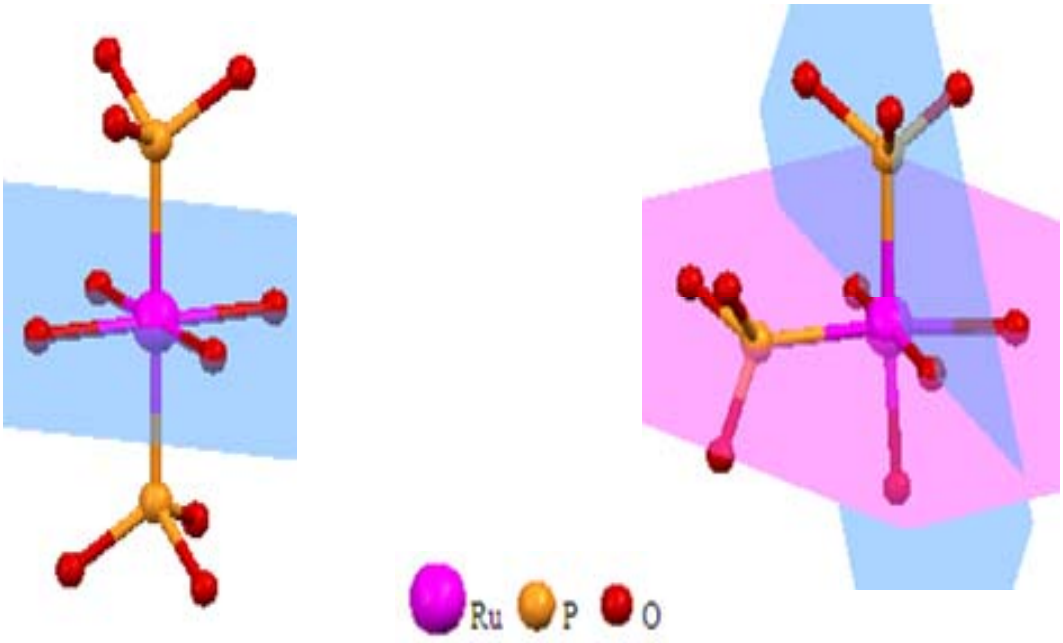

Figure 3.38. Basal planes of the coordination geometry for the Ru(II) ion in the trans (a) and in the cis (b) structures.

The average bond distances are Ru-P = 2.2061, Ru′-P′ = 2.2106 and Ru-O = 2.084 Å (Table 2). Compared to the bond distances in the *trans*-complex, the Ru-P distances of *cis*-structure are smaller while the Ru-O distance are nearly the same. Ruthenium(II) coordination involves bond angles ranging between 83.01(14)-96.01(5)° and 81.24(13)-94.12(10)° for two asymmetric units of *cis*-structure, the smallest values belonging to the O5-Ru-O10 83.01(14)° and O5'-Ru'-O10' 81.24(13)° and the largest values belonging to the P1-Ru-P2 96.01(5)° and P1'-Ru'-O5' 94.12(10)°. The average coordination wide angles are 173,43 and 173,25° for asymmetric unit of *cis*-structure. The P1…P2 distance is 3.152(2) Å (Table 3.5).

Table 3.5. Selected bond lengths and angles for compounds (Å,°).

trans		***Cis***	
Ru – P1	2.3175(14)	Ru – P (aver)	2.2061
Ru – O (aver)	2.066	Ru – O (aver)	2.084
P – O (aver)	1.597	P – O (aver)	1.595
Ru' – P1'	2.3089(15)	Ru' – P' (aver)	2.2106
Ru' – O' (aver)	2.065	Ru' – O' (aver)	2.084
P' – O' (aver)	1.597	P' – O' (aver)	1.580
P1··· $P1^{i}$	4.635(2)	P1 ··· P2	3.152(2)
	trans		
P1 – Ru – O4	91.82(11)	P1' – Ru' – O4'	90.81(11)
P1 – Ru – O5	88.96(11)	P1' – Ru' –O5'	91.30(12)
O4 – Ru – O5	92.96(15)	O4' – Ru' – O5'	92.94(16)
O4 – Ru – $(O5)^{i}$	87.04(15)	O4' – Ru' – $(O5')^{ii}$	87.06(16)
	Cis		
P1 – Ru – P2	96.01(5)	P1' – Ru' – P2'	90.93(6)
P – Ru – O (aver)	91.42	P' – Ru' – O' (aver)	93.03
P – Ru – O (aver)	173.00	P' – Ru' – O' (aver)	173.44
Wide angle			
O4 – Ru – O5	90.04(14)	O4' – Ru' – O5'	90.94(13)
O9 – Ru – O10	89.98(14)	O9' – Ru' – O10'	90.57(13)
O5 – Ru – O9	86.54(13)	O5' – Ru' – O9'	83.46(13)
O5 – Ru – O10	83.01(14)	O5' – Ru' – O10'	81.24(13)
O4 – Ru – O10	85.07(14)	O4' – Ru' – O10'	84.20(13)
O4 – Ru – O9	174.30(13)	O4' – Ru' – O9'	172.87(13)

i = -x, -y, -z and ii = 1-x,1-y,1-z

(Atoms names written with (') symbol shows the second symmetry independent molecule in the unit cell.)

Hydrogen bond and molecular packing geometry of the title molecules were calculated with PLATON [120] and hydrogen bonding geometry is summarized in Table 3.6. In the case of cis-structure, a maximum and minimum residual electron density of 1.448 e/$Å^3$ and -0.591 e/$Å^3$ were observed at a distance of 0.86 Å from Ru and 0.66 Å from O6' atom, respectively. For the trans-structure the highest peak 1.118 e/$Å^3$ and deepest hole -1.616 e/$Å^3$ were observed at distances of 1.12 Å from P1' and 0.84 Å from Ru atom, respectively.

Table 3.6. Hydrogen-bonding geometry (Å,°)

	D – O···A	H···A	D···A	D – H···A
	C1 – H1B···O4	2.32	3.127(8)	141
trans	C1' – H1F···O4'	2.41	3.191(8)	139
	C3 – H3C···O5	2.49	3.206(7)	132
	C3' – H1E···O5'	2.35	3.146(9)	140
	C1 – H1B···O4	2.44	3.165(8)	133
	C3 – H3A···O9	2.37	3.278(7)	157
	C9 – H9C···O9	2.41	3.166(9)	135
	C10 – H10C···O8	2.52	2.912(8)	104
cis	C11 – H11C···O4	2.53	3.180(9)	125
	C1' – H1F···O4'	2.37	3.174(8)	140
	C2' – H2F···O3'	2.56	2.959(9)	105
	C3' – H3D···O9'	2.33	3.131(9)	141
	C10' – H10F···O8'	2.38	2.803(10)	106

3.13. Catalytic activity of trans- and cis-[Ru(acac)$_2${P(OMe)$_3$}$_2$] in hydrogen generation from the hydrolysis of sodium borohydride

The *trans*-[Ru(acac)$_2${P(OMe)$_3$}$_2$] and *cis*-[Ru(acac)$_2${P(OMe)$_3$}$_2$] complexes were tested as homogeneous catalyst in the hydrolysis of sodium borohydride for hydrogen generation. Figure 3.39 shows the hydrogen volume plots versus time for the hydrolysis of sodium borohydride performed using a) *cis*-[Ru(acac)$_2${P(OMe)$_3$}$_2$], b) *trans*-[Ru(acac)$_2${P(OMe)$_3$}$_2$], c) *trans*-[Ru(acac)$_2${P(OMe)$_3$}$_2$] plus 2 equivalents of P(OMe)$_3$, d) [Ru(acac)$_3$], e) [Ru(acac)$_3$] plus 2 equivalents of P(OMe)$_3$, f) *cis*-[Ru(acac)$_2${P(OMe)$_3$}$_2$] plus 2

equivalents of $P(OMe)_3$ all with 0.6 mM Ruthenium complex and 450 mM sodium borohydride at 25 ± 0.1 °C. It is observed that none of the two complexes alone is an effective catalyst in the hydrolysis of sodium borohydride. Amount of hydrogen gas liberated from the hydrolysis of sodium borohydride in the presence of sole *trans* or *cis*-$[Ru(acac)_2\{P(OMe)_3\}_2]$ complexes is less than 100 mL, which is negligible in comparison with the amount of hydrogen acquired by using $[Ru(acac)_3]$ (1200 mL) in the same period of time. Since the addition of trimethylphosphite highly improves the catalytic activity of ruthenium(III) acetylacetonate [52], the catalytic activity of *trans*- and *cis*- $[Ru(acac)_2\{P(OMe)_3\}_2]$ complexes was also tested in the hydrogen generation of sodium borohydride in the presence of two equivalents of trimethylphosphite. Figure 3.39 shows that catalytic activity of trans isomer in the presence of two equivalents of trimethylphosphite is slightly improved, though still lower than that of sole $Ru(acac)_3$. On contrary to the trans isomer, the catalytic activity of *cis*-$[Ru(acac)_2\{P(OMe)_3\}_2]$ is greatly enhanced in the presence of two equivalents of trimethylphosphite. Accordingly, although the *cis* isomer is not an efficient catalyst in the hydrogen generation of sodium borohydride, the significant improvement in its catalytic activity obtained by addition of 2 equivalents of trimethylphosphite indicates the formation of an active ruthenium species containing more than two phosphine ligands. It is noteworthy that changing the mole ratio of trimethylphosphite to trans- or cis-$[Ru(acac)_2\{P(OMe)_3\}_2]$ in the range of 1-4 does not affect on the hydrogen generation rate or in other words, regardless of different concentrations of trimethylphosphite, one active ruthenium species involving more than two phosphorus ligands is formed during hydrolysis of sodium borohydride starting with cis-$[Ru(acac)_2\{P(OMe)_3\}_2]$ or $Ru(acac)_3$ [54] in the presence of trimethylphosphite. The observation that catalytic activity of cis-$[Ru(acac)_2\{P(OMe)_3\}_2]$ is greatly improved in the presence of two equivalents of trimethylphosphite, prompted us to isolate and characterize the active ruthenium species formed in aqueous solution during hydrolysis of sodium borohydride starting with $Ru(acac)_3$ plus $P(OMe)_3$.

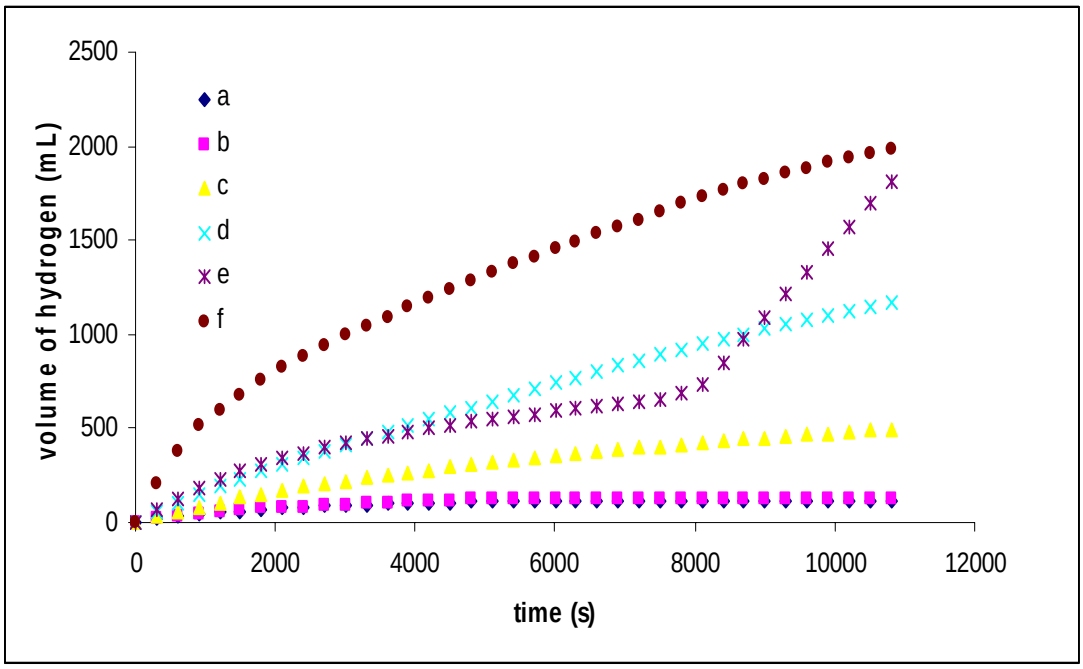

Figure 3.39. Volume of hydrogen versus time for the hydrolysis of sodium borohydride using compounds : a) *cis*-[Ru(acac)$_2${P(OMe)$_3$}$_2$], b) *trans*-[Ru(acac)$_2${P(OMe)$_3$}$_2$], c) *trans*-[Ru(acac)$_2${P(OMe)$_3$}$_2$] plus 2 equivalents of P(OMe)$_3$, d) [Ru(acac)$_3$], e) [Ru(acac)$_3$] plus 2 equivalents of P(OMe)$_3$, f) *cis*-[Ru(acac)$_2${P(OMe)$_3$}$_2$] plus 2 equivalents of P(OMe)$_3$.

3.14. Attempts to isolate the active catalyst after finishing the catalytic hydrolysis of sodium borohydride starting with Ru(acac)$_3$ and P(OMe)$_3$ along with UV-Visible spectroscopic measurements during the catalytic reaction

To isolate and characterize the active catalyst formed from the Ru(acac)$_3$ and P(OMe)$_3$ under the reducing conditions, after finishing of catalytic hydrolysis of $NaBH_4$, the mixture was extracted with dichloromethane and the combined organic extracts containing ruthenium complexes were collected for further characterization. Extraction by dichloromethane is an easy and effective technique to separate ruthenium complexes from $NaBH_4$ or metaborates forming as a side product during hydrolysis of $NaBH_4$. ^{1}H NMR spectroscopy of combined organic extracts (Figure 3.40) shows a singlet at δ = 3.49 ppm which is a promising sign of coordination P(OMe)$_3$ to ruthenium. In addition, ^{13}C NMR spectroscopy of organic extracts

(Figure 3.41) supports formation of a ruthenium complex containing trimethylphosphite ligands by a singlet at δ = 50.9 ppm. Apart from peaks in the region of [δ (^{1}H) 3.49, δ (^{13}C) 50.9] attributed to the methyl groups of trimethylphosphite (Figure 3.40 and 3.41), other broad peaks [δ (^{1}H) -5.66, δ (^{13}C) -23.5] with very high intensity are observed in very high-field regions, attributed to paramagnetic ruthenium(III) acetylacetonato complexes that nmr shifts of paramagnetic transition metal acetylacetonates has been useful for investigating a number of solution properties such as bonding, kinetics and thermodynamics of stereochemical equilibria [121,122]. Accordingly, based on ^{1}H and ^{13}C NMR spectroscopy of organic extracts (Figure 3.40 and 3.41), a mixture of compounds containing paramagnetic ruthenium(III) acetylacetonate complex and a ruthenium complex with trimethylphosphite ligands are obtained after finishing catalytic hydrolysis of $NaBH_4$ starting with $Ru(acac)_3$ and $P(OMe)_3$.

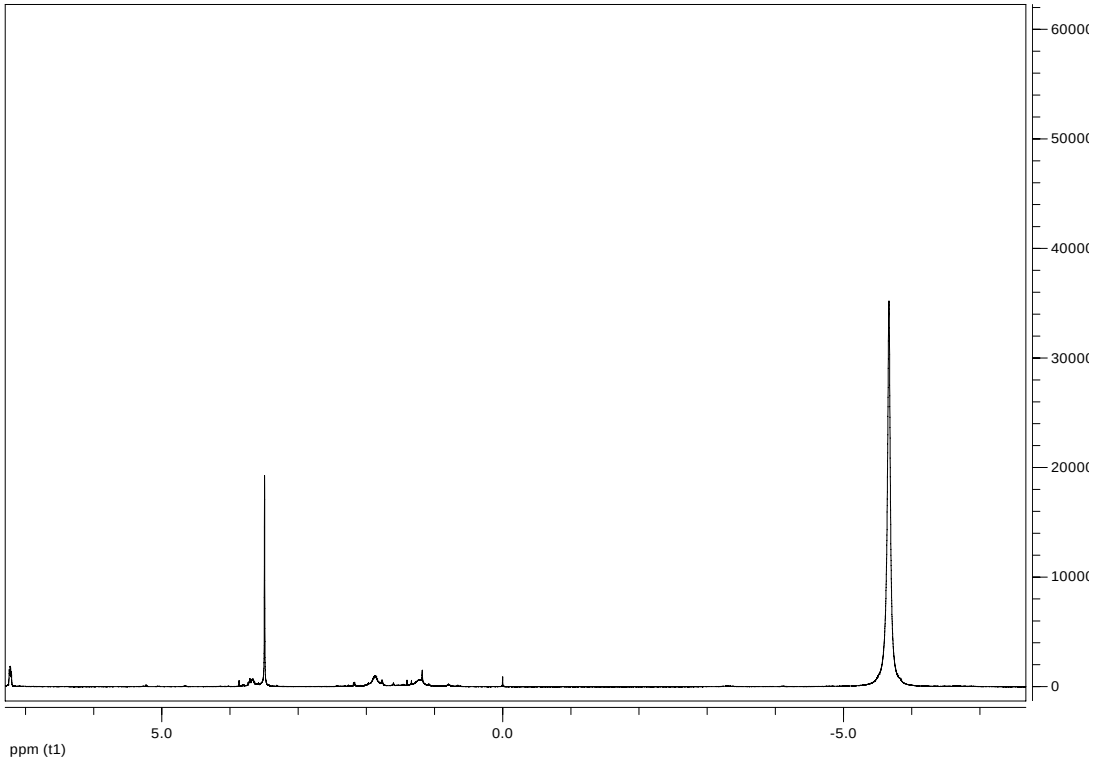

Figure 3.40. ^{1}H NMR spectroscopy of combined paramagnetic $Ru(acac)_3$ and ruthenium complex with trimethylphosphite ligands.

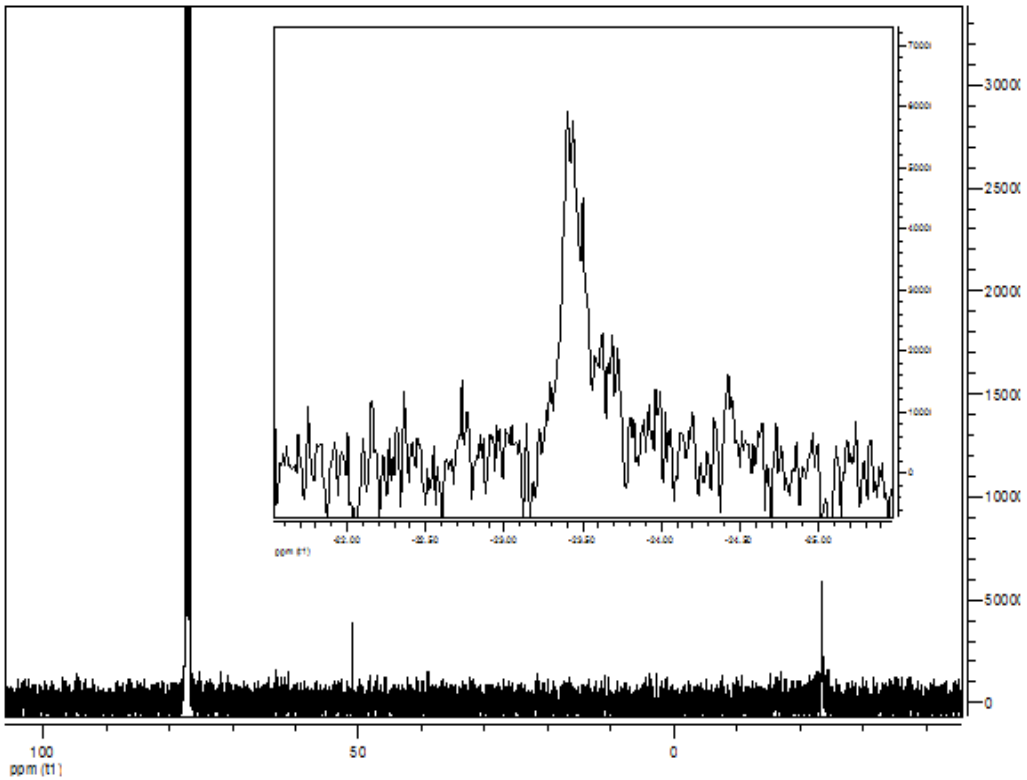

Figure 3.41. ^{13}C NMR spectroscopy of combined paramagnetic $Ru(acac)_3$ and ruthenium complex with trimethylphosphite ligands.

Monitoring the UV-visible electronic absorption spectra during the catalytic hydrolysis of $NaBH_4$ starting with $Ru(acac)_3$ and $P(OMe)_3$ gives some insights into the nature of active catalyst. Figure 3.42 displays three UV-Visible spectra taken at different stages of the catalytic reaction. The spectrum taken from the mixture before the reaction (before adding sodium borohydride, Figure 3.42a) shows three prominent absorption bands at 270, 350 and 509 nm assigned to charge transfer transitions and a d-d transition of $Ru(acac)_3$, respectively [123]. The UV-visible spectrum taken from the reaction solution during the reaction after induction period (Figure 3.42b) exhibits one absorption band at 480 nm with higher intensity compared to that of $Ru(acac)_3$ and another band at 275 nm. These two bands retain during the whole reaction and should be due to the active catalyst. The spectrum taken at the end of the catalytic reaction (Figure 3.42c) shows essentially the same absorption features as the ones of $Ru(acac)_3$ before the reaction. This observation indicates that the active catalyst is alive during the catalysis, but converted to the

parent $Ru(acac)_3$ when the hydrolysis of sodium borohydride is over. The UV-visible spectrum observed for the active catalyst during the catalytic reaction (Figure 3.42b) resembles the electronic absorption spectra of three octahedral ruthenium(II) complexes known in literature: $[Ru(en)_2IP]^{2+}$, $[Ru(en)Phen]^{2+}$, (IP: imidazo[4,5-f][1,10]phenanthroline and Phen: 1,10 – phenanthroline) [124] and cis-$[Ru(acac)_2\{P(OMe)_3\}_2]$ [54]. This resemblance implies that the active catalyst is most likely a ruthenium(II) species.

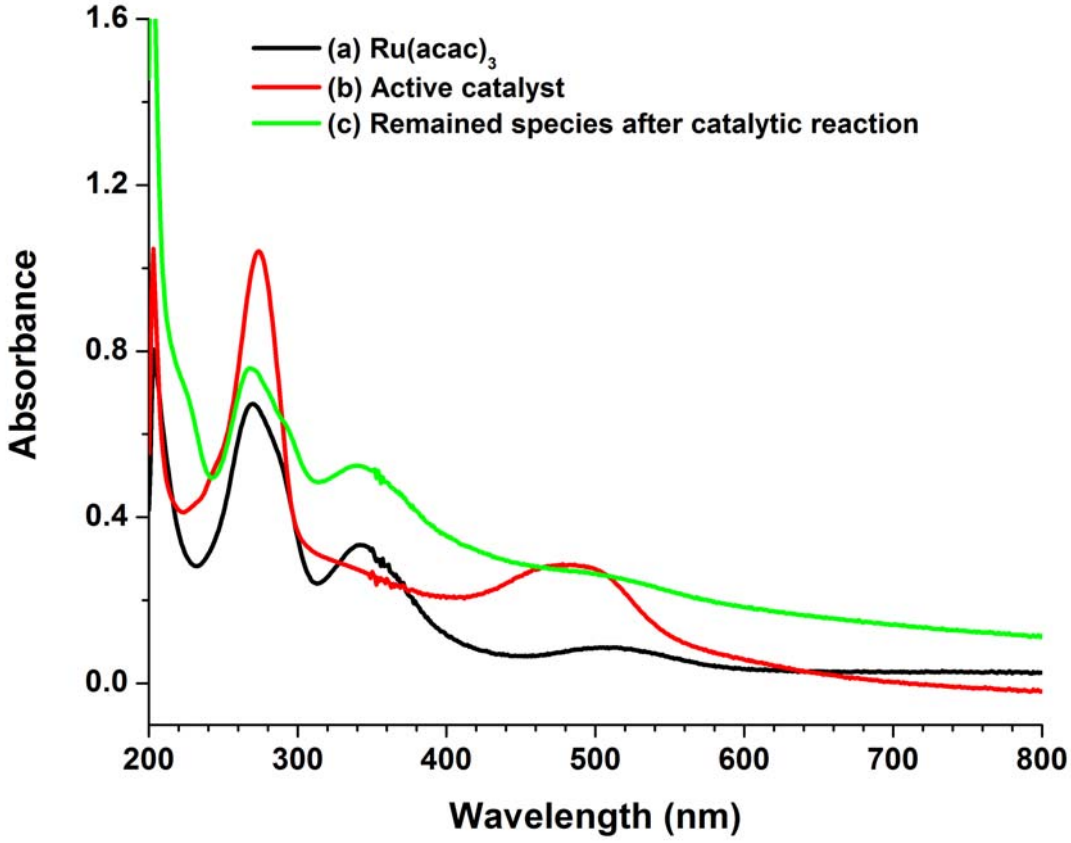

Figure 3.42. UV-Visible spectroscopic measurements during hydrolysis of $NaBH_4$ (450 mM) starting with 2 mM $Ru(acac)_3$ and $P(OMe)_3$ (4-8 mM) in THF-H_2O (1:9) at 25 °C.

That the active catalyst is alive as long as hydrogen generation continues, i.e. as long as sodium borohydride is present in solution, leads to a long catalytic lifetime (*vide infra*). However, the active catalyst is immediately converted back to the parent

ruthenium(III) acetylacetonate when the hydrogen generation stops, i.e. no more $NaBH_4$ in the catalytic solution is left. The reformation of ruthenium(III) acetylacetonate was confirmed by the ^1H and ^{13}C NMR spectra of the crude organic extract obtained from the solution after the catalytic reaction.

It is noteworthy that performing the same catalytic hydrolysis starting with different ratios of $P(OMe)_3$ to $Ru(acac)_3$ in the range of 1-4 gives the same UV-Visible electronic absorption spectra indicating that changing the ratio of $P(OMe)_3$ to $Ru(acac)_3$ does not affect the structure of active catalyst or mechanism of catalytic hydrolysis of $NaBH_4$.

3.15. Isolation and characterization of $[Ru\{P(OMe)_3\}_4H]$ complex

The organic extracts collected after finishing the catalytic hydrolysis of $NaBH_4$ and extraction by dichloromethane, were dissolved in cold hexane and due to low solubility of $Ru(acac)_3$ in hexane, it was separated from another ruthenium complex containing trimethylphosphite ligands. Colorless crystals of hydridotetrakis(trimethylphosphite)ruthenium(I) complex as a minor product after finishing the catalytic hydrolysis of $NaBH_4$, were obtained by the crystallization from hexane at 0°C after 10 days. Based on UV-Visible spectroscopic measurements (Figure 3.42) along with ^1H and ^{13}CNMR spectroscopy (Figure 3.40 and 3.41) of organic extracts, the in-situ active catalyst is a Ru(II) species which mostly converts back to ruthenium(III) acetylacetonate after finishing the hydrogen generation and some traces of active catalyst is reduced to Ru(I) species in the form of $[Ru\{P(OMe)_3\}_4H]$ complex as a minor product which is isolable after finishing the catalytic hydrolysis of $NaBH_4$ starting with $Ru(acac)_3$ and $P(OMe)_3$. Single crystals of the Ru(I) species, $[Ru\{P(OMe)_3\}_4H]$, were used for the XRD structure determination. The complex crystallizes in the triclinic space group P-1 with three asymmetric unit formula of $[Ru\{P(OMe)_3\}_4H]$ in the unit cell (Fig. 3.43). Projection of the crystal structure of the $[Ru\{P(OMe)_3\}_4H]$ complex involving a Unit cell with three asymmetric molecules and three inversion symmetry related molecules is shown in Figure 3.44. The coordination around the Ru atoms involves four P atoms

from $P(OMe)_3$ ligands and one H atom. The five bond angles within the coordination sphere are in the range of 96.2(2)- 101.3(3)°, the sixth bong angle has a maximum deviation of the angle from ideal value of 109°. The values of this angles for three molecules are 153.73(18) - 154.2(2) - 155.4(2)°. A H atom locates at this wide angle position in the coordination sphere. Crystal data and experimental details of the title compound plus the average values of selected bond lengths and angles are given in Table 3.7 and 3.8, respectively.

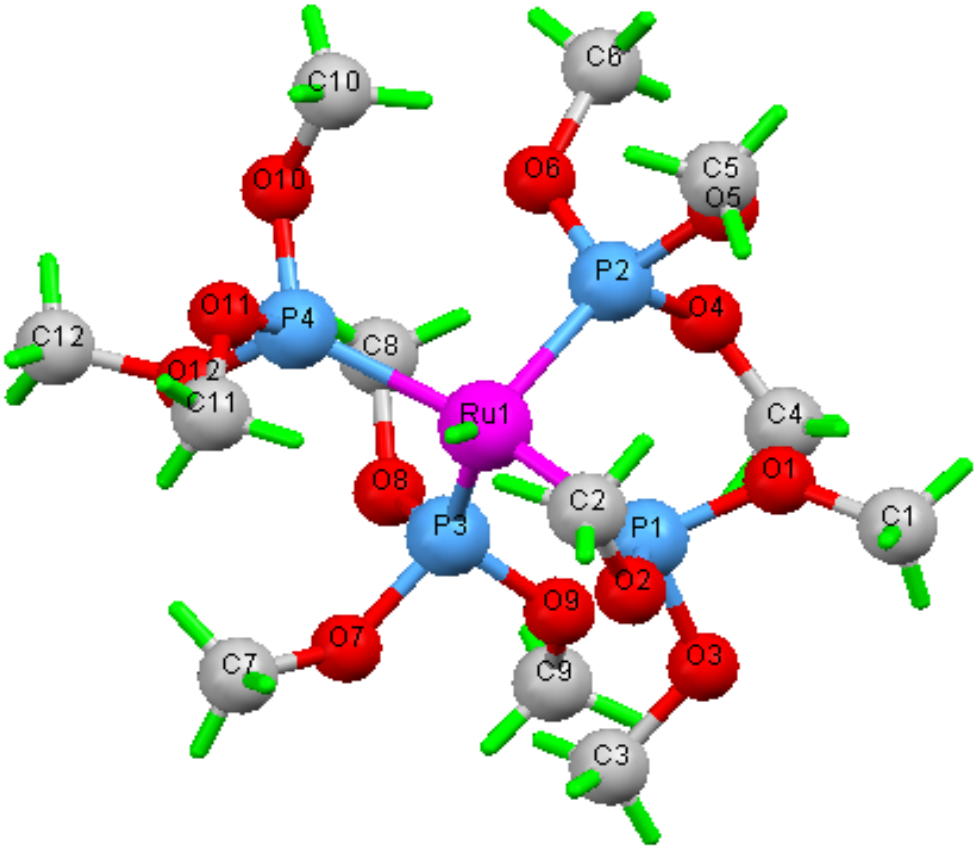

Figure 3.43. X-ray crystal structure of $[Ru\{P(OMe)_3\}_4H]$ complex

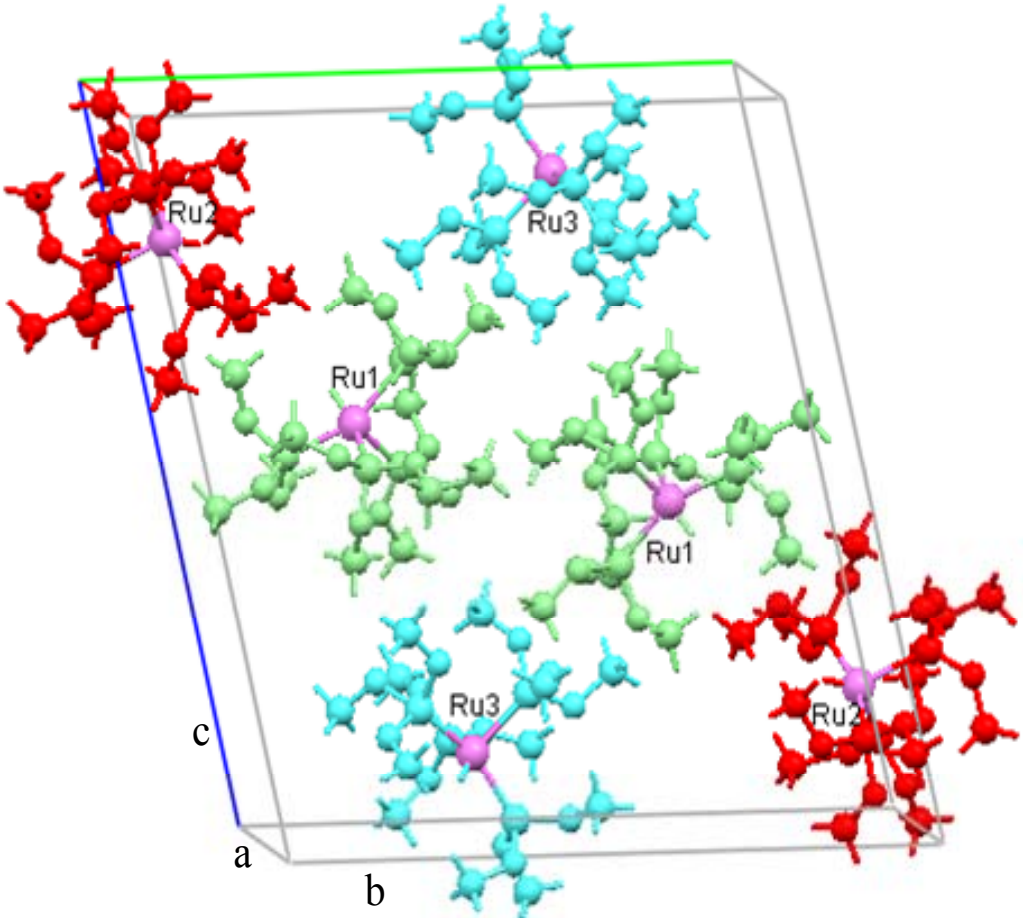

Figure 3.44. Projection of the crystal structure of $[Ru\{P(OMe)_3\}_4H]$ complex

Table 3.7. Crystal data and experimental details of the title compound

Compound	[Ru{P(OMe)$_3$}$_4$H]
Formula	$C_{12}H_{37}O_{12}P_4Ru$
Formula weight	598.37
Temperature (K)	295(2)
Space group	P-1
a (Å)	10.066(2)
b (Å)	19.108(3)
c (Å)	20.938(4)
α (º)	78.839(14)
β (º)	87.308(16)
γ (º)	79.506(14)
Volume (Å^3)	3884.7(13)
Z	6
Density (calculated) (Mg/m^3)	1.535
μ (mm^{-1})	0.901
F(000)	1854
θ range for data collection (º)	2.16 - 24.98
Reflections measured collected/unique	14137
Independent observed reflections	13324
Independent reflections [$I > 2\sigma$]	6153
Data/restraints/parameters	13324 / 0 / 478
R_{int}	0.0897
R indices [I>2σ(I)]	$R_1 = 0.1035$, $wR_2 = 0.3134$
Goodness of fit on F^2	1.163

Table 3.8 Selected/average bond length [Å] and angles [°] for the three asymmetric units of [Ru{P(OMe)$_3$}$_4$H]

[Ru{P(OMe)$_3$}$_4$H]		
Assymetric unit I	Assymetric unit II	Assymetric unit III
Ru1 P4 2.253(5)	Ru2 P8 2.231(5)	Ru3 P10 2.251(5)
Ru1 P2 2.266(7)	Ru2 P5 2.260(5)	Ru3 P9 2.255(5)
Ru1 P3 2.273(6)	Ru2 P7 2.278(6)	Ru3 P11 2.265(5)
Ru1 P1 2.275(6)	Ru2 P6 2.287(6)	Ru3 P12 2.287(5)
Ru1-P (aver) 2.267	Ru2-P (aver) 2.264	Ru3-P 2.265
P4 Ru1 P2 101.3(3)	P8 Ru2 P5 155.4(2)	P10 Ru3 P9 153.73(18)
P4 Ru1 P3 96.9(2)	P8 Ru2 P7 96.3(2)	P10 Ru3 P11 97.30(19)
P2 Ru1 P3 96.6(3)	P5 Ru2 P7 100.1(2)	P9 Ru3 P11 100.19(19)
P4 Ru1 P1 154.2(2)	P8 Ru2 P6 100.0(2)	P10 Ru3 P12 100.65(18)
P2 Ru1 P1 96.7(3)	P5 Ru2 P6 96.4(2)	P9 Ru3 P12 96.79(18)
P3 Ru1 P1 99.3(2)	P7 Ru2 P6 96.3(2)	P11 Ru3 P12 96.2(2)
P4 Ru1 H1 75.9	P8 Ru2 H2 77.8	P10 Ru3 H3 76.3
P2 Ru1 H1 130.3	P5 Ru2 H2 77.6	P9 Ru3 H3 77.4
P3 Ru1 H1 133.1	P7 Ru2 H2 131.8	P11 Ru3 H3 131.8
P1 Ru1 H1 78.3	P6 Ru2 H2 131.9	P12 Ru3 H3 131.9

$(Ru - P)_{ave}$	2.265(7)	$(P - Ru - P)_{ave}$	98.1(3)	small angle
$(P - O)_{ave}$	1.59(2)	$(P - Ru - P)_{ave}$	154.4(2)	large angle
$(O - C)_{ave}$	1.46(3)	$(O - P - Ru)_{ave}$	120.1(8)	
		$(O - P - O)_{ave}$	97.0(1)	
		$(P - O - C)_{ave}$	123.4(2)	

Solution NMR data of hydridotetrakis(trimethylphosphite)ruthenium(I), [Ru{P(OMe)$_3$}$_4$H], are also in good agreement with the single crystal structure. The ^{1}H NMR spectrum (Figure 3.45) taken from chloroform-d solution gives two peaks at 3.45 and 3.47 ppm for the P(OMe)$_3$ groups located at axial and equatorial positions, respectively . A singlet peak is observed at -5.71 ppm (the inset in Figure 3.45) for the hydrogen atom which is directly coordinated to ruthenium and broadness of this singlet peak is a characteristic of the paramagnetic 17-electron ruthenium complex.

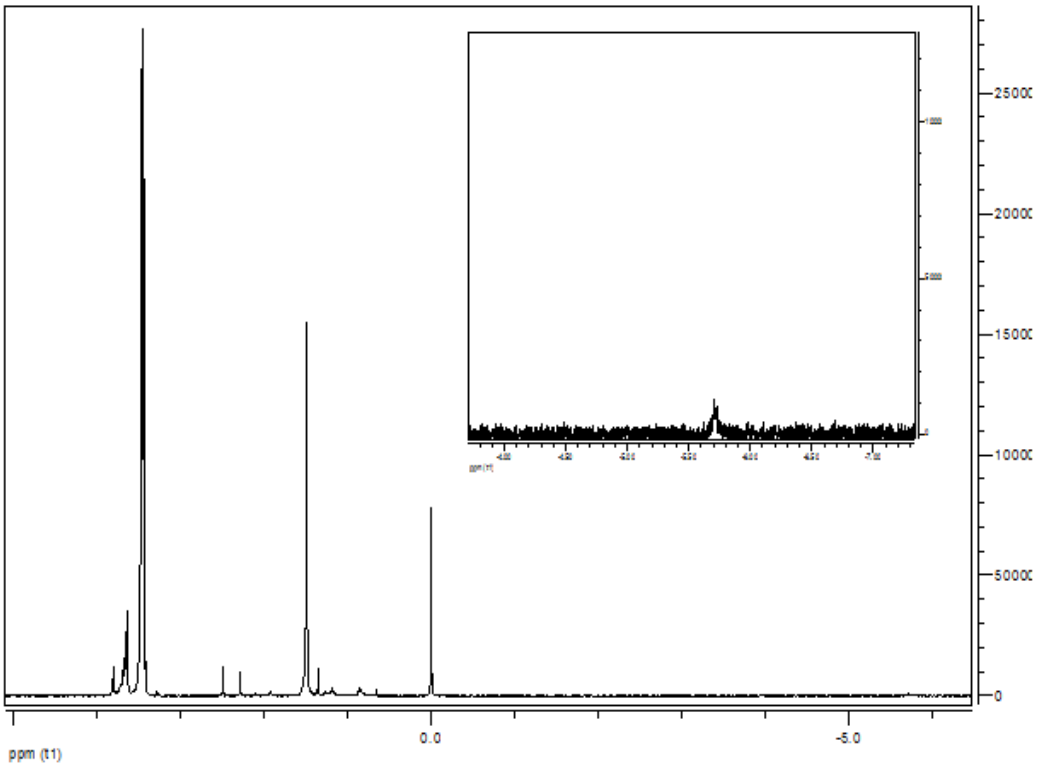

Figure 3.45. ^{1}H NMR spectrum of [Ru{P(OMe)$_3$}$_4$H] complex taken in $CDCl_3$

^{13}C NMR spectrum (Figure 3.46), gives two singlets at 49.32 and 49.80 ppm for the P(OMe)$_3$ groups and due to closeness of the carbons to electronegative oxygen atoms, the related singlets locates at a nearly down-field region.

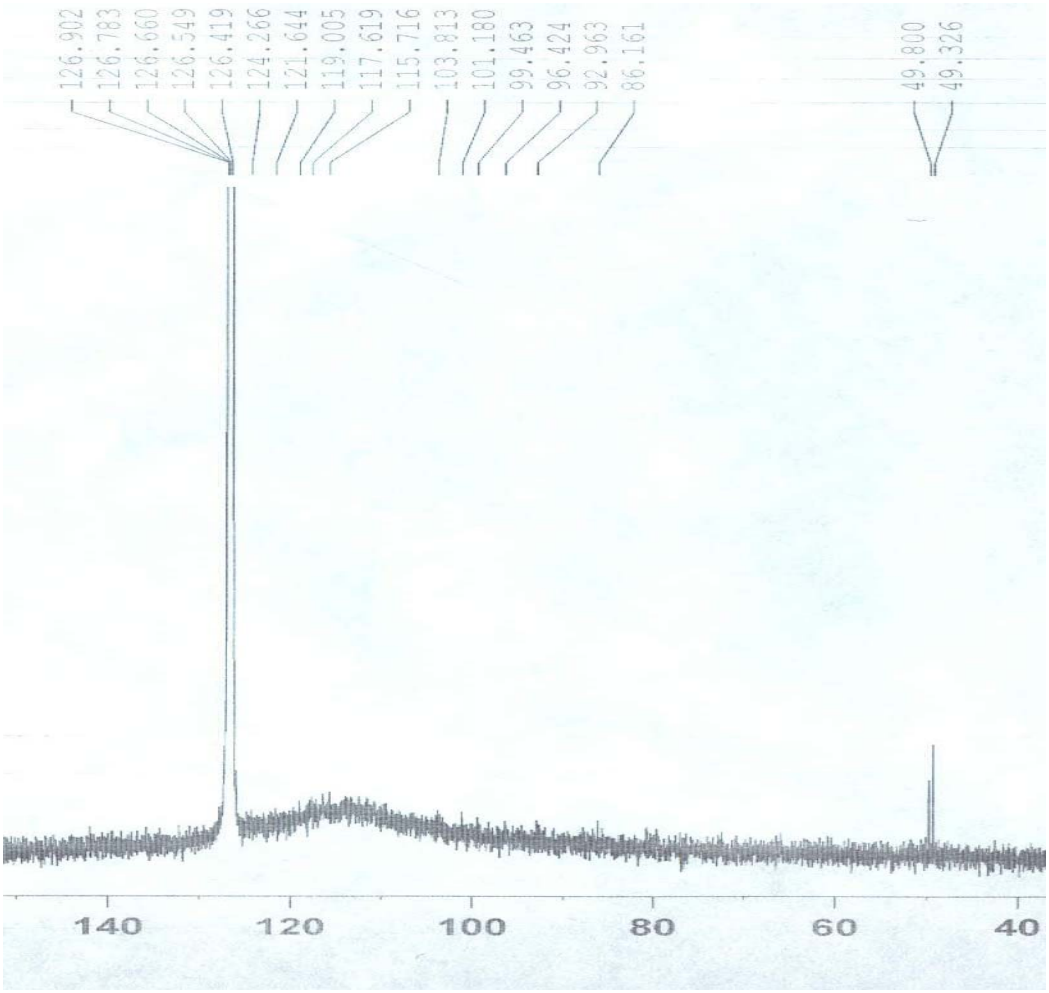

Figure 3.46. ^{13}C NMR spectrum of $[Ru\{P(OMe)_3\}_4H]$ complex taken in $CDCl_3$

In accordance with molecular structure, the ^{31}P NMR spectrum (Figure 3.47), gives two separate peaks at 169.65 and 172.4 ppm with an intensity ratio of 3 to 1. The peak at the region of 172.4 ppm with three times intensity in comparison with another peak, is attributed to three phosphorus atoms located at equatorial positions, while another peak at 169.5 ppm is for a single phosphorus atom located at a nearly trans position to hydrogen atom which is directly coordinated to ruthenium. In the case of $[Ru\{P(OMe)_3\}_4Cl_2]$ complex [58], ^{31}P NMR shows a peak at 131ppm which is about 40 ppm more shielded than corresponding peak in $[Ru\{P(OMe)_3\}_4H]$ complex. Consequently, Cl atoms which are σ-donor and π-donor ligands, make the ruthenium more electron-rich and ruthenium make a stronger bond with phosphorus atoms via stronger π-back electron donation ability, while hydride (H^-) which is a σ-

donor ligand, make the ruthenium less electron rich and ruthenium estabilish a weaker bond with phosphorus atoms due to weaker π-back electron donation ability and that is why ^{31}PNMR peak for [Ru{P(OMe)$_3$}$_4$H] complex is about 40 ppm more unshielded in comparison with another complex containing two Cl ligands.

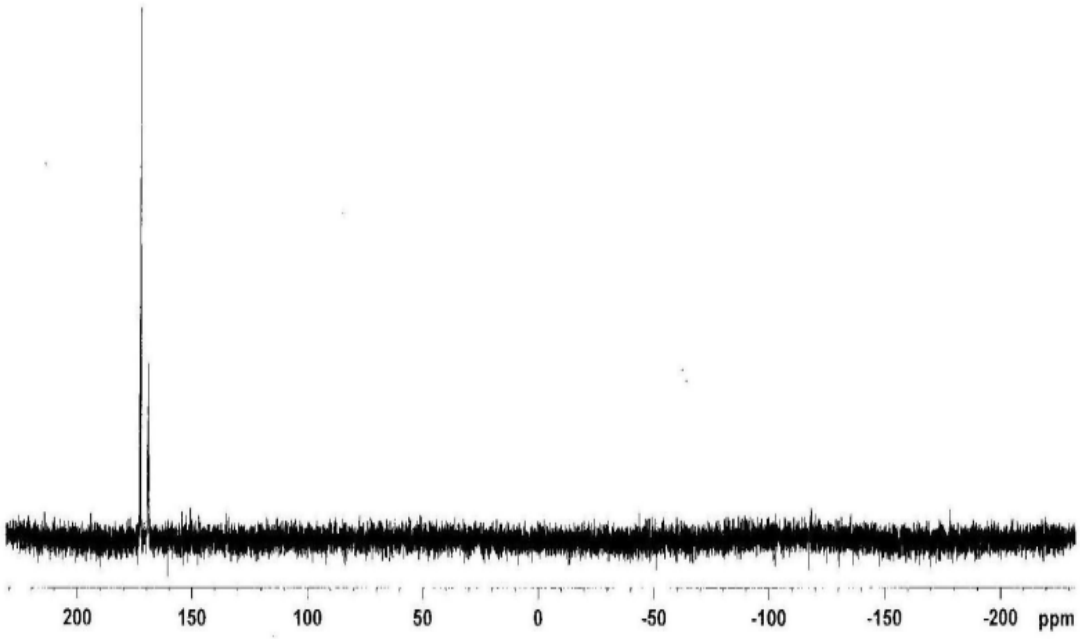

Figure 3.47. ^{31}P NMR spectrum of [Ru{P(OMe)$_3$}$_4$H] complex taken in $CDCl_3$

UV-Visible spectrum (Figure 3.48) of [Ru{P(OMe)$_3$}$_4$H] shows a prominent and very intense absorption band at 295 nm clearly distinguishable from UV-Visible of in-situ active catalyst (Figure 3.42) which is a Ru(II) species and formed temporarily during catalytic hydrolysis of sodium borohydride.

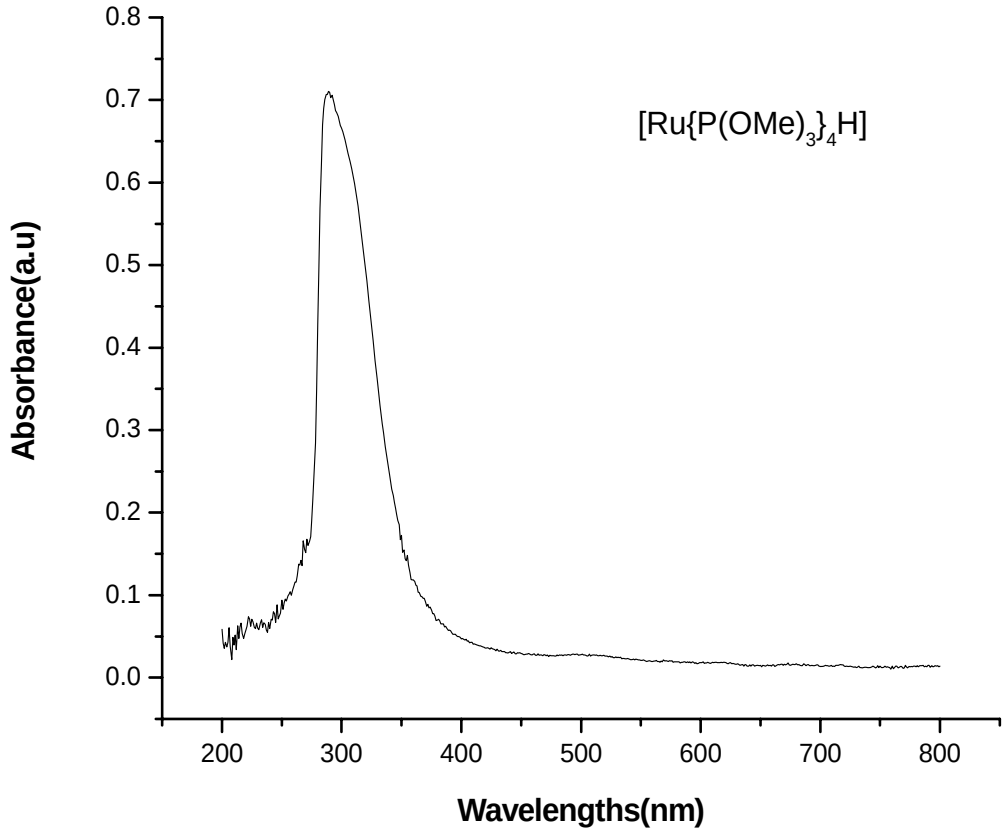

Figure 3.48. UV-Visible spectrum of $[Ru\{P(OMe)_3\}_4H]$ complex taken in THF

The FTIR spectrum of $[Ru\{P(OMe)_3\}_4H]$ complex (Figure 3.49) shows three absorption bands at 1066, 1580-1720 and 2928 cm^{-1} assigned as P-O, Ru-H and C-H stretchings, respectively. Moreover, two other weak absorption bands at 1375 and 1445 cm^{-1} are attributed to C-H bendings. Mass spectrum of $[Ru\{P(OMe)_3\}_4H]$ complex (figure 3.50) obtained by a Micro TOF-LC/ESI/Ms system, shows M^+ molecular ion peak as the base peak at m/z = 597 along with another peak at m/z = 473 for the $[M\text{-}P(OMe)_3]^+$ fragment.

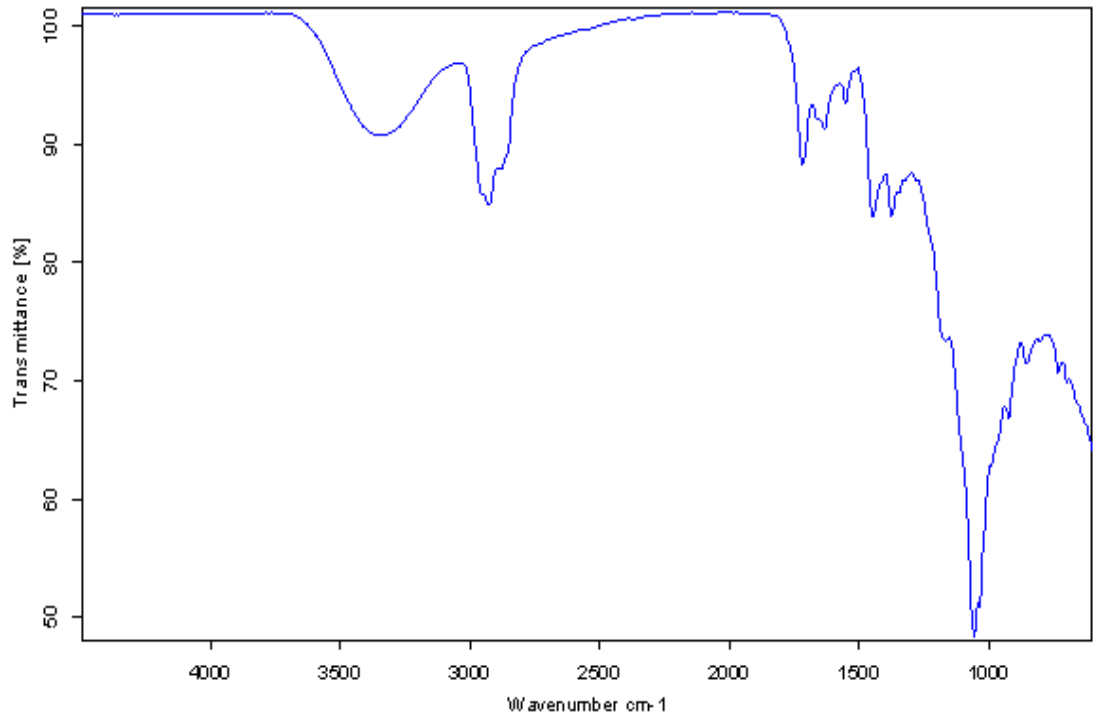

Figure 3.49. FTIR spectrum of [Ru{P(OMe)$_3$}$_4$H] complex taken by ATR/FTIR spectrometer

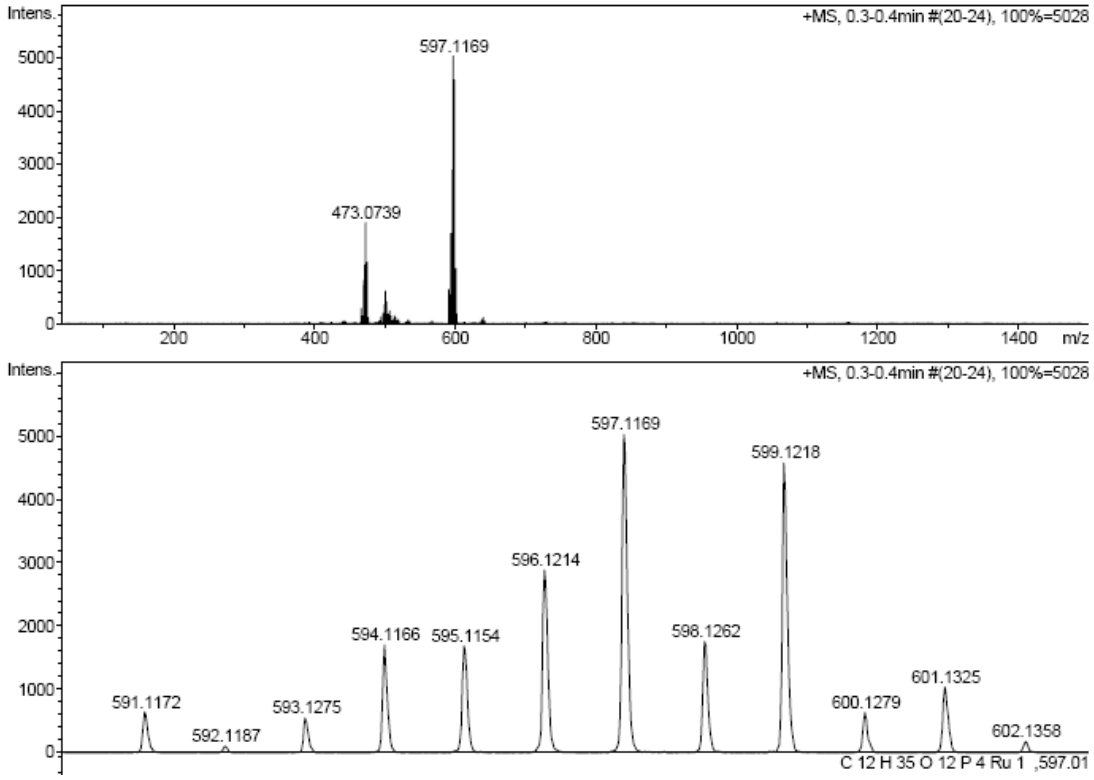

Figure 3.50. Mass spectrum of [Ru{P(OMe)$_3$}$_4$H] complex

3.16. Testing catalytic activity of [Ru{P(OMe)$_3$}$_4$H] complex as a homogeneous catalyst in hydrogen generation from the hydrolysis of sodium borohydride

After isolation of [Ru{P(OMe)$_3$}$_4$H] complex at the end of catalytic hydrolysis of $NaBH_4$ starting with Ru(acac)$_3$ and P(OMe)$_3$, it was applied as a homogeneous catalyst at the beginning of hydrolysis of $NaBH_4$ in order to evaluate its catalytic activity and make a comparison with catalytic activity of other complexes such as Ru(acac)$_3$, trans and cis-[Ru(acac)$_2${P(OMe)$_3$}$_2$] [54] and these complexes in the presence of two equivalents of trimethylphosphite. According to Figure 3.51, catalytic activity of [Ru{P(OMe)$_3$}$_4$H] complex in hydrogen generation of $NaBH_4$ is slightly lower than Ru(acac)$_3$, while catalytic activity of Ru(acac)$_3$ [52] or cis-[Ru(acac)$_2${P(OMe)$_3$}$_2$] [54] are significantly enhanced by the addition of two equivalents of trimethylphosphite per ruthenium into the medium.

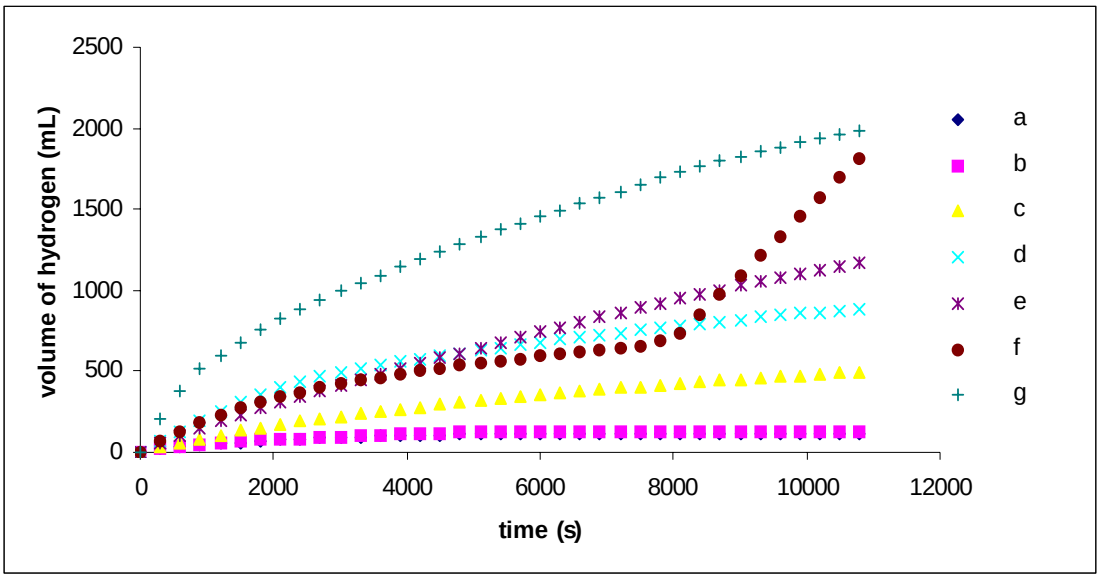

Figure 3.51. Volume of hydrogen versus time for the hydrolysis of $NaBH_4$ (450 mM) using 0.6 mM of ruthenium compounds : a) *cis*-[Ru(acac)$_2${P(OMe)$_3$}$_2$], b) *trans*-[Ru(acac)$_2${P(OMe)$_3$}$_2$], c) *trans*-[Ru(acac)$_2${P(OMe)$_3$}$_2$] plus 2 equivalents of P(OMe)$_3$, d) [Ru{P(OMe)$_3$}$_4$H] e) [Ru(acac)$_3$], f) [Ru(acac)$_3$] plus 2 equivalents of P(OMe)$_3$, g) *cis*-[Ru(acac)$_2${P(OMe)$_3$}$_2$] plus 2 equivalents of P(OMe)$_3$.

Based of Figure 3.42 and 3.51, we can make a conclusion that when $Ru(acac)_3$ or cis-$[Ru(acac)_2\{P(OMe)_3\}_2]$ are applied as homogeneous catalysts in the presence of $P(OMe)_3$, a new in-situ Ru(II) species with very high catalytic activity is formed and after reduction of in-situ Ru(II) species to Ru(I), $[Ru\{P(OMe)_3\}_4H]$, at the end of catalytic reaction, its catalytic activity is decreased.

3.17. Stabilization, isolation and characterization of catalytically very active in-situ Ru(II) species formed temporarily during catalytic hydrolysis of sodium borohydride starting with $Ru(acac)_3$ and $P(OMe)_3$

In order to stabilize the in-situ active catalyst formed temporarily during hydrolysis of $NaBH_4$ starting with $Ru(acac)_3$ and $P(OMe)_3$, 2,2′-bipyridine was found as a suitable substance for stabilization and isolation of in-situ active catalyst from aqueous solution. To stabilize the in-situ active catalyst by 2,2′-bipyridine, a catalytic reaction containing 2 mM of $Ru(acac)_3$ in the presence of $P(OMe)_3$ and 450 mM $NaBH_4$ in 50 mL H_2O-THF at 25°C was setup and the catalytic reaction was followed by UV-Visible spectroscopic measurements. About 1 h after starting the catalytic reaction, the in-situ active catalyst is formed that its formation is understandable by its clear UV-visible spectrum (Figure 3.42) accompanied by a sudden increase in the hydrogen generation rate simultaneously. After formation of in-situ active catalyst, 2,2′-bipyridine (2.5 mM) was immediately added into catalytic solution and the reaction was followed by UV-Visible spectroscopic measurements. As it was explained by UV-Visible spectra in Figure 3.42, the active catalyst is formed temporarily and after finishing the hydrogen generation, it is immediately recycled to ruthenium(III) acetylacetonate along with formation of hydridotetrakis(trimethylphosphite)ruthenium(I) as a minor product. However, the in-situ active catalyst remains stable in the presence of 2,2′-bipyridine and based on Figure 3.52, the stabilized active catalyst is not recycled even few hours after finishing the catalytic reaction. Figure 3.52 nicely shows that the stabilized active catalyst by 2,2′-bipyridine is stable and isolable from the aqueous solution. In addition, UV-Visible spectrum of stabilized active catalyst shows three absorption

bands at 235, 285 and 460 nm and on contrary to UV-Visible spectrum of $Ru(acac)_3$, the absorption band at 350 nm is disappeared.

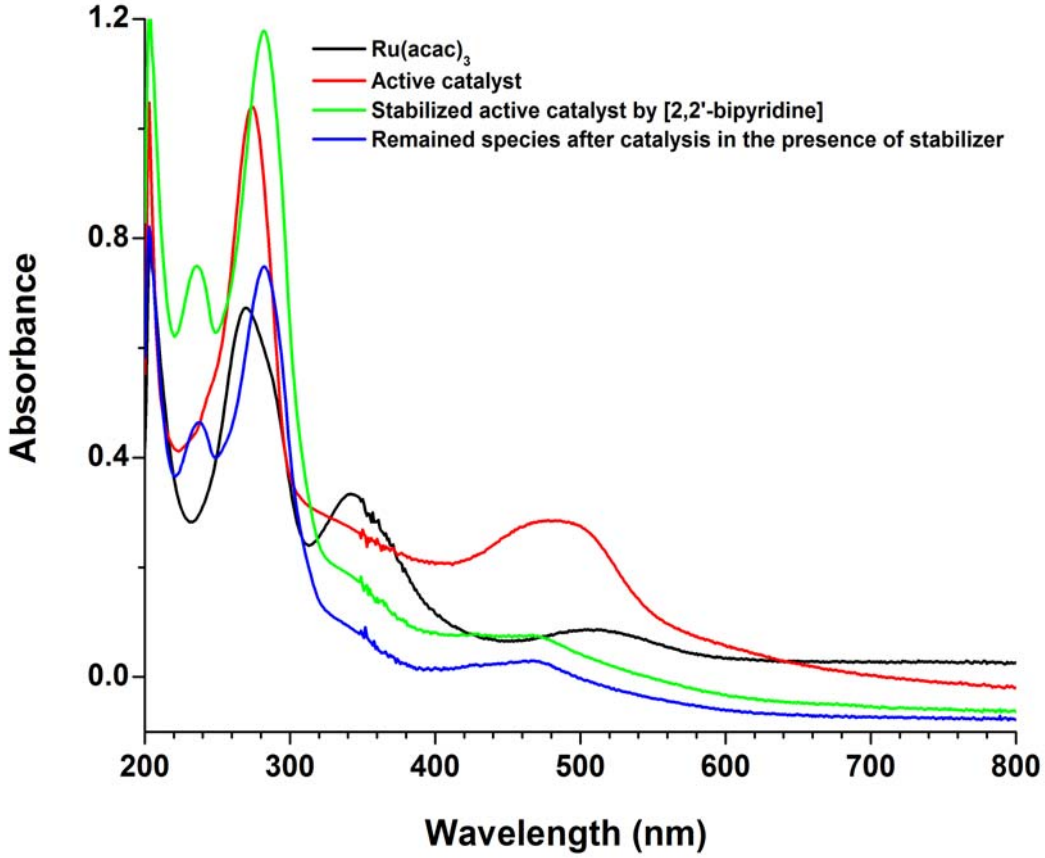

Figure 3.52. UV-Visible spectroscopic measurements during hydrolysis of $NaBH_4$ (450 mM) starting with 2mM $Ru(acac)_3$ and 3 equivalents of $P(OMe)_3$ along with stabilization by 2,2´-bipyridine (2.5 mM).

It is worthy to note that for stabilization of in-situ active catalyst by 2,2´-bipyridine, it is vital to apply lower concentrations of $Ru(acac)_3$ and $NaBH_4$ and perform the catalytic reaction at room temperature. If we apply very high concentrations of $Ru(acac)_3$ or $NaBH_4$ or catalytic reaction is performed at a very high temperature, the in-situ active catalyst is formed and recycled faster and its stabilization by 2,2´-bipyridine is getting more difficult, too. However, applying higher concentrations of 2,2´-bipyridine as a stabilizer, is beneficial to have an easier

stabilization and unreacted amount of 2,2′-bipyridine after finishing the catalytic reaction, is easily washed by cold hexane and separated from stabilized complex.

Following the same procedure used in the isolation procedure for [Ru{P(OMe)$_3$}$_4$H] complex, the stabilized ruthenium complex by 2,2′-bipyridine was isolated via extraction of catalytic solution by dichloromethane and , then, recrystallization of organic extracts in the mixture of chloroform-hexane gives [Ru(acac)(bipy){P(OMe)$_3$}H] as the stabilized active catalyst. According to Figure 3.53, the ^{1}H NMR spectrum of [Ru(acac)(bipy){P(OMe)$_3$}H] taken from chloroform-d solution gives a singlet at-5.59 ppm for the hydrogen atom which is directly coordinated to ruthenium, a broad peak at 1.45 ppm for the hydrogens of methyl groups belonging to acetylacetonate ligand, a singlet at 3.42 ppm for the hydrogens of trimethylphosphite ligands and two multiplates at 6.45 and 6.99 ppm for the hydrogens of 2,2′-bipyridine ring which is coordinated to ruthenium via two nitrogen atoms.

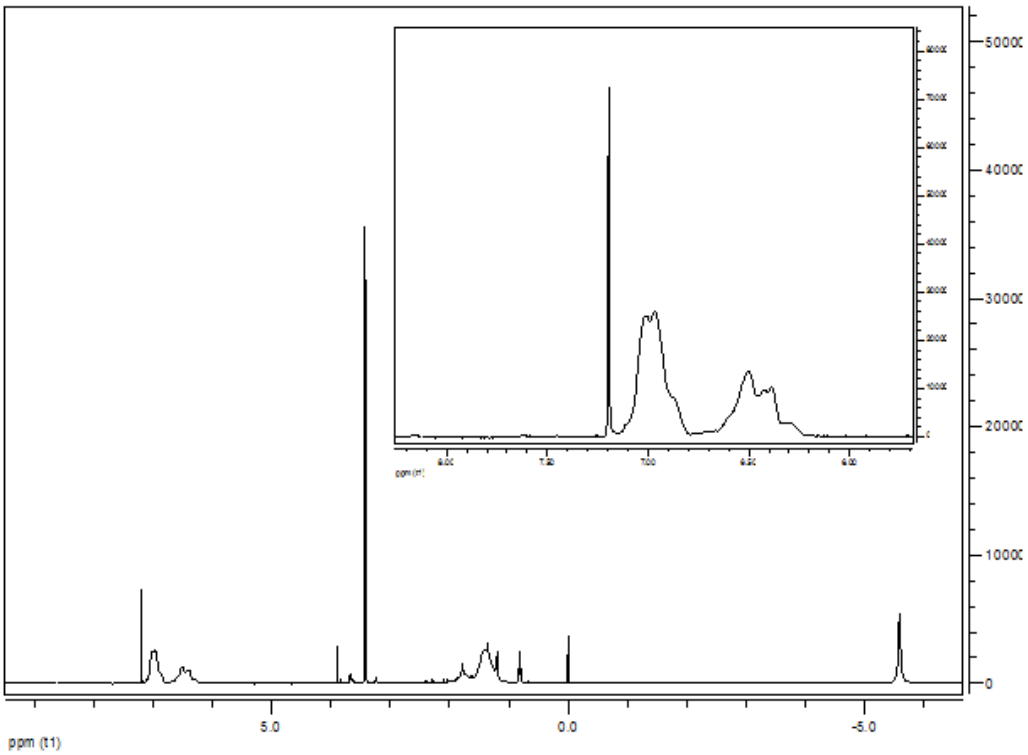

Figure 3.53. ^{1}H NMR of [Ru(acac)(bipy){P(OMe)$_3$}H] complex taken in $CDCl_3$

^{13}C NMR spectrum (Figure 3.54) of [Ru(acac)(bipy){$P(OMe)_3$}H] complex , gives a multiplate at 40.5 ppm for methyl carbons of acetylacetonate ligand, two singlet peaks at 50.91 and 100.02 ppm for the carbons of $P(OMe)_3$ group and C-H of acetylacetonate group respectively, two multiplates at 125.6 and 127.8 ppm for the carbons of 2,2′-bipyridine ring and one doublet at 145.18 ppm for the carbonyls of acetylacetonate group.

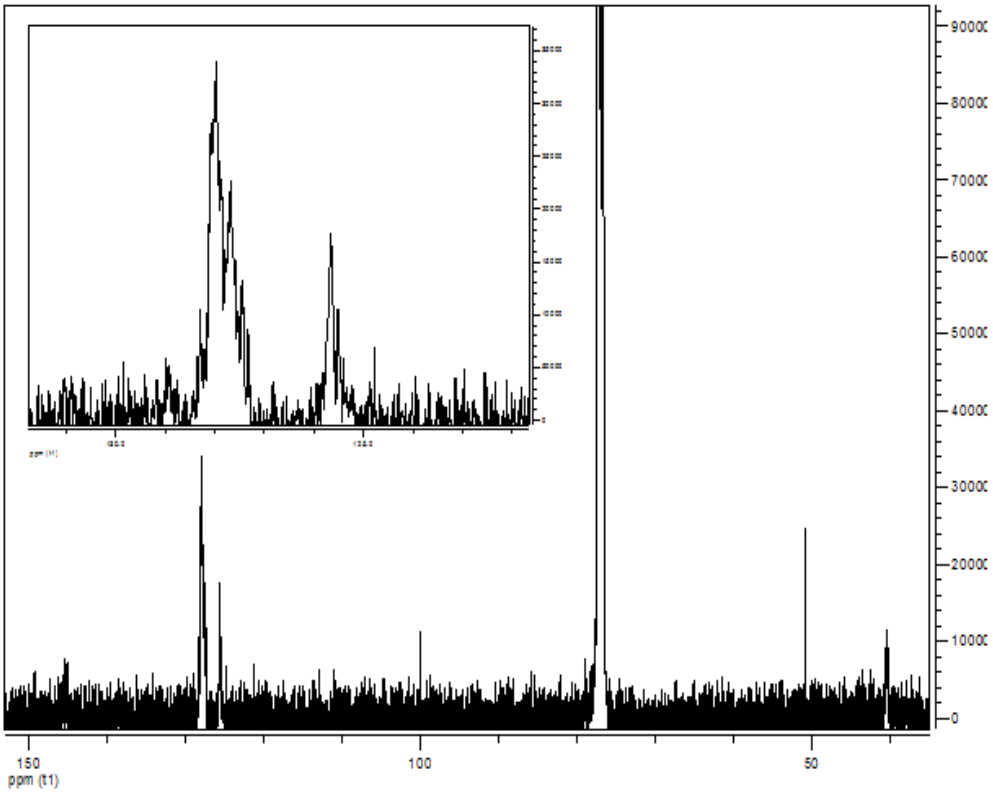

Figure 3.54. ^{13}C NMR of [Ru(acac)(bipy){$P(OMe)_3$}H] complex taken in $CDCl_3$

^{31}P NMR spectrum (Figure 3.55) of [Ru(acac)(bipy){$P(OMe)_3$}H] complex shows a peak at 163.22 ppm for a single phosphorus atom of $P(OMe)_3$ group.

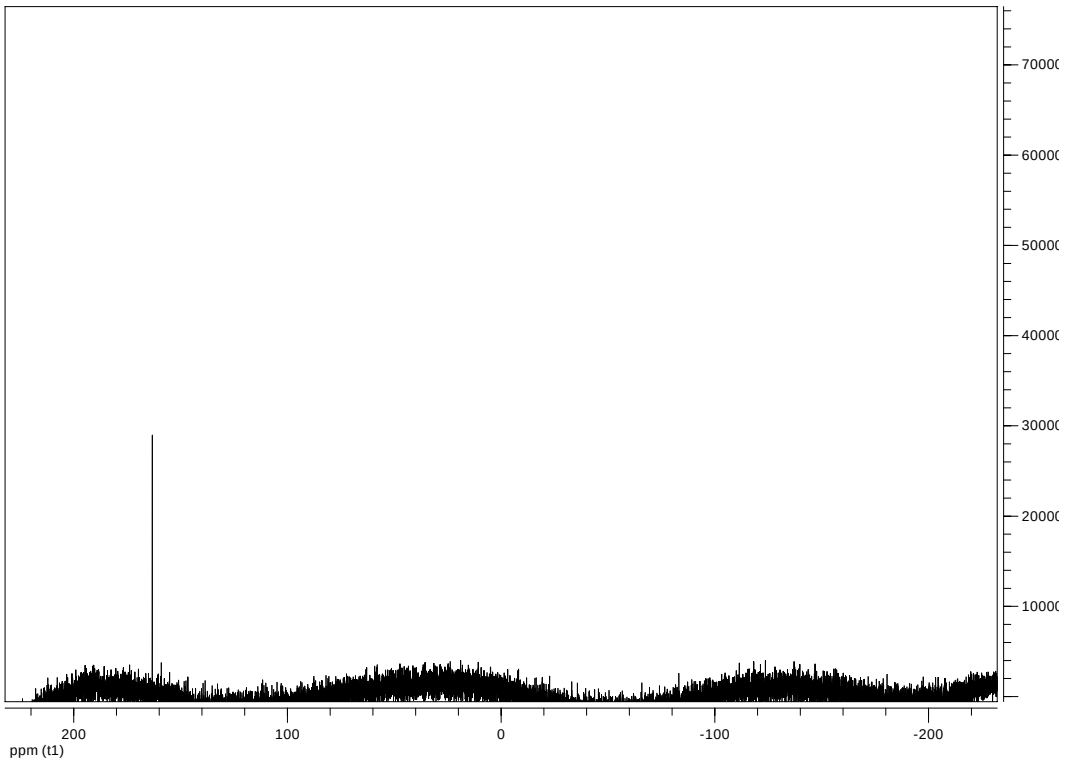

Figure 3.55. ^{31}P NMR spectrum of [Ru(acac)(bipy){P(OMe)$_3$}H] complex

FTIR spectrum of [Ru(acac)(bipy){P(OMe)$_3$}H] complex (Figure 3.56) shows an absorption band at the region of 1490-1550 cm^{-1} assigned as C=C stretching of 2,2′-bipyridine ring which shifts about 30 cm^{-1} to lower wave number region in comparison with the corresponding absorption band for uncoordinated 2,2′-bipyridine compound. 2,2′-bipyridine acts as a σ-donor and π-acceptor ligand and both of nitrogens inside the rings make strong bonds with ruthenium making bond energy of C=C of rings weaker and for that reason frequency of vibration in coordinated 2,2′-bipyridine is getting decreased. Mass spectrum of [Ru(acac)(bipy){P(OMe)$_3$}H] complex (Figure 3.57) obtained by a Micro TOF-LC/ESI/Ms system, shows a very stable fragment, [Ru(bipy){P(OMe)$_3$}(OCH$_2$CH$_2$CH$_2$O)]$^+$, at m/z = 456.

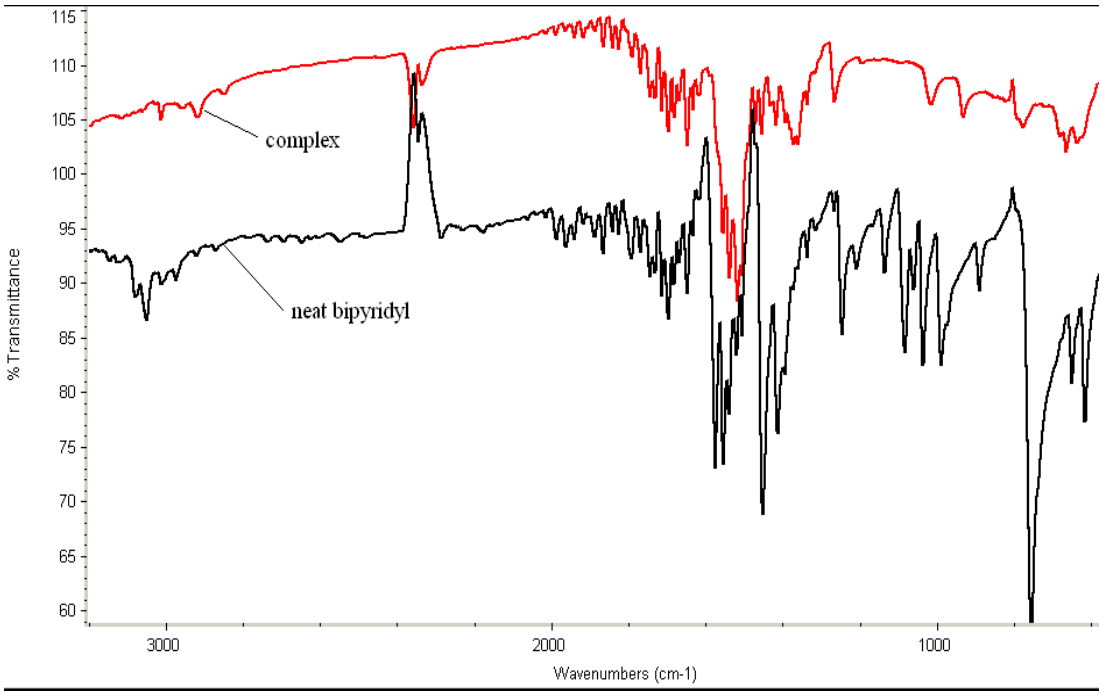

Figure 3.56. FTIR spectrum of [Ru(acac)(bipy){P(OMe)$_3$}H] complex

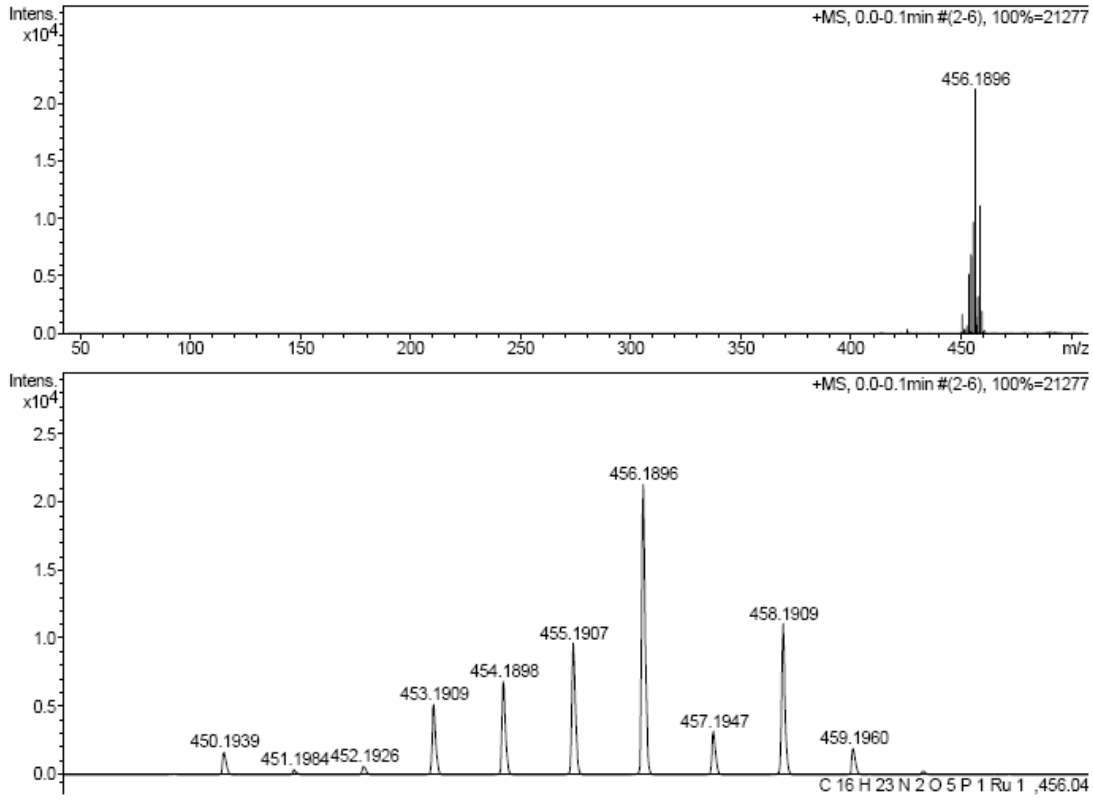

Figure 3.57. Mass spectrum of [Ru(acac)(bipy){P(OMe)$_3$}H] complex

At the next stage, one question needed to be addressed: the question is whether one chelate acetylacetonate ligand (acac) or two monodentate trimethylphosphite ligands are replaced by 2,2′-bipyridine in order to make the in-situ active catalyst stabilized. To reply this question, one catalytic reaction containing $Ru(acac)_3$, $NaBH_4$ and 2,2′-bipyridine without using trimethylphosphite, was performed and followed by UV-Visible spectroscopic measurements for 24 h. After one day following the reaction, there was no change in the UV-Visible spectrum of ruthenium(III) acetylacetonate or in other words, acetylacetonato ligands are not directly replaced by 2,2′-bipyridine even after a very long time in the presence of $NaBH_4$. This observation indicates unequivocally that two phosphorus ligands are replaced by 2,2′-bipyridine to make the in-situ active catalyst stabilized and accordingly, the in-situ active catalyst is $[Ru(acac)\{P(OMe)_3\}_3H]$. So, the in-situ active catalyst is a Ru(II) species and it is in accordance with what we expected regarding reduction of ruthenium center during hydrolysis of $NaBH_4$ (Figure 3.42). In addition, it has been reported that catalytic activity of cis-$[Ru(acac)_2\{P(OMe)_3\}_2]$ in the hydrolysis of $NaBH_4$ is significantly enhanced by the addition of two equivalents of $P(OMe)_3$ per ruthenium into the medium, while catalytic activity of trans-$[Ru(acac)_2\{P(OMe)_3\}_2]$ in the presence of $P(OMe)_3$ is slightly improved [54]. So, we can make a conclusion that in-situ active catalyst has three phosphorus ligands in facial form not meridional and because trans-$[Ru(acac)_2\{P(OMe)_3\}_2]$ already has two phosphorus ligands at the trans position, so formation of active catalyst with three phosphorus ligands in facial form is not possible. Meridional form of $[Ru(acac)\{P(OMe)_3\}_3H]$ is sterically less favorable for attaching substrate and producing hydrogen in comparison with fac-$[Ru\{P(OMe)_3\}_3(acac)H]$. Moreover, the Ru(I) species, $[Ru\{P(OMe)_3\}_4H]$, containing four bulky trimethylphosphite ligands is sterically less favorable to act as an active catalyst in comparison with $[Ru(acac)\{P(OMe)_3\}_3H]$.

3.18. Comparison the catalytic activity of in-situ active catalyst without stabilization, [Ru(acac){P(OMe)$_3$}$_3$H], and in the case of stabilization by 2,2´-bipyridine, [Ru(acac)(bipy){P(OMe)$_3$}H], in hydrogen generation of sodium borohydride

Other catalytic experiments concerning hydrolysis of $NaBH_4$ (450 mM) in the presence of $Ru(acac)_3$ (2 mM) and 3 equivalents of $P(OMe)_3$ were performed to compare the catalytic activity of in-situ active catalyst without stabilization, [Ru(acac){P(OMe)$_3$}3H], and after stabilization by 2,2´-bipyridine (2.5 mM) as [Ru(acac)(bipy){P(OMe)$_3$}H] complex. Based on Figure 3.58, the rate of hydrogen generation for the in-situ active catalyst is 83 mL H_2/minute, while hydrogen generation rate after stabilization of active catalyst by 2,2´-bipyridine, becomes 8 mL H_2/minute. Accordingly, catalytic activity of in-situ active catalyst is highly decreased after stabilization. However, stabilization of in-situ active catalyst by 2,2´-bipyridine is very useful to get insight into mechanism and structure of active catalyst forming temporarily during hydrolysis of $NaBH_4$.

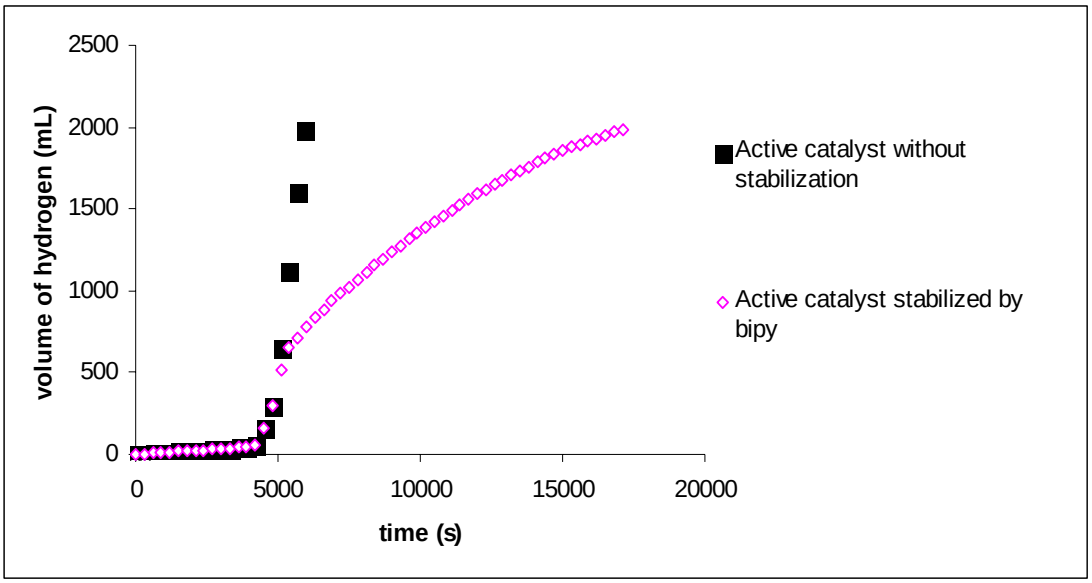

Figure 3.58. Volume of H_2 versus time for the hydrolysis of $NaBH_4$ (450 mM) starting with 2 mM $Ru(acac)_3$ in the case of a) in-situ active catalyst, [Ru(acac){P(OMe)$_3$}$_3$H], b) active catalyst stabilized by 2,2´-bipyridine, [Ru(acac)(bipy){P(OMe)$_3$}H].

3.19. Preparation, characterization and single crystal X-ray diffraction of 1,2-bis(diphenylphosphinoborane)ethane

1,2-bis(diphenylphosphinoborane)ethane, $[Ph_2P(BH_3)CH_2]_2$, was unexpectedly formed during hydrolysis of sodium borohydride catalyzed by $Ru(acac)_3$ plus 1,2-bis(diphenylphosphino)ethane, $[Ph_2PCH_2]_2$. Accordingly, in this catalytic reaction, sodium borohydride acts not only as a substrate to produce hydrogen, but also as a BH_3 supplier for formation of phosphanylborohydrides such as 1,2-bis(diphenylphosphinoborane)ethane, dppe$(BH_3)_2$. When an aqueous solution of sodium borohydride is added to a solution of 1,2-bis(diphenylphospino)ethane, dppe, in tetrahydrofurane under rigorous stirring in an inert atmosphere at 25.0 °C, a reaction occurs together with the hydrogen generation yielding 1,2-bis(diphenylphosphinoborane)ethane, dppe$(BH_3)_2$, which can be isolated by extraction in dichloromethane. Colorless crystals of dppe$(BH_3)_2$ were obtained by crystallization from the hexane-dichloromethane solution at 0°C. Table 3.9 shows the crystal data and crystal refinement of dppe$(BH_3)_2$. Table 3.10 shows selected bond lengths and bond angles of the compound. ORTEP drawing of the dppe$(BH_3)_2$ complex with the atomic numbering scheme is given in Figure 3.59.

Single crystal X-ray diffraction analysis of the colorless crystal shows the crystallization in monoclinic system with space group $P2_1$ and two asymmetric units with a formula of $C_{26}H_{30}B_2P_2$ and four molecules per unit cell. All molecular properties of two asymmetric units of the molecule I are similar of the molecule II as given in Table 3.10.

The average bond angles around P atoms are 112.9, 113.1, 105.8, and 105.5 for B-P-C, B'-P'-C', C-P-C and C'-P'-C', respectively. Study of the interactions between P atoms and contact atoms in sphere of coordination with average distances (P-B: 1.876 Å for the molecule I, 1.905 Å for II and P-C: 1.804 Å for I, 1.809 Å for II) reveals that the P atoms are surrounded by four atoms (one boron and three carbon atoms) as nearly ideal tetrahedral. The conformations of molecules were analyzed using PLATON. Both molecules in an asymmetric unit have a similar three-dimensional conformation. Dihedral angles between the least square planes of

phenyl rings in coordination sphere of P atoms are Cg1-Cg2 = 76.4(3), Cg3-Cg4 = 88.2(3) for molecule (I) and Cg5-Cg6 = 71.2(3), Cg7-Cg8 = 71.5(3) for molecule(II). Rings are composed of atoms Cg1 = C1/C6, Cg2 = C7/C12, Cg3 = C15/C20, Cg4 = C21/C26, Cg5 = C1'/C6', Cg6 = C7'/C12', Cg7 = C15'/C20', Cg8 = C21'/C26'. There is no classic hydrogen bond in the structure but the title compound includes several pi-ring interactions between two asymmetric moieties. Details of the pi-ring interaction geometry are given in Table 3.11.

Table 3.9. Crystal data and structure refinement for $DPPE(BH_3)_2$.

Chemical Formula	$C_{26}H_{30}B_2P_2$
Formula weight [g/mol]	426.06
Crystal system, Space group	monoclinic, $P2_1$
a (Å)	11.657(2)
b (Å)	17.237(2)
c (Å)	12.764(2)
β (°)	98.735(14)
Cell volume ($Å^3$)	2535.0(7)
Z, calculated density	4, 1.116 g/cm^3
Absorption coefficient	0.182 mm^{-1}
F(000)	904
Crystal size	0.3 x 0.3 x 0.3 mm
θ-range for data collection	2.21-26.29º
Limiting indices	$-14 \leq h \leq 0$, $0 \leq k \leq 21$, $-15 \leq l \leq 15$
Reflections collected / Unique	5542 / 5286 [R_{int}= 0.0492]
Completeness to data	Up to θ 26.29º 99.2 %
Data / restrains / parameters	5286 / 553 / 4
Goodness-of-fit on F^2	1.001
Final R indices [I>2σ(I)]	R_1 =0.0558, wR_2 = 0.1301
R indices (all data)	R_1 =0.1719, wR_2 = 0.1644
Largest diff. peak and hole	0.519 and -0.303 e/$Å^3$

Table 3.10. Selected bond length [Å] and angles [°] for two asymmetric units of $DPPE(BH_3)_2$.

Molecule (I)		Molecule (II)	
B1 – P1	1.882(8)	B1' – P1'	1.896(9)
B2 – P2	1.870(9)	B2' – P2'	1.914(10)
P1 – C1	1.809(7)	P1' – C1'	1.802(8)
P1 – C7	1.788(7)	P1' – C7'	1.799(7)
P1 – C13	1.832(7)	P1' – C13'	1.837(8)
P2 – C14	1.805(7)	P2' – C14'	1.818(8)
P2 – C15	1.784(9)	P2' – C15'	1.805(7)
P2 – C21	1.803(7)	P2' – C21'	1.794(8)
C13 – C14	1.521(9)	C13' – C14'	1.533(11)
B1 – P1 – C1	112.8(4)	B1' – P1' – C1'	112.1(4)
B1 – P1 – C7	115.3(4)	B1'– P1' – C7'	113.6(5)
B1 – P1 – C13	110.2(4)	B1' – P1' – C13'	112.0(5)
B2 – P2 – C14	111.8(5)	B2' – P2' – C14'	112.7(5)
B2 – P2 – C15	114.3(5)	B2' – P2' – C15'	115.6(5)
B2 – P2 – C21	113.2(4)	B2' – P2' – C21'	112.8(5)
C1 – P1 – C7	107.2(3)	C1' – P1' – C7'	107.2(3)
C1 – P1 – C13	104.0(3)	C1' – P1' – C13'	105.3(4)
C7 – P1 – C13	106.5(3)	C7' – P1' – C13'	106.0(4)
C14 – P2 – C15	105.8(5)	C14' – P2' – C15'	105.8(4)
C14 – P2 – C21	106.5(3)	C14' – P2' – C21'	103.7(4)
C15 – P2 – C21	104.6(4)	C15' – P2' – C21'	105.2(3)
P1 – C13 – C14	111.8(5)	P1' – C13' – C14'	110.4(5)
P2 – C14 – C13	111.0(5)	P2' – C14' – C13'	111.7(5)

Table 3.11. Structural parameters of pi-ring interaction geometry (Å,°) for the title compound.

D – H ··· Cg	**D–H**	**Cg···H**	**D·····Cg**	**D–H···Cg**
C9 –H9···Cg8	0.93	2.81	3.685(14)	158
C11′–H11′···Cg1^{i}	0.93	2.79	3.634(12)	151
C25′ –H25′···Cg5^{ii}	0.93	2.91	3.662(12)	138

Symmetry codes [i: x, y, 1+z and ii: 1-x, ½+y,1-z]

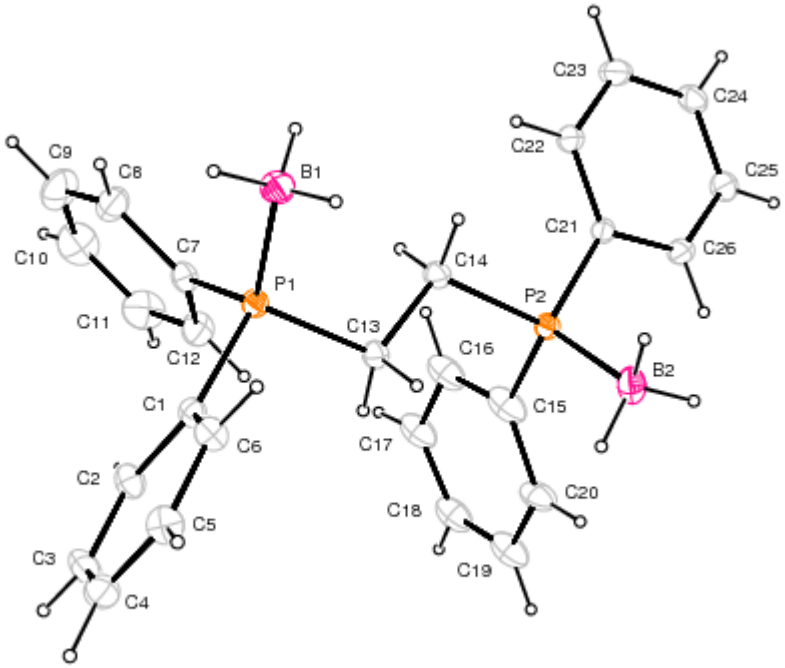

Figure 3.59. ORTEP drawing of the title compound with the atomic numbering scheme for DPPE$(BH_3)_2$ complex

The solution NMR data of 1,2-bis(diphenylphosphinoborane)ethane, DPPE$(BH_3)_2$, obtained on a Bruker Avance (III) 400 MHz spectrometer are also in good agreement with the single crystal structure. The ^{1}HNMR spectrum (Figure 3.60) taken from dichloromethane-d solution gives a triplet at 1.99 ppm for the hydrogens of borane groups which are coordinated to phosphorus atoms. Two doublet diastereopic peaks are observed at 2.15 and 2.38 ppm for the hydrogens of methylene groups due to their different chemical environments arisen from their different distances to borane groups. On contrary to DPPE$(BH_3)_2$ complex, in the case of meso-$[HP(BH_3)(Ph)CH_2]_2$ one singlet was reported for the hydrogens of methylene groups at 1.69 ppm due to their same distances to borane groups [87]. A multiplate is observed at 7.38 ppm for the hydrogens of phenyl rings located at meta and para positions. Two separated multiplates at 7.54 and 7.61 ppm are attributed to ortho-hydrogens of phenyl rings and similar to hydrogens of methylene groups, ortho-hydrogens of phenyl rings are not identical due to their different positions to borane groups.

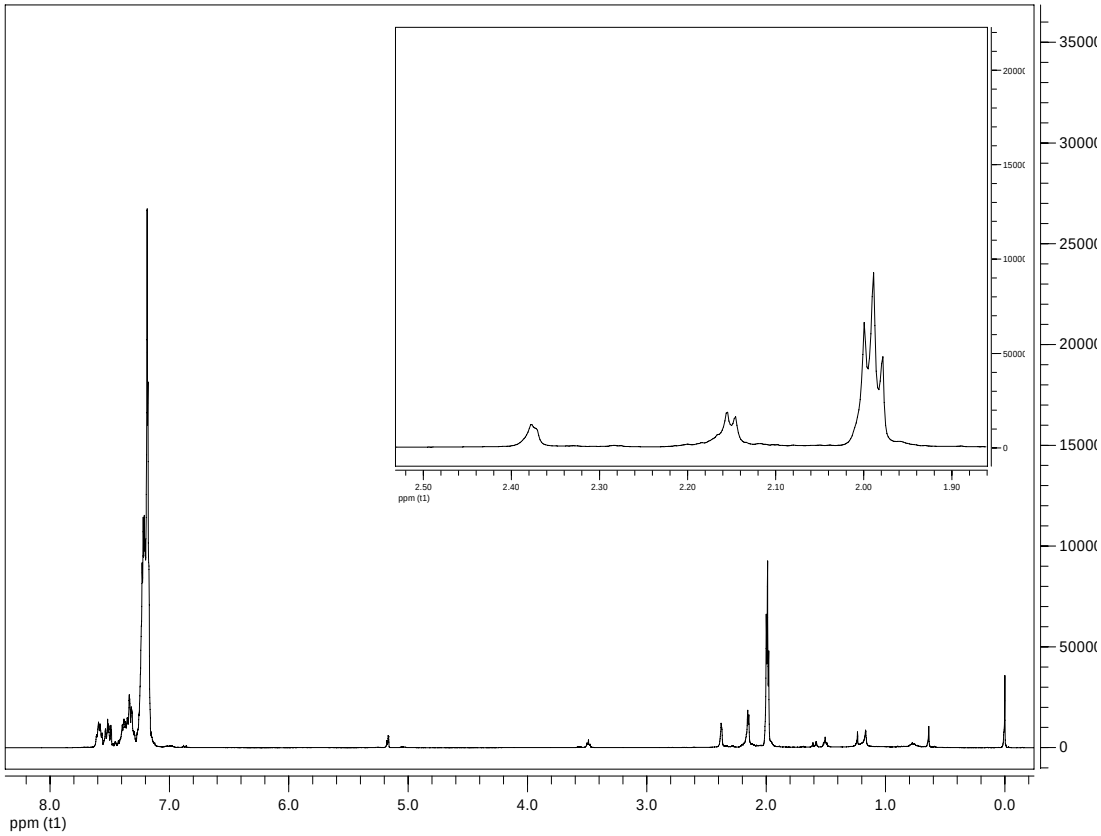

Figure 3.60. ^{1}H NMR of $DPPE(BH_3)_2$ taken in CD_2Cl_2

In accordance with molecular structure, the ^{13}C NMR spectrum (Figure 3.61) gives a singlet at 22.93 ppm for methylene carbons, a multiplate at 127.81 ppm for phenyl ring carbons coordinated to phosphorus atoms directly and three multiplates at 129.87, 131.85 and 137.59 ppm for meta-, para-, and ortho-carbons of phenyl rings, respectively. ^{31}P NMR spectrum (Figure 3.62) of $DPPE(BH_3)_2$ complex, $[Ph_2P(BH_3)CH_2]_2$, shows a peak at -12.5 ppm which is about 10 ppm more shielded than corresponding peak of meso-$[HP(BH_3)(Ph)CH_2]_2$ complex [87], showing that $DPPE(BH_3)_2$ complex containing more phenyl rings, has more electron-rich phosphorus atoms.

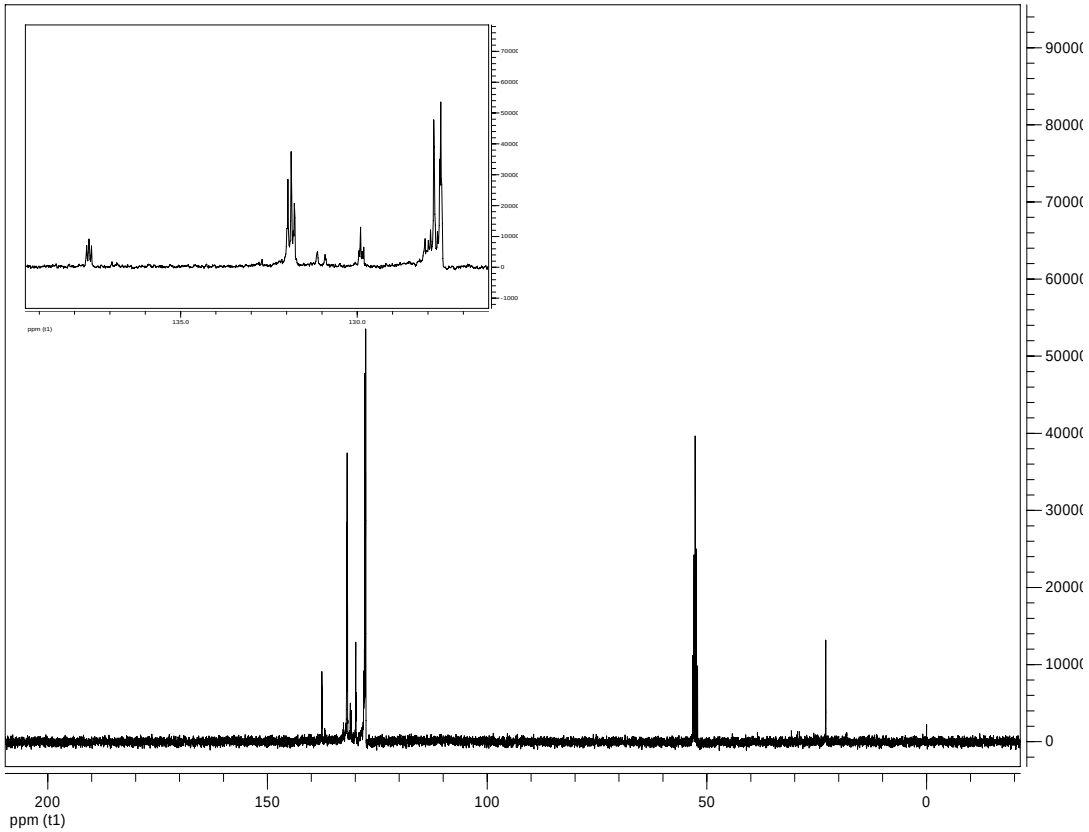

Figure 3.61. ^{13}C NMR of $DPPE(BH_3)_2$ taken in CD_2Cl_2

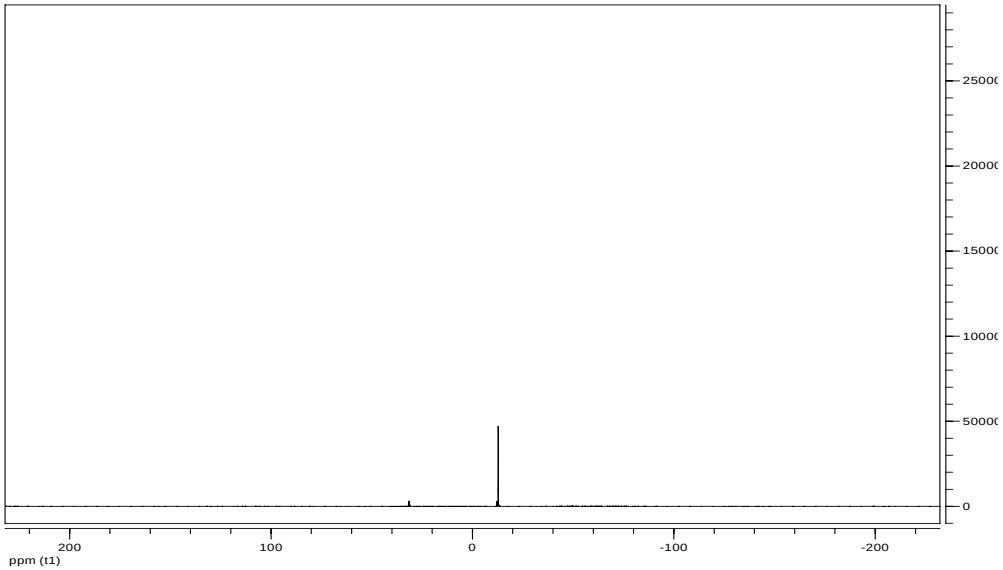

Figure 3.62. ^{31}P NMR of $DPPE(BH_3)_2$ taken in CD_2Cl_2

However, ^{11}B NMR (Figure 3.63) gives a peak at -40.06 ppm for borane groups comparable to the value of -41.6 ppm reported for meso-$[HP(BH_3)(Ph)CH_2]_2$ complex [87].

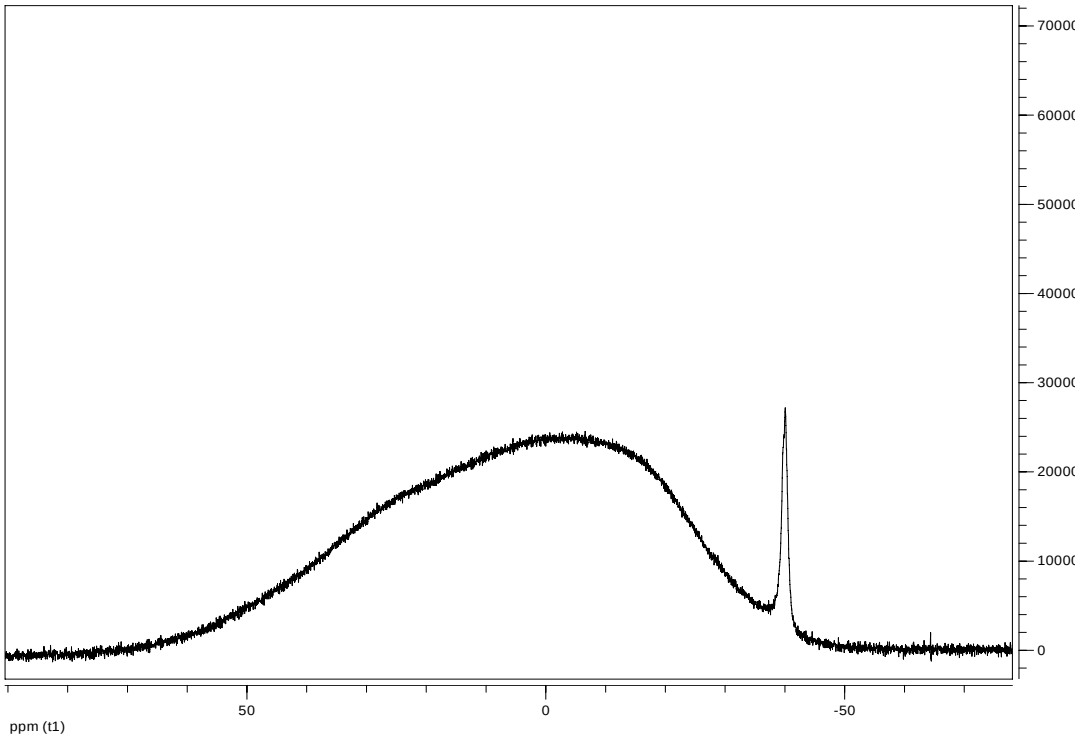

Figure 3.63. ^{11}B NMR of $DPPE(BH_3)_2$ taken in CD_2Cl_2

Mass spectrum, taken by a Micro TOF-LC/ESI/Ms system, does not show the molecular ion peak expected at m/z = 425. Instead, it shows peaks at m/z = 429 or 431 due to oxidation of $dppe(BH_3)_2$ during the sampling/ionization whereby BH_3 groups are replaced by the oxo groups.

CHAPTER 4

CONCLUSION

In summary, our study on the hydrolysis of sodium borohydride catalyzed by $Ru(acac)_3$ plus different phosphorus ligands such as $P(OMe)_3$ or $P(OPh)_3$ has led to the following conclusions and insights :

(i) $Ru(acac)_3$ acts as a homogeneous catalyst in the hydrolysis of sodium borohydride in the presence of different phosphorus compounds such as $P(OMe)_3$ or $P(OPh)_3$.

(ii) Phosphorus compound, usually known as poison in catalysis, is involved in the formation of a species (active catalyst) after induction time with a higher catalytic activity in comparison to sole $Ru(acac)_3$.

(iii) The observation of the fact that the rate of hydrogen generation for the hydrolysis of sodium borohydride starting with $Ru(acac)_3$ and a phosphine is highly increased after an induction time, is indicative of formation of a new ruthenium species containing phosphorus compound.

(iv) In all of experiments involving catalytic hydrolysis of sodium borohydride by $Ru(acac)_3$ and a phosphine, applying higher temperatures or using higher concentrations of $Ru(acac)_3$ lead to a faster formation of active catalyst or a lower induction time.

(v) Varying the phosphorus compound affects the lifetime of the catalyst. The active catalyst containing $Ru(acac)_3$ plus $P(OMe)_3$ has a total turnover number (TTON) of

20700 (over 3 days), while the active catalyst involving $Ru(acac)_3$ and $P(OPh)_3$ has a TTON of 2850 (over 17 hours) in hydrogen generation of sodium borohydride. Both of active catalysts containing $P(OMe)_3$ and $P(OPh)_3$ compounds have higher TTON in comparison with sole $Ru(acac)_3$ (TTON = 1200 over 3 hours) showing that catalytic activity and lifetime of $Ru(acac)_3$ in the hydrolysis of sodium borohydride is improved in the presence of phosphorus compounds.

(vi) Varying the phosphorus compound affects not only the catalytic activity and lifetime of the catalyst but also the kinetics and activation parameters of the hydrolysis of $NaBH_4$. Both the activation energy (58 ± 2 $kJ.mol^{-1}$) and the enthalpy of activation (56 ± 2 $kJ.mol^{-1}$) for the active catalyst containing trimethylphosphite are very similar to the values reported for the sole $Ru(acac)_3$ (58.2 and 55.7 $kJ{\cdot}mol^{-1}$), respectively. While active catalyst involving $Ru(acac)_3$ and $P(OPh)_3$ has lower activation energy and activation enthalpy values (Ea = 52 $kJ.mol^{-1}$, $\Delta H^{\#}$ = 48 $kJ.mol^{-1}$) in comparison with $Ru(acac)_3$ alone. It is noteworthy that the activation entropy has large negative value for both of active catalysts containing trimethylphosphite ($\Delta S^{\#}$ = -64 J/mol.K) and triphenylphosphite ($\Delta S^{\#}$ = -95 J/mol.K) compounds, showing an associative nature in the transition state for the catalytic hydrolysis of sodium borohydride.

(vii) For both of $P(OMe)_3$ and $P(OPh)_3$ compounds, the hydrogen generation was found to be zero order regarding the substrate concentration and first order with respect to the catalyst concentration.

(viii) Varying the mole ratio of different phosphorus compounds to $Ru(acac)_3$ does not affect the rate of hydrogen generation or in other words, the mechanism of reaction or structure of the active catalyst formed during hydrolysis of sodium borohydride are independent of phosphine concentration.

(ix) Trans- and cis-$[Ru(acac)_2\{P(OMe)_3\}_2]$ complexes, do not show significant catalytic activity in hydrogen generation of sodium borohydride. However, catalytic activity of cis-$[Ru(acac)_2\{P(OMe)_3\}_2]$ complex is highly increased in the presence of

two equivalents of trimethylphosphite, indicating that the active catalyst formed during hydrolysis of sodium borohydride starting with $Ru(acac)_3$ or cis-$[Ru(acac)_2\{P(OMe)_3\}_2]$, has more than two phosphine ligands. Taking all the results together, we propose that the in-situ formed active catalyst operating in hydrogen generation from the hydrolysis of sodium borohydride starting with ruthenium(III) acetylacetonate and trimethylphosphite is most likely the fac-$[Ru(acac)\{P(OMe)_3\}_3H]$ complex which can be generated not only from $Ru(acac)_3$ but also from cis-$[Ru(acac)_2\{P(OMe)_3\}_2]$ in the presence of trimethylphosphite during the hydrolysis of sodium borohydride.

(x) $[Ru(acac)_2(\eta^2\text{-}C_8H_{14})_2]$ complex which is easily accesible via reduction of $Ru(acac)_3$ by zinc amalgam in the presence of cyclooctene, provides a convenient entry into a wide range of trans- and cis-$[Ru(acac)_2L_2]$ complexes (L = Py, bipy, $CNBu^t$, NMe_3, PMe_3, $P(OMe)_3$, $P(OPh)_3$, PEt_3, PMe_2Ph or $SbPh_3$) such as trans- and cis-$[Ru(acac)_2\{P(OMe)_3\}_2]$ complexes. Trans-$[Ru(acac)_2\{P(OMe)_3\}_2]$ which is a kinetically stable product due to π-competition of phosphines, converts to its cis isomer on heating.

(xi) One in-situ active catalyst is formed temporarily during hydrolysis of sodium borohydride starting with $Ru(acac)_3$ and $P(OMe)_3$. The in-situ active catalyst which is a Ru(II) species is alive as long as the hydrogen generation continues. After finishing the hydrogen generation, the in-situ active catalyst converts back to paramagnetic ruthenium(III) acetylacetonate species as a major product along with formation of a Ru(I) species containing four trimethylphosphite ligands, $[Ru\{P(OMe)_3\}_4H]$, as a minor product.

(xii) The in-situ active catalyst is stabilized by 2,2´-bipyridine and isolated from the aqueous solution as $[Ru(acac)(bipy)\{P(OMe)_3\}H]$ complex. The structure of in-situ active catalyst is compatible with fac-$[Ru(acac)\{P(OMe)_3\}_3H]$ complex which is producible not only by $Ru(acac)_3$ but also by cis-$[Ru(acac)_2\{P(OMe)_3\}_2]$ in the presence of trimethylphosphite.

(xiii) fac-[Ru(acac){P(OMe)$_3$}$_3$H] is sterically more favorable to act as an homogeneous catalyst to produce hydrogen in comparison with its meridional form with one active site between two bulky trimethylphosphite ligands or [Ru{P(OMe)$_3$}$_4$H] complex containing four bulky ligands.

(xiv) The in-situ active catalyst, fac-[Ru(acac){P(OMe)$_3$}$_3$H] has much higher catalytic activity in comparison with its stabilized complex by 2,2′-bipyridine, [Ru(acac)(bipy){P(OMe)$_3$}H].

(xv) sodium borohydride acts not only as a substrate to produce hydrogen, but also as a BH_3 supplier in forming phosphanylborohydrides such as 1,2-bis(diphenylphosphinoborane)ethane, DPPE$(BH_3)_2$.

REFERENCES

[1] Fakioglu, E.; Yurum, Y.; Veziroglu, T.N., *A review of hydrogen storage systems based on boron and its compounds*, **2004**.

[2] Zuttel, A., *Naturwissenschaften*, **2004**, 91, 157.

[3] Kim, J.H.; Kim, K.T.; Kang, Y.M.; Kim, S.K.; Song, M.S.; Lee, J.Y., *J. Alloys. Compd*., **2004**, 379, 222.

[4] Kim, J.H.; Lee, H.; Han, S.C.; Kim, H.S.; Song, M.S.; Lee, J.Y., *Int. J. Hydrogen Energy*, **2004**, 29, 263.

[5] Kojima, Y.; Suzuki, K.I.; Fukumoto, K.; Sasaki, M.; Yamamoto, T.; Kawai, Y.; Hayashi, H., *Int. J. Hydrogen Energy*, **2002**, 27, 1029.

[6] Schaller, K.V.; Gruber, C., *Fuel cell derive and high dynamic energy storage systems- opportunities for the future city bus. Fuel cells bull*, **2000**, 27, 9.

[7] Ogston, J.M.; Kreutz, T.G.; Steinbugler, M.M., *Fuels for fuel cell vehicles. Fuel cell bull*, **2000**, 16, 5.

[8] Levy, A.; Brown, J.B.; Lyons, C.J., *Ind. Eng. Chem*., **1960**, 52, 211.

[9] Gardiner, J.A.; Collat, J.W., *J. Am. Chem. Soc*., **1965**, 87, 1692.

[10] Atkinson, K.; Roth, S.; Hirscher, M.; Grunwald, W., *Carbon nanotubes: an efficient hydrogen storage medium for fuel cells? Fuel cells bull*, **2001**, 38, 9.

[11] Sandrock, G., *State-of-the-art review of hydrogen storage in reversible metal hydrides for military fuel cell applications*. Final report contract N00014-97-M-0001, **1997**.

[12] Aiello, R.; Sharp, J.H.; Matthews, M.A., *Int. J. Hydrogen Energy*, **1999**, 24, 1123.

[13] Sifer, N.; Gardner, K., *J. Power Sources*, **2004**, 132, 135.

[14] Kong, V.C.Y.; Foulkes, F.R.; Kirk, D.W.; Hinatsu, J.T., *Int. J. Hydrogen Energy*, **1999**, 24, 665.

[15] Amendola, S.C.; Onnerud, P.; Kelly, M.T.; Petillo, P.J.; Sharp, G.L.;Binder, M., *J. Power Sources*, **2000**, 85, 186.

[16] Amendola S.C.; Janjua, J.M.; Spencer, N.C.; Kelly, M.T.; Petillo, P.J.; Sharp, G.L.; Binder, M., *Int. J. Hydrogen Energy*, **2000**, 25, 969.

[17] Lee, J.Y.; Lee, H.H.; Lee, J.H.; Kim, D.M.; Kim, J.H., *J. Electrochem. Soc*., **2002**, 149, 603.

[18] Li, Z.P.; Liu, B.H.; Arai, K.; Morigazaki, N.; Suda, S., *J. Alloys. Compd*. **2003**, 356, 469.

[19] Liu, B.H.; Li, Z.P., *J. Power Sources*, **2009**, 187, 527.

[20] Basic research needs for the hydrogen economy, *Report of the basic energy sciences workshop on hydrogen production, storage and use*, May 13-15, **2003**, office of science, US Department of Energy, www.sc.doe.gov/bes/hydrogen.pdf.

[21] Annual Energy Outlook 2005 With Projections To 2025, *Energy Information Administration*, February **2005**, www.eia.doe.gov/oiaf/aeo/pdf/0383(**2005**).pdf.

[22] Turner, J.; Sverdrup, G.; Mann, K.; Maness, P.G.; Kroposki, B.; Ghirardi, M.; Evans, R.J.; Blake, D., *Int. J.Energy Res*., **2008**, 32, 379.

[23] IAC Report, *Lighting the way towards a sustainable energy futures*, Interacademy Council, Amsterdam, **2007**.

[24] Xia, Z.T.; Chan, S.H., *J. Power Sources*, **2005**, 152, 46.

[25] James, B.D.; Wallbridge, M.G.H., *Metal tetrahydroborates. Prog. Inorg. Chem*., **1970**, 11, 99.

[26] Schlesinger, H.I.; Brown, H.C.; Finhold, A.E.; Gilbert, J.R.; Hoekstra, H.R.; Hyde, E.K., *J. Am. Chem. Soc*., **1953**, 75, 21.

[27] Pecsok, R.L., *J. Am. Chem. Soc.*, **1953**, 75, 286.

[28] Levy, A.; Brown, J.B.; Lyons, C.J., *Ind. Eng. Chem.*, **1960**, 52, 211.

[29] Brown, H.C.; Brown, C.A., *J. Am. Chem. Soc.*, **1962**, 84, 1493.

[30] Stockmayer, W.H.; Miller, R.R.; Zeto, R.J., *J. Phys. Chem.*, **1961**, 65, 1076.

[31] Davis, R.E.; Bromels, E.; Kibby, C.L., *J. Am. Soc.*, **1962**, 84, 885.

[32] Davis, R.E.; Swain, C.G., *J. Am. Soc.*, **1960**, 82, 5950.

[33] Mesmer, R.E.; Jolly, W.L., *Inorg. Chem.*, **1962**, 1, 608.

[34] Gardiner, J.A.; Collatt, J.W., *J. Am. Chem. Soc*., **1964**, 86, 3165.

[35] Sen, B.; Kaufman, C.M., *J. Chem. Soc. Dalton Trans.*, **1985**, 307, 64.

[36] Kojima, Y.; Kawai, Y.; Suzuki, K.I.; Fukumoto, K.; Kimbara, M.; Nakashi, H.; Matsumoto, S., *J. Power Sources*, **2004**, 125, 22.

[37] Kojima, Y.; Kawai, Y.; Nakashi, H.; Matsumoto, S., *J. Power Sources*, **2004**, 135, 36.

[38] Hanxi, Y.; Hua, D.; Xinping, A.; Chuansin, C., *Int. Journal of Hydrogen Energy*, **2003**, 28, 1095.

[39] Lee, J.Y.; Kim, J.H.; Han, S.C.; Kim, H.S.; Song, M.S., *Int. Jourmal of Hydrogen Energy*, **2004**, 29, 263.

[40] Wu, C.; Zhang, H.; Yi, B., *Catalysis Today*, **2004**, 93, 477.

[41] Wu, C.; Wu, F.; Bai, Y.; Zhang, H., *Materials Letters*, **2005**, 59, 1748.

[42] Yang, T.H.; Krisshan P.; Lee, W.Y.; Kim, C.S., *J. Power Sources*, **2005**, 143, 17.

[43] Korobov, I.I.; Mozgina, N.G.; Blinova, L.N., *Kinet. Catal*., **1995**, 48, 380.

[44] Hua, D.; Hanxi, Y.; Xinping, A.; Chuansain, C., *Int. J. Hydrogen Energy*, **2003**, 28, 1095.

[45] Ozkar, S.; Zahmakiran, M., *J. Alloys Compd*., **2005**, 404, 728.

[46] Zahmakiran, M.; Ozkar, S., *J. Mol. Cat A: Chemical*, **2006**, 258, 95.

[47] Metin, O.; Ozkar, S., *Int. J. Hydrogen Energy*, **2007**, 32, 1707.

[48] Rakap, M.; Ozkar, S., *Appl. Catal. B*, **2009**, 91, 21.

[49] Metin, O., Ozkar, S., *J. Mol. Cat A: Chemical*, **2008**, 295, 39.

[50] Keceli, E.; Ozkar, S., *J. Mol. Cat A: Chemical*, **2008**, 286, 87.

[51] Widegren, J.A.; Finke, R.G., *J. Mol. Cat A: Chemical*, **2003**, 198, 317.

[52] Masjedi, M.; Demiralp, T.; Ozkar, S., *J. Mol. Cat A: Chemical*, **2009**, 310, 59.

[53] Demiralp, T., *Master Thesis*, METU, Ankara, June **2008**.

[54] Masjedi, M.; Yildirim, L.T.; Ozkar, S., *Inorg. Chim. Acta*, **2010**, 363, 1713.

[55] Sommerer, S.O.; Palenik, G.J., *Organometallics*, **1991**, 10, 1223.

[56] Funaioli, T.; Cavazza, C.; Marchetti, F.; Fachinetti, G., *Inorg. Chem*., **1999**, 38, 3361.

[57] Papp, G.; Horvath, H.; Katho, A.; Joo, F., *Helv. Chim. Acta*. **2005**, 88, 566.

[58] Goncalves, N.S.; Mazzetto, S.E., *Transition Met. Chem*., **2002**, 27, 646.

[59] Bruce, M.; Kelly, D.; Mclaughlin, G.; Robertson, G.; Tomkins, I.; Wallis, R. *Aus. J. Chem*. **1980**, 33, 195.

[60] Hanyu, A.; Takezawa, E.; Sakaguchi, S.; Ishii, Y., *Tetrahedron Lett*. **1998**, 39, 5557.

[61] Raveendran, R.; Pal, S., *Eur. J. Inorg. Chem*., **2008**, 5540.

[62] *EU Patent*. **1994**, Publication No : 0612 757 A_1.

[63] Getty, A.D.; Tai, C.-C.; Linehan, J.C.; Jessop, P.G.; Olmstead, M.M.; Rheingold, A.L., *Organometallics*, **2009**, 28, 5466.

[64] Munshi, P.; Main, A.D.; Linehan, J.C.; Tai, C.-C.; Jessop, P.G., *J. Am. Chem. Soc*. **2002**, 124, 7963.

[65] Tai, C.-C.; Pitts, J.; Linehan, J.C.; Main, A.D.; Munshi, P.; Jessop, P.G., *Inorg. Chem*., **2002**, 41, 1606.

[66] Jessop, P.G.; Hsiao, Y.; Ikariya, T.; Noyori, R., *J. Am. Chem. Soc*., **1996**, 118, 344.

[67] Yin, C.; Xu, Z.; Yang, S.-Y.; Ng, S.M.; Wong, K.Y.; Lin, Z.; Lau, C.P., *Organometallics*, **2001**, 20, 1216.

[68] Borowski, A.J.F.; Sabo-Etienne S.; Donnadieu, B.; Chaudret, B., *Organometallics*, **2003**, 22, 1630.

[69] *US Patent*. **1995**, Publication No: 5, 430, 179.

[70] Teunissen, H.T.; Elsevier, C.J., *Chem. Commun*., **1998**, 1367.

[71] Teunissen, H.T.; Elsevier, C.J., *Chem. Commun*., **1997**, 667.

[72] Engelen, M.C.; Teunissen, H.T.; Vries, J.G.; Elsevier, C.J., *J. Mol. Cat. A: Chemical*, **2003**, 206, 185.

[73] Masjedi, M.; Yildirim, L.T.; Ozkar, S., Novel homogeneous catalyst comprising ruthenium and trimethylphosphite for the hydrolysis of sodium borohydride at room temperature, submitted to Dalton Transaction.

[74] Masjedi, M.; Yildirim, L.T.; Ozkar, S., A facile route to phosphanylborohydrides: synthesis, crystal structure and spectroscopic properties of

1,2-bis(diphenylphosphinoborane)ethane, *Journal of Molecular Structure*, Submitted **2010**.

[75] Stephan, O.; Riegel, N.; Juge, S., *J. Electroanal. Chem*., **1997**, 421, 5.

[76] Dornhaus, F.; Bolte, M.; Lerner, H.-W.; Wagner, M., *J. Organomet. Chem*., **2007**, 692, 2949.

[77] Geanangel, R.A., *J. Inorg. Nucl. Chem*., **1974**, 36, 1397.

[78] Jugie, G.; Laussac, J.P.; Laurent, J.P., *Bulletin de la societe chimique de France*, **1970**, 7, 2542.

[79] Juge, S.; Stephan, M.; Laffitte, J.A.; Genet, J.P., *Tetrahedron Lett*., **1990**, 31, 6357.

[80] Juge, S.; Stephan, M.; Merdes, R.; Genet, J.P.; Halut-Desportes, S., *J. Chem. Soc., Chem. Commun*., **1993**, 531.

[81] Kaloun, B.El.; Merdes, R.; Genet, J.P.; Uziel, J.; Juge, S., *J. Organomet. Chem*., **1997**, 529, 455.

[82] Schmidbaur, H.; Sigl, M.; Schier, A., *J. Organomet. Chem*., **1997**, 529, 323.

[83] Nunez, R.; Vinas, C.; Teixidor, F.; Sillanpaa, R.; Kivekas, R., *J. Organomet. Chem*., **2002**, 657, 224.

[84] Baban, J.A.; Roberts, B.P., *J. Chem. Soc. Perkin Trans. II*, **1986**, 1607.

[85] Schmidbaur, H.; Mueller, G.; Blaschke, G., *Chem. Ber*., **1980**, 113, 1480.

[86] Dornhaus, F.; Bolte, M.; Lerner, H.-W.; Wagner, M., *Eur. J. Inorg. Chem*., **2006**, 1777.

[87] Dornhaus, F.; Bolte, M.; Lerner, H.-W.; Wagner, M., *Eur. J. Inorg. Chem*., **2006**, 5138.

[88] Angerer, W.; Scheldrick, W.S.; Malisch, W., *Chem. Ber*., **1985**, 118, 1261.

[89] Hoic, D.A.; Davis, W.M.; Fu, G.C., *J. Am. Chem. Soc*., **1996**, 118, 8176.

[90] Gaumont, A.-C.; Hursthouse, M.B.; Coles, S.J.; Brown, J.M., *Chem. Commun*., **1999**, 63.

[91] Dorn, H.; Jaska, C.A.; Singh, R.A.; Lough, A.J.; Manners, I., *Chem. Commun*., **2000**, 1041.

[92] Muller, G.; Brand, J., *Organometallics*, **2003**, 22, 1463.

[93] Jaska, C.A.; Lough, A.J.; Manners, I., *Inorg. Chem*., **2004**, 43, 1090.

[94] Brauer, G., *Handbook of preparative Inorganic chemistry*, academic press, New York, **1965**, vol.2, P.1806.

[95] Bennett, M.A.; Chung, G.; Hockless, D.C.R.; Neumann, H.; Willis, A.C., *J. Chem. Soc., Dalton Trans*., **1999**, 3451.

[96] Enraf–Nonius. *CAD-4 EXPRESS*. Enraf–Nonius, Delft, The Netherlands (**1994**).

[97] XCAD4: Harms, K.; Wocadlo, S., *XCAD4*, University of Marburg, Germany (**1995**).

[98] SIR92: Altomare, A.; Cascarano, G.; Giacovazzo, C.; Guagliardi, A.; Burla, M.C.; Polidori, G.; Camalli. M., *J. Appl. Cryst*., **1994**, 27, 435.

[99] SHELX: Sheldrick. G.M., *Acta Cryst. A*., **2008**, 64, 112.

[100] ORTEP-3: Farrugia. L.J., *J. Appl. Cryst*., **1997**, 30, 565.

[101] MERCURY: Macrae, C.F.; Edgington, P.R.; McCabe, P.; Pidcock, E.; Shields, G.P.; Taylor, R.; Towler, M.; Streek. J.V. D., *J. Appl. Cryst*., **2006**, 39, 453.

[102] North, A.C.T.; Phillips, D.C.; Mathews, F.S., *Acta Cryst. A*., **1968**, 24, 351.

[103] WinGX: Farrugia, L. J., *J. Appl. Cryst*., **1999**, 32, 837.

[104] Amirnasr, M.; Houriet, R.; Meghdadi, S., *Journal of thermal analysis and calorimetry*, **2002**, 67, 523.

[105] Connors, K.A., *Theory of chemical kinetics*, VCH publishers, New York (**1990)**.

[106] Twigg, M.V., *Mechanisms of Inorganic and Organometallic reactions*, Plenum press, New York (**1994**).

[107] Prasad, E.; Flowers, R.A., *J. Am. Chem. Soc*., **2002**, 124, 6357.

[108] Maechling, S.; Zaja, M.; Blechert, S., *Adv. Synth. Catal*., **2005**, 347, 1413.

[109] Bennett, M.A.; Byrnes, M.J.; Willis, A.C., *Dalton Trans*. **2007**, 1677.

[110] Bennett, M.A.; Byrnes, M.J.; Willis, A.C., *Organometallics*, **2003**, 22, 1018.

[111] Bennett, M.A.; Byrnes, M.J.; Chung, G.; Edwards, A.J.; Willis, A.C., *Inorg. Chim. Acta*, **2005**, 358, 1692.

[112] Bennett, M.A.; Byrnes, M.J.; Kovacik, I., *J.Organomet.Chem*., **2004**, 689, 4463.

[113] Atwood, J.D., *Inorganic and organometallic reaction mechanisms*, 2nd edn., VCH, Weinheim, **1997**, P. 87.

[114] Elian, M.; Hoffmann, R., *Inorg. Chem*., **1975**, 14, 1058.

[115] Burdett, J.K., *J. Chem. Soc., Faraday Trans*., **1974**, 2, 1599.

[116] Placa, S.J.La; Ibers, J.A., *Inorg. Chem*., **1965**, 4, 778.

[117] Appleton, T.G.; Clark, H.C.; Manzer, L.E., *Coord. Chem. Rev*., **1973**, 10, 335.

[118] Lupin, M.S.; Shaw, B.L., *J. Chem. Soc A*, **1968**, 741.

[119] Grobelny, R.; Jeowska-Trzebiatowska, B.; Wojciechowski, W., *J. Inorg. Nucl. Chem*., **1966**, 28, 2715.

[120] PLATON: Spek. A.L., *J. Appl. Cryst*., **2003**, 36, 7.

[121] Johnson, A.; Everett, G.W.Jr., *J. Am. Chem. Soc*., **1970**, 92, 6705.

[122] Eaton, D.R., *J. Am. Chem. Soc*., **1965**, 87, 3097.

[123] R. Grobelny, B. Jeowska-Trzebiatowska, W. Wojciechowski, J. Inorg. Nucl. Chem. 1966, **28**, 2715.

[124] P. Nagababu, J.N.L. Latha, S. Satyanarayana, Chem. Biodiversity 2006, **3**, 1219.

CURRICULUM VITAE

Personal Information

Surname; Name: Masjedi, Mehdi
Nationality: Iranian
Date and Place of Birth: 01.09.1974, Tehran
Marital Status: Single
Email: mehdimasjedi@yahoo.com

Education

1993-1997	Department of Chemistry, Faculty of Arts and Sciences, Lorestan University, Iran (Bs in Pure Chemistry) (Graduation CGPA : 3.2 / 4)
1998-2001	Department of Chemistry, Faculty of Arts and Sciences, Gilan University, Iran (Ms in Inorganic Chemistry) (Graduation CGPA : 3.6 / 4)
2005-2010	Graduate School of Natural and Applied Sciences, Middle East Technical University, Turkey (PhD in Inorganic Chemistry) (Graduation CGPA : 3.86 / 4)
Awards	PhD Fellowship from Technological and Scientific Research Council of Turkey (TUBITAK) for 4 years (2006-2010)

Publications

(1) K. Tabatabaeian, M. Mamaghani, A. Neshat, M. Masjedi. Synthesis and spectroscopic studies of new substituted Dinuclear 4,5,6,7-Tetrahydroindenyl Ruthenium complexes. Russian Journal of Coordination Chemistry (2003), 29(7), 501-504.

(2) M.W. Pitcher, Y. Arslan, P. Edinc, M. Kartal, M. Masjedi, O.Metin, F. Sen, O. Turkarslan, B. Yigitsoy. Recent advances in the synthesis and applications of inorganic polymers. Phosphorus, silicon, sulfur and related elements (2007), 182, 2861-2880.

(3) M. Masjedi, T. Demiralp, S. Ozkar. Testing catalytic activity of Ruthenium(III)acetylacetonate in the presence of trialkylphosphite or trialkylphosphine in hydrogen generation from the hydrolysis of sodium borohydride. Journal of molecular catalysis A: Chemical 310 (2009) 59-63.

(4) M. Masjedi, L.T. Yildirim, S. Ozkar. Crystal structure of trans- and cis-bis(acetylacetonato)bis(trimethylphosphite)ruthenium(II) and testing their catalytic activity in hydrogen generation from the hydrolysis of sodium borohydride, Inorganica Chimica Acta, 363 (2010) 1713-1718.

(5) M. Masjedi, L.T.Yildirim, S. Ozkar. A facile route to phosphanyl-borohydrides: synthesis, crystal structure and spectroscopic properties of 1,2- bis(diphenylphosphino borane) ethane, Submitted to Journal of Molecular Structure.

(6) M. Masjedi, L.T. Yildirim, S. Ozkar. Novel homogeneous catalyst comprising ruthenium and trimethylphosphite for the hydrolysis of sodium borohydride at room temperature, submitted to Dalton Transactions.